# Eruptive history of Ohachidaira volcano and evolution of the summit caldera, Taisetsu volcano group, central Hokkaido, Japan

Yasuda, Yuki

(Degree)
博士（学術）

(Date of Degree)
2018-03-25

(Date of Publication)
2020-03-25

(Resource Type)
doctoral thesis

(Report Number)
甲第7125号

(URL)
https://hdl.handle.net/20.500.14094/D1007125

# Doctoral Dissertation

**Eruptive history of Ohachidaira volcano and evolution of the summit caldera, Taisetsu volcano group, central Hokkaido, Japan**

**（北海道大雪山御鉢平火山の噴火史と、山頂カルデラの形成過程）**

**January, 2018**

**Graduate School of Science, Kobe University**

**Yuki Yasuda**

**安田　裕紀**

# 博　士　論　文

# 北海道大雪山御鉢平火山の噴火史と、山頂カルデラの形成過程

平成 30 年 1 月

神戸大学大学院理学研究科

安田　裕紀

# Doctoral Dissertation

**Eruptive history of Ohachidaira volcano and evolution of the summit caldera, Taisetsu volcano group, central Hokkaido, Japan**

January, 2018

Graduate School of Science, Kobe University

Yuki Yasuda

# Contents

# Eruptive history of Ohachidaira volcano and evolution of the summit caldera, Taisetsu volcano group, central Hokkaido, Japan

By Yuki Yasuda

## Abstract

The 34 ka Sounkyo eruption is the most voluminous explosive volcanic event of Ohachidaira volcano in the Taisetsu volcano group (central Hokkaido, Japan) and made a substantial contribution to the formation of the 2-km-diameter summit caldera (Ohachidaira caldera). This eruption provides an ideal opportunity to study small calderas and their formation mechanisms. In Chapter 1 of this thesis, I present a short review of the current understanding of caldera formation mechanisms based on geological studies, and highlight major challenges in the field that I deal with. In Chapter 2, I present a brief description of the evolution of the Taisetsu volcano group and the stratigraphy of its basement. I also review previous studies of Ohachidaira volcano and its summit caldera in terms of eruptive history and detect what is lacking in such studies. In Chapter 3, I reconstruct the eruptive history of Ohachidaira volcano on the basis of field and paleomagnetic data and investigate how the summit caldera developed in relation to each eruptive event, with special focus on the Sounkyo eruption in Chapter 4. Finally, in Chapter 5, I summarize the major findings in this study.

Ohachidaira volcano is an andesitic to dacitic stratovolcano located in the center of the Taisetsu volcano group. Early volcanism (600 ka–) at Ohachidaira was characterized by an alternation of effusive and explosive activities, producing 0.17 $km^3$

of lava flows, the Ohachidaira lava, and intermittent pyroclastic deposits to construct the main lower edifice of Ohachidaira. The 80–40 ka Hb-type ignimbrite (>4.6 $km^3$ in bulk volume), whose source was believed to be the Ohachidaira caldera, attains at least 130 m thick on the foot of the Taisetsu volcano group and appears to overlie the Ohachidaira lava on the southern side of Ohachidaira volcano. However, my geological data indicates that there is no proof for or against its source to be the Ohachidaira caldera, and in fact supports the inference that the ignimbrite was vented from somewhere in the Taisetsu volcano group rather than the Ohachidaira caldera. Between 80–40 ka and 34 ka, Ohachidaira produced two relatively small explosive eruptions, the Kobachidaira ignimbrite and Mamiyadake Scoria Member. The Kobachidaira ignimbrite (0.04 $km^3$ in bulk volume) occurs only in the summit area, covering the middle to lower flanks of Ohachidaira volcano and overlain by the Mamiyadake Scoria Member, and is a <30-m-thick, lithic-rich, pyroclastic density current (PDC) deposit. Its coarseness (<5.5 m) and abundance (~50 vol%) of lithic fragments throughout the deposit reflects a vent opening and development. The Mamiyadake Scoria Member (0.08 $km^3$ in bulk volume) forms a tephra ring as much as ~60 m thick, occurring around the caldera and comprising the upper edifice of Ohachidaira. The tephra ring is dominated by pyroclastic breccia and stratified and cross-stratified lapilli-tuff beds with interstratified fine-ash beds, formed by phreatomagmatic and magmatic activities. The tephra ring deposits are generally enriched in lithic clasts (~40 vol%), whose assemblage is dominated by shallow-origin volcanic rocks, indicating that the shallow conduit and vent were progressively widened as the eruption proceeded. The total volume of lithic fragments ejected during the two small explosive eruptions is estimated to be ~0.05 $km^3$.

The 34 ka Sounkyo eruption produced 7.6 $km^3$ of tephra (~5 $km^3$ DRE) as fallout, ignimbrite, and lithic breccia units. The Sounkyo eruption products are made up of five eruptive units (SK-A to -E) in proximal (near source) regions, corresponding to the distal deposits, a 1- to 2-m-thick pumice fallout and the Px-type ignimbrite up to 220 m thick. The eruption began with a fallout phase, producing unstable low eruption columns during the earlier phase to form a <7-m-thick succession of well-stratified fallouts, occasionally interrupted by thin PDC beds suggestive of small-scale column

collapse (SK-A1 and the lower part of the distal fallout). The eruption column reached up to 25 km high (subplinian to plinian) and became more stable at the late of the phase, producing a <60-m-thick, pumice-dominated fallout (SK-A2 and the upper part of the distal fallout). The second phase, the climax of the Sounkyo eruption, produced a widespread, valley-filling ignimbrite in both proximal and distal regions (SK-B and the Px-type ignimbrite). This phase culminated in extensive failure of the wall-rock of the shallow conduit, generating dense, lithic-rich, low-mobile PDCs to form a >27-m-thick, unstratified and ungraded, coarse lithic breccia (SK-C). The failure in turn choked the conduit and stopped the eruption. After a short eruptive hiatus, as evidenced by the occurrence of a fine-ash layer or reworked deposit sandwiched between SK-C lithic breccia and SK-D, the eruption resumed with a short-lived fall phase, establishing an eruption column up to 16 km high and producing a <6-m-thick scoria fallout (SK-D) in the vicinity of the source. Finally, the eruption ended with the generation of PDCs by eruption column collapse to form a 5- to 15-m-thick ignimbrite in the proximal area (SK-E). The PDCs may have traveled down to accumulate the Px-type ignimbrite.

The caldera volume (0.35 $km^3$) is an order of magnitude less than that of magma ejected and is comparable with that of lithic fragments ejected (0.28 $km^3$) during the Sounkyo eruption, suggesting that the caldera was not essentially formed by caldera collapse but, instead, by vent widening as a consequence of explosive erosion and failure of the shallow conduit. The dominance of shallow-origin volcanic rocks in the lithic fraction throughout the Sounkyo eruption products implies the development of a flaring funnel-shaped vent. Hence, the occurrence of lithic breccias within small caldera-forming eruption products does not necessarily reflect the presence and the timing of caldera collapse, as commonly assumed in literature. Lithic breccias commonly overlie climactic ignimbrite/fallout deposits in small caldera-forming eruptions, and a new model for the formation of such lithic breccias is proposed based on comparison my results with other small caldera-forming events. In the model, I hypothesize that (1) the shallow conduit has been explosively eroded and enlarged with consequent fragmentation and brecciation of the walls before and during an eruption climax (e.g. SK-A to -B), (2) the subsequent waning of the eruption lead to the collapse of unstable fractured walls and the production of lithic breccias (e.g. SK-C), and (3) the

collapsing mixture composed predominantly of fragments of basement rocks with minor eruptive materials contributes, at least in part, its caldera fill.

Remanence data from juvenile clasts and welded tuff collected at nine sites within the Kobachidaira ignimbrite, Mamiyadake Scoria Member, and Sounkyo Member (SK-A, -B, and -E) have been used to determine the paleomagnetic directions of each eruptive episodes and to correlate the deposits. Stable primary components of remanence were isolated through thermal demagnetization experiments. The within-site dispersion of characteristic remanent magnetization (ChRM) directions for each site is small ($k$ >100, $\alpha_{95}$ <6°), suggesting that the estimated site mean directions are representative of the ChRM for the deposits of that location. Moreover, the between-site mean ChRM directions for each eruptive episodes has moderate to low dispersion and is significantly distinct each other, indicating that the estimated ChRM may record the direction of the Earth's magnetic field at the time of emplacement and thus allows correlation of deposits. ChRM directions for the Sounkyo Member (SK-A,-B, and -E) are statistically indistinguishable from the paleomagnetic direction for the Px-type ignimbrite estimated by Yasuda et al. (2015; *Bulletin of the Volcanological Society of Japan*), together with their lithological and petrological characteristics, confirms a correlation between them.

# Chapter 1

# General introduction

## 1.1. Explosive caldera-forming eruptions

Calderas are large volcanic depressions, more or less circular in form, the diameters of which are many times greater than those of any included vents (Williams, 1941). Moderate to large explosive eruptions produce ignimbrites (pyroclastic-flow deposits) and/or plinian fallouts, ranging from a few to thousands of cubic kilometers, often associated with formation of calderas at their source areas (Lipman, 1997). The greater the volume of magma is ejected, the larger the size of the resulting caldera is (Spera and Crisp, 1981; Scandone, 1990; Geshi et al., 2014).

Explosive caldera-forming eruptions are amongst the most devastating of volcanic phenomena. Pyroclastic flows from such eruptions are hot (hundreds of degrees Celsius), rapidly moving (e.g. >200 m/s, the A.D. 186 Taupo eruption; Wilson and Walker, 1985) mixtures of particles and gas that hug the ground and thus destroy everything in their path, as much as tens to hundreds of kilometers. Co-ignimbrite ash falls, which are derived from collapsing eruption columns and moving pyroclastic flows and may have a comparable volume to the associated ignimbrite, are very extensive, covering over millions square kilometers (Sparks and Walker, 1977; Costa et al., 2012). The 1815 Tambora eruption, the largest caldera-forming event of recorded history, expelled ~50 $km^3$ of magma and caused the death of thousands of people (Self et al., 1984). To mitigate the hazard from explosive caldera-forming eruptions requires understanding of how the eruptions initiate, progress, and end, along with the timing and styles of caldera formation, which may have a significant impact on the course of eruption and the type of products ejected.

The small (VEI 5–6) caldera-forming eruptions occur more frequently than the

large (VEI >7) caldera-forming eruptions (Tatsumi and Suzuki-Kamata, 2014; Nakada, 2015). For example, VEI 5–6 eruptions have occurred at least eight times in the past one hundred years in the world, while the last VEI 7 eruption is the 1815 Tambora eruption (Global Volcanism Program, 2013). In this thesis, I mainly address the more frequent small caldera eruptions.

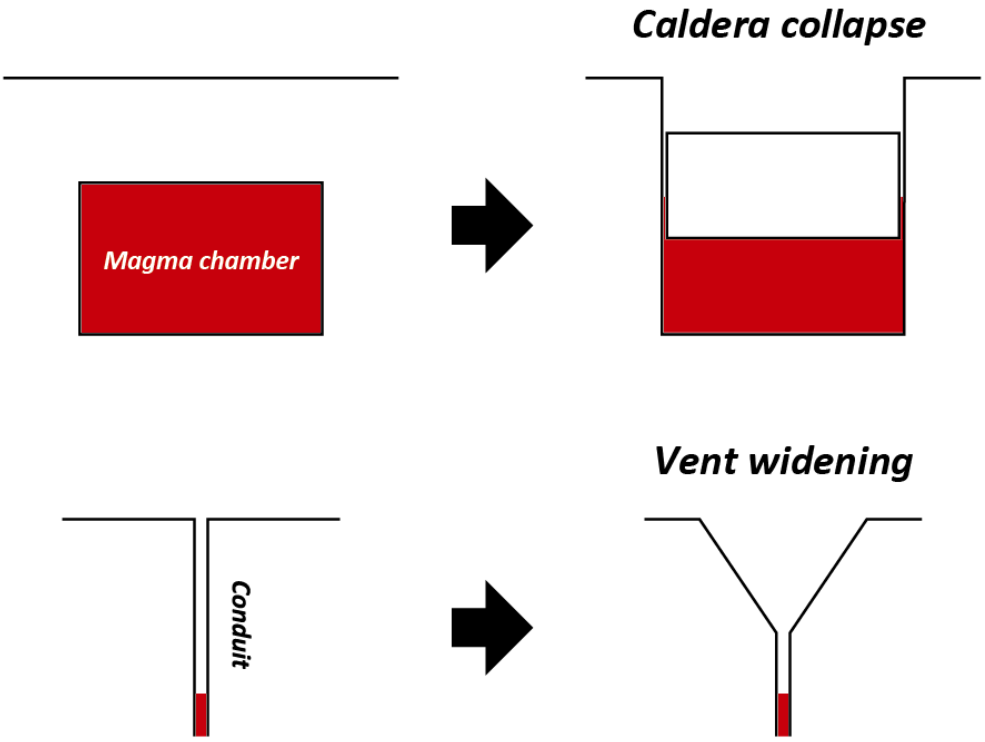


**Figure 1.1:** Two end member mechanisms of caldera formation associated with explosive eruptions.

## 1.2. Origin of caldera depressions

How calderas form in association with explosive eruptions has been a matter of debate over the last decades. Such calderas can be formed by collapse (subsidence) of the roof of the magma chamber due to magma evacuation, "caldera collapse" or by enlargement of a vent as a result of explosive erosion and failure of the shallow part of conduit walls, "vent widening" (Fig. 1.1). No matter how the roof is fragmented or brecciated, the process should be referred to as caldera collapse as long as the roof subsides into the chamber (see Fig. 1.2, 1.3, and 1.4). The essential difference between the two types is that the presence of a magma chamber is necessary for caldera collapse, but not for vent widening. Calderas formed by the former process are called *collapse calderas*, while those by the latter process are called *explosion calderas* in the sense of Stearns and Clark (1930). In this thesis, I avoid the usage of the term *explosion caldera*, because failure or slumping of conduit walls into a central vent may play a significant role in establishing the overall size of the caldera in the latter case (Escher, 1929; Lipman, 1997).

### 1.2.1. Calderas formed by "caldera collapse"

Large calderas (>5–10 km in diameter) are generally inferred to have been formed by caldera collapse. Lipman (1976) first identified that accumulation of landslide breccias that interfinger with thick pumiceous ignimbrite in the caldera fill sequence in four large Oligocene eroded calderas in the San Juan Mountains, and interpreted that these breccias have been derived from the caldera walls during caldera subsidence and emplaced simultaneously with the accumulating intracaldera ignimbrite. Such intracaldera accumulations have been reported in other large calderas elsewhere (Lipman and Sawyer, 1985; Lipman et al., 1993; Branney and Kokelaar, 1994; Fiske and Tobisch, 1994; Hildreth, 1996; Yamamoto, 2003; Sato et al., 2016).

The great discrepancy between the volume of a caldera and that of pre-existing rock fragments in the erupted material has been regarded as strong evidence for caldera collapse (Williams, 1942), despite the difficulty of obtaining accurate volumes of

pyroclastic ejecta. In the climactic eruption of Mount Mazama, for instance, the volume of the missing edifice was ~50 $km^3$, but that of lithic fragments in the deposits of the eruption was ~6 $km^3$ (Bacon, 1983). This discrepancy can be readily explained by collapse of the roof of the magma chamber due to magma evacuation because the total erupted magma volume was very similar to the missing volume (Bacon, 1983).

Ring fracture systems that accommodate caldera subsidence are usually identified as ring dykes composed mainly of plutonic intrusions in ancient eroded volcanic fields (Smith and Bailey, 1968; Miura, 1999; Kennedy and Stix, 2007; Kokelaar, 2007) or as the presence along an annular line of post-caldera lava domes in younger caldera fields (Heiken et al., 1986; Kennedy et al., 2012).

There are two models invoked to explain the cause of caldera collapse. A conventional model is that underpressure in the magma chamber created by pre-climactic eruption trigger collapse (Druitt and Sparks, 1984; Geshi et al., 2014). An alternative model is that overpressure in the magma chamber due to magma chamber growth leads to extensive uplift in the overlying roof and development of faults that trigger eruption and caldera collapse (Gregg et al., 2012).

### 1.2.2. Calderas formed by "vent widening"

Small calderas (<3 km in diameter) may be formed by vent widening. Such calderas are defined by its flaring funnel-shaped conduit without a caldera-bounding ring fault or a coherent subsided block. A typical example is the Nigorikawa caldera in southwestern Hokkaido, Japan, whose subsurface structures are well understood from deep geothermal drilling as deep as >3 km (Ando, 1983; Kurozumi and Doi, 2003). The caldera fill comprises a significant volume of landslide debris derived from the conduit walls, implying that conduit wall failure contributes vent enlargement (see Chapter 4 for detail).

The 2-km-diameter Novarupta crater in Alaska formed in response to the 1912 plinian eruption (~13 $km^3$ of magma) is inferred to have a funnel-shaped conduit (Hildreth, 1983, 1987; Hildreth and Fierstein, 2012). Hildreth at first appreciated the contributions not only from explosive excavation of lithic debris, but also from inward

slumping of conduit walls to form the Novarupta depression (Hildreth, 1983). In fact he described that there may be some of intravent lithic fallback debris (Hildreth, 1983, 1987). Nevertheless, he currently drew a schematic cross section of Novarupta vent in which the funnel is mostly backfilled by welded tuff of the vent-excavation episode, stressing eruptive excavation as a major process in the evolution of the funnel (Hildreth and Fierstein, 2012).

The relative importance of the two processes—(1) explosive erosion and (2) inward collapse of the walls—for the development of such calderas is unclear, but may provide a key to understanding their origin. In addition, what triggers the inward wall collapse and how such a process links with the pyroclastic ejecta outside the caldera are also problems that should be explained in order to elucidate formation mechanisms of such calderas.

The term "funnel-shaped caldera" is ambiguous and should be carefully used when one considers the origin of calderas, because it potentially includes both of calderas formed by caldera collapse and by vent widening. This term has been traditionally referred to some young Japanese large calderas, such as Aira, Aso, Kutcharo, Shikotsu (Aramaki, 1983, 1984). These calderas develop a local negative Bouguer anomaly with relatively low at the center, implying a shallow funnel-shaped

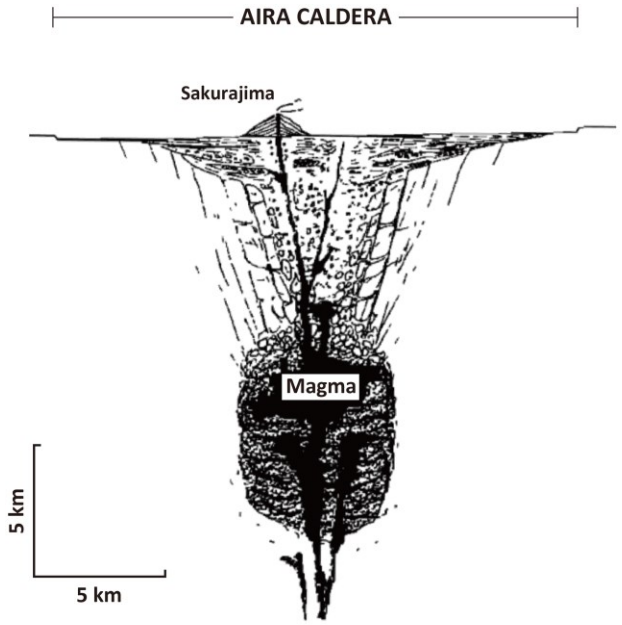


**Figure 1.2:** A hypothetical cross section of the Aira caldera (modified after Aramaki, 1984).

subsurface structure filled by lighter debris (Yokoyama, 1963, 1983). Aramaki (1983, 1984) suggested that the fracturing and sinking of the overlying roof along steeply inward dipping faults into the evacuated magma chamber resulted in the formation of a shallow funnel-shaped caldera floor (Fig. 1.2). In genetic terms, such a process to form a caldera should be called caldera collapse. However, he unconvincingly mentioned that such calderas merge in geometry with the Nigorikawa caldera, in spite of the fact that its origin is vent widening. Lipman (1997) has already realized the nomenclatural problem, stressing out that any types of calderas associated with ignimbrite eruptions—plate (piston), piecemeal, downsag, or vent funnel—are considered to be funnel-shaped in overall geometry. Even plate (piston) collapse calderas, which involve the subsidence of a relatively coherent roof block into an emptying chamber, can have negative Bouguer anomalies due to the presence of caldera-wall slide breccias accumulated near the caldera margins (Lipman, 1997).

Yokoyama (1983, 1993, 2005, 2016) has been proposing an alternative hypothesis for the origin of funnel-shaped calderas. From his point of view, funnel-shaped calderas—calderas with negative Bouguer gravity anomalies—are formed by violent explosions accompanied by a large amount of pyroclastic ejecta, irrespective of caldera size, and their formation has nothing to do with the subsurface magma chamber. Small calderas can be formed by a single explosive eruption; larger calderas can be developed by multiple nested destructive eruptions. Some large funnel-shaped calderas, such as Aira and Aso in Kyushu (Japan), comprise multiple low-gravity-anomaly centers, which is consistent with his hypothesis. He might be an only volcanologist who strongly disagrees with “caldera collapse” model. The evidence against caldera collapse he has provided includes: (1) the main basis for caldera collapse—the similarity in volume between pyroclastic ejecta and disrupted volcanic edifices and the deficiency of lithic debris in the ejecta—is ambiguous owing to the difficulty of estimating the accurate ejecta volume (estimated errors ranging over an order of magnitude, Yokoyama, 2015); (2) from a perspective of stress distribution, the destructive stress caused by magma evacuation from a chamber at a reasonable depth may not reach the Earth’s surface and hence cannot form a caldera depression; and (3) it is unrealistic that collapsed volcanic edifices sink downward against the upward force of the violent explosions.

His hypothesis relies on the geophysical and geomorphological data. What is missing in his conceptual model is (1) the certification of the large volume of disrupted volcanic edifices (>50 $km^3$ in the case of large calderas) as lithic fragments in the ejecta outside the caldera and (2) the linkage between the dynamics of caldera formation and the geological features (i.e. sequence, lithofacies, and stratigraphic architecture) of the caldera-forming eruptive deposits. The first task is very challenging as Yokoyama noted, but the second task could be achieved by focusing on lithic debris in the preserved deposits around calderas as described below.

## 1.3. Lithic breccias and their implications for caldera formation

Explosive caldera-forming eruptions are commonly accompanied by a sudden increase in the flux of lithic debris part way through the course of the eruptions, emplacing coarse lithic-rich deposits on the ground surface. Such lithic-rich deposits are often associated with pumiceous ignimbrites in proximal (near-source) areas and are referred to as various terms, *co-ignimbrite lag fall deposits* (Wright and Walker, 1977) or *lag breccias* (Druitt and Sparks, 1982; Walker, 1985), or *proximal co-ignimbrite breccias* (Valentine and Wohletz, 1989). Geological studies addressing small caldera-forming eruptions, however, demonstrated that some of these eruptions are dominated by plinian-fall deposits with accompanying lithic-rich horizons (e.g. Gardner and Tait, 2000). Accordingly, in this thesis, the term *lithic breccias* is used in a non-genetic, lithological sense to refer the lithic-rich deposits. Lithic fragments in pyroclastic deposits are basically originated from wall-rocks of the vent, conduit, and magma chamber, so that the variations in abundance and assemblages of lithic fragments may provide insights into the evolution of magma chamber/conduit/vent geometries and provide constraints on how and when caldera formation proceeds in the eruptions.

### 1.3.1. Lithic breccias associated with large calderas

Large caldera-forming eruptions tend to begin with a plinian-fall phase immediately followed by the emplacement of voluminous ignimbrites and “contemporaneous” coarse lithic breccias. Such field observations encouraged Druitt and Sparks to propose a two-stage model for caldera formation (Fig. 1.3); in which (1) an eruption begins with emission of small to moderate volumes of magma through a central vent while the chamber is overpressured, and then (2) the chamber pressure decreases sufficiently for the chamber roof to collapse, leading to eruption of large volumes of magma along a ring fault. They interpreted that the sudden appearance of lithic breccias marks the onset of the second stage (i.e. caldera collapse). The origin of the lithic breccias during caldera collapse can be explained by (1) a rapid increase in magma discharge rate due to opening of new vents and conduit enlargement, which, in turn, lead to the enhancement of vent-conduit erosion (Druitt, 1985; Walker, 1985), (2) explosive disruption of hydrothermal systems cut by dilating caldera faults (Rosi et al., 1996; Kokelaar, 2007), or (3) slumping and sliding of the oversteepened caldera walls (Lipman, 1997). The lithic breccias are apparently derived from variable depths and include hydrothermally altered rocks (Suzuki-Kamata et al., 1993; Rosi et al., 1996; Druitt, 2014), which is consistent with such inferred processes. It is therefore widely accepted that coarse lithic breccias mark the onset of caldera collapse.

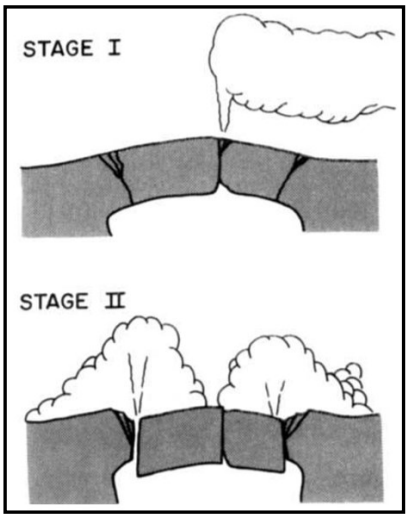


**Figure 1.3:** Two-stage model for caldera formation (modified after Druitt and Sparks, 1984). An initial plinian eruption from a central vent decompresses an overpressured magma chamber (Stage I). When the chamber pressure falls sufficiently for the chamber roof to collapse, a ring fault develops along with the emission of a voluminous ignimbrite (Stage II).

In the climactic eruption of Mount Mazama (Crater Lake caldera), azimuthal differences in lithic types in the lithic breccia, associated with the voluminous ignimbrite, correlate well with the geology of the adjacent caldera walls, supporting the presence of multiple vents along a caldera ring faults (Suzuki-Kamata et al., 1993). At Long Valley caldera, no lithic breccias have been found although the assemblage of dispersed lithic fragments in the ejecta suggests the change from the single-vent Plinian phase to the ring-vents climactic ignimbrite phase simultaneously with caldera collapse (Hildreth and Mahood, 1986).

Simmons et al. (2017a) has pointed out that coarse lithic breccias associated with moderate-sized calderas (~10 km in diameter) show the increase in deeper-origin basement and hydrothermally altered lithic clasts within the stratigraphy of each eruption sequence, proposing an attractive model for caldera formation (Fig. 1.4). They interpreted such lithic breccias as reflecting a deepening of the magma fragmentation level and consequent explosive widening of conduit walls at depth, which is necessary for subsidence of the chamber roof block along vertical or inward-dipping faults that initially inhibit the subsidence by friction. Such interpretations are consistent with numerical simulations which predict rapid increases in mass discharge rate and in magma decompression accompanied by a progressive deepening of the magma fragmentation level when the transition from a central-vent to a fissure vent occurs at the onset of caldera collapse (Folch and Martí, 2009).

### 1.3.2. Lithic breccias associated with small calderas

Small caldera-forming eruptions often produce lithic breccias “after” the climactic ignimbrite or plinian fallout deposits. Such stratigraphic relationship was first recognized by Scott et al. (1996) in the 1991 Pinatubo eruption and has been reported in other small caldera eruptions over the past two decades (Gardner and Tait, 2000; Browne and Gardner, 2004; Andrews et al., 2007; Andrews, 2014). These authors believed that the lithic breccias atop the climactic products mark caldera collapse and that the caldera collapse happened near the end of the eruption. Such beliefs led them to propose models in which subsidence of the caldera block (or fragmented blocks) along

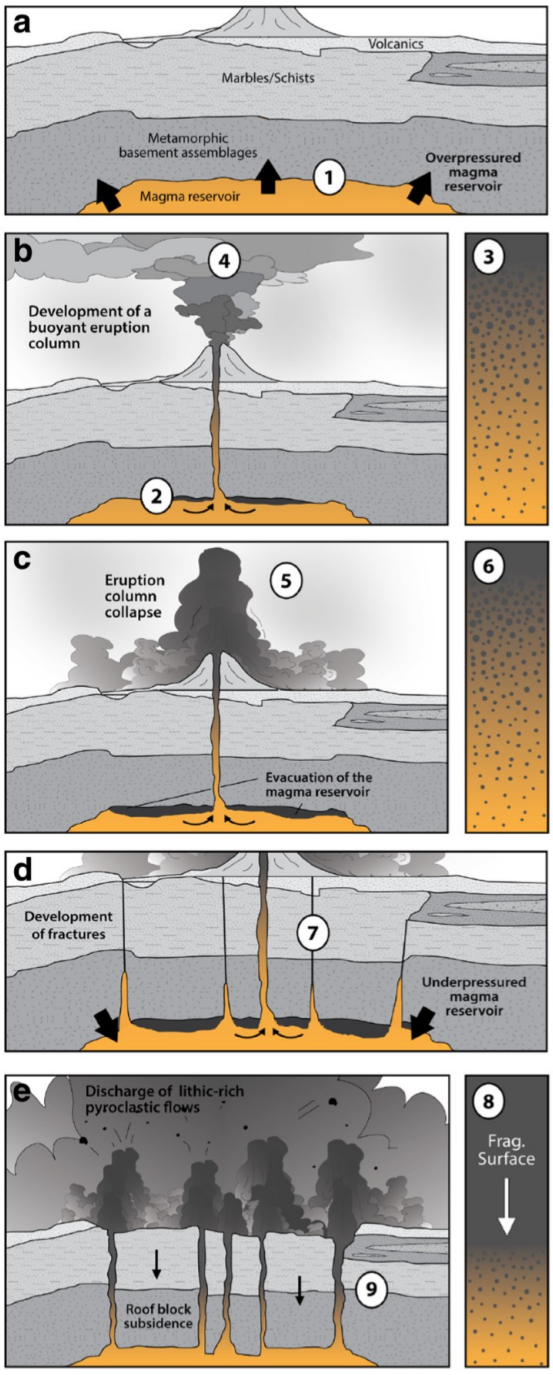


**a. GROWTH OF THE MAGMA RESERVOIR**

**1.** Overpressure in the magma reservoir at 7-8 km depth (storage pressures of 130-220 MPa). Driven by: i. The intrusion of basaltic magmas into the main rhyodacitic reservoir. ii Volatile exsolution, supercritical bubble nucleation and growth.

**b. INITIATION OF THE ERUPTION FROM A POINT SOURCE VENT**

**2.** Magma reservoir overpressures, dyke propagation and magma ascent.
**3.** Decompression of the ascending magma, volatile exsolution and bubble growth.
- Moderate magma decompression rates of 7-9 MPa $s^{-1}$ immediatly prior to fragmentation at shallow crustal depths.
**4.** Discharge of juvenile pyroclasts at MDR of ~$10^6$ - $10^7$ kg $s^{-1}$ and the development of a buoyant eruption column (LP1-A).

**c. ERUPTION COLUMN COLLAPSE**

**5.** Explosive widening of the vent and the injection of lithics into the eruption column resulted in column collapse the development of valley-confined pyroclastic flows (LP1-B).
**6.** Minimal change in magma decompression rates or fragmentation depths.
- 7-11 MPa $s^{-1}$
- Shallow fragmentation depths
- MDR ~$10^6$ - $10^7$ kg $s^{-1}$

**d. TRANSITION TO CALDERA COLLAPSE**

**7.** Magma evacuation and underpressurisation of the magma reservoir led to the propagation of sub-vertical to inwards dipping fractures.
- Fracture orientation and friction along the fracture surface inhibited roof block subsidence.
**8.** Rapid decompression of the magmatic system (15-28 MPa $s^{-1}$), associated with the development of fractures, resulted in high rates of bubble nucleation, the downward propagation of the fragmentation surface and deep fragmentation depths (LP1-C).

**e. CALDERA COLLAPSE AND THE OPENING OF MULTIPLE FRACTURE VENTS**

**9.** A deepening of the fragmentation surface led to the explosive widening of fractures and the discharge of lithic-rich pyroclastic flows at MDR ~$10^8$ kg $s^{-1}$ (LP1-C).
- Widening of the fracture vents was necessary to reduce friction between the bounding roof blocks and enable caldera collapse.

**Figure 1.4:** Caldera formation model for the 184 ka Lower Pumice 1 eruption, Santorini, Greece (from Simmons et al., 2017a).

inward-dipping faults immediately closes the conduit and terminates the eruption (Scott et al., 1996; Browne and Gardner, 2004; Andrews, 2014). However, these models include a serious problem that needs to be explained; how does the caldera block (or fragmented blocks) subsides along downward narrowing peripheral faults? As Yokoyama (1993) suggested, sand grains in an hourglass smoothly fall downward through the narrow passage; however, disrupted volcanic edifices may not be able to do so. Moreover, such collapse models for small calderas tend to lack the linkage with the lithology of the lithic fragments in the deposits.

## 1.4. Purpose of this thesis

Two completely different models proposed for the formation of small calderas are "vent widening" model as demonstrated in the Nigorikawa caldera (Ando, 1983; Kurozumi and Doi, 2003) and "caldera collapse" model as inferred in some small calderas (Scott et al., 1996; Browne and Gardner, 2004; Andrews, 2014). Even if these models may partially explain the dynamics of caldera formation, to develop a comprehensive understanding of the formation mechanisms and eruptive dynamics of small calderas it is necessary to link and explain the relationship among the subsurface structures, dynamics of eruption and caldera formation, and nature and stratigraphy of the eruptive products.

In order to achieve this, I have chosen to work on Ohachidaira volcano and its summit caldera (Ohachidaira caldera). This is because (1) the volcano provides a detailed record of the eruptive history along with a high-resolution stratigraphy of the caldera-forming eruption sequence via rarely well-exposed and well-preserved exposures and (2) the Ohachidaira caldera is typical of small calderas due to its small diameter and the late appearance of the associated lithic breccia so that it may provide essential information about small caldera dynamics.

# Chapter 2

# Geological background

## 2.1. Basement of Taisetsu volcano group

The Taisetsu-Tokachi volcanic chain, extending from northeast to southwest approximately 80 km in central Hokkaido, is located at the southwestern end of the Kuril arc and formed in response to the subduction of the Pacific plate beneath the North American plate to the northwest (Fig. 2.1; e.g. Kita et al., 2014). The Taisetsu volcano group, comprising the northern part of the volcanic chain, has been active since ~1 Ma (NEDO, 1990). This volcano group covers Neogene volcanic rocks, which in turn overlie the Hidaka Supergroup (Fig. 2.2; Konoya et al., 1966; Katsui et al., 1979). The Neogene volcanic rocks consist of andesitic to rhyolitic lavas and tuffs, reaching as high as 1600 m asl on the flanks of the Taisetsu volcano group (Katsui et al., 1979). The Hidaka Supergroup comprising slate, sandstones, and cherts is the oldest rocks (pre-Neogene) exposed in the study area and is occasionally intruded by granodiorites (Katsui et al., 1979; NEDO, 1989). The slate belonging to the Hidaka Supergroup is found up to ~1000 m asl along the Kurodakesawa Creek (Konoya et al., 1966; Katsui et al., 1979). The ~1–2 Ma rhyolitic ignimbrites are only exposed on the northern to western margins of the Taisetsu volcano group, and are distinguished from deposits of the Taisetsu volcano group by the abundance of coarse quartz phenocrysts (Konoya et al., 1966; Katsui et al., 1979; Nishiki et al., 2017) .

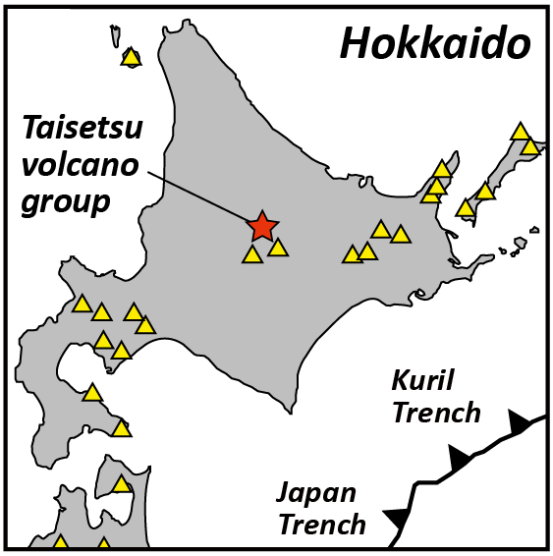


**Figure 2.1:** Map showing the location of the Taisetsu volcano group (star) and active volcanoes (triangles).

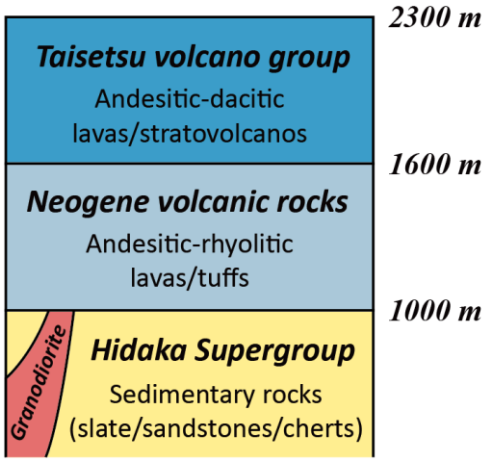


**Figure 2.2:** Generalized stratigraphic column showing the sequence of the Taisetsu volcano group and its basements. The maximum height where the top of each group can be found is shown in the right of column.

**Figure 2.3:** Taisetsu volcano group (photograph taken from west). The highest peak is Asahidake (2291 m asl).

## 2.2. Taisetsu volcano group

The Taisetsu volcano group is constructed from a series of overlapping andesitic to dacitic lava domes and stratovolcanos, whose peaks attain a height of 1700–2300 m (Fig. 2.3; Katsui et al., 1979). The volcano group has developed at two distinct stages (Ishige, 2017): older stage (1–0.7 Ma) and younger stage (0.2 Ma–now). At the older stage, andesitic lava flows, domes, and stratovolcanoes were erupted from multiple vents along north to south of the volcano group (Ishige, 2017). From 0.2 Ma, the eruptive activity of the volcano group is characterized by explosive moderate-volume ignimbrite eruptions alternating with the formation of andesitic to dacitic lava domes and stratovolcanoes such as Hakuundake, Koizumidake, Hokuchindake, and Kurodake, whose sources are located in the center to north of the volcano group (Ishige, 2017).

## 2.3. Previous studies of eruptive history of Ohachidaira volcano

Here I define Ohachidaira volcano as a stratovolcano whose edifice is built by lavas and pyroclastics sourced within the Ohachidaira caldera. Ohachidaira volcano was known formally as the central stratovolcano or cone (Doi et al., 1962; Katsui et al., 1979). These authors used the term "central" because they believed that the volcano was formed in the center of a 4- × 6-km-diameter older caldera. The older caldera was suggested by these authors as the distribution of lava domes and stratovolcanoes around the "central" volcano seem to be circular, although there is no topographic caldera rim. The Aizankei welded tuff, which they correlated with the formation of the older caldera, may correspond to the ~1–2 Ma rhyolitic ignimbrites. Thus, I discount the presence of the older caldera and avoid the term "central" to describe the volcano.

The eruptive history of Ohachidaira volcano has been reconstructed by field mapping conducted at distal and proximal areas (Doi et al., 1962; Konoya et al., 1966; Katsui et al., 1979; Metsugi, 1987; Wakasa et al., 2006; Sato and Wada, 2012; Yasuda et al., 2015). For distal area, Doi et al. (1962) first identified a widespread ignimbrite sheet at the foot of the Taisetsu volcano group, named "Sounkyo welded tuff", and correlated

it with the formation of the Ohachidaira caldera. Katsui et al. (1979) and Metsugi (1987) also recognized the same ignimbrite sheet and termed "Ohachidaira pumice-flow deposit" and "Taisetsu pyroclastic-flow deposit", respectively. Wakasa et al. (2006) and Sato and Wada (2012), however, found that the superficially indistinguishable ignimbrite sheet can be divided into two petrological distinct ignimbrites. The older one is composed of hornblende-rich pumice fragments (hornblende > pyroxene) and termed Hb-type ignimbrite, and the younger one is composed pyroxene-rich pumice fragments (hornblende < pyroxene) and termed Px-type ignimbrite (Sato and Wada, 2012). Yasuda et al. (2015) identified the detailed distribution of the two ignimbrites (Fig. 2.4), and they demonstrated that paleomagnetic directions for the two ignimbrites are significantly distinct at 95% confidence limits, suggesting a time interval of 100 ± 40 years or more between these two ignimbrite eruptions. The Hb-type ignimbrite has a zircon fission-track age of 58 ± 18 ka (Nishiki et al., 2017) while the Px-type ignimbrite has a $^{14}C$ age of 34 ka (Ishige and Nakagawa, 2017).

The proximal deposits from Ohachidaira volcano were descried by Metsugi (1987). He identified lavas, pumiceous pyroclastic deposit, scoriaceous pyroclastic deposit, lithic pyroclastic deposit, pumice falls, base-surge deposit, and welded scoria falls, based on the field mapping and correlation for proximal products distributed around the volcano. The eruption stratigraphy reconstructed by Metsugi (1987), however, has a serious problem in correlation: he regarded the welded scoria falls that occur in some isolated areas as a product of the same eruptive episode and as a key bed, but despite being from different eruptive episodes. Moreover, the correlation between such proximal deposits and the distal ignimbrites remains still unclear. Accordingly, it is necessary to conduct a new field survey to reconstruct the detailed eruption stratigraphy of Ohachidaira volcano.

The caldera floor (1900 m asl) is 100–300 m lower than the caldera rim. The lacustrine sediments locally exposed on the caldera floor indicate the past existence of a caldera lake (Katsui et al., 1979).

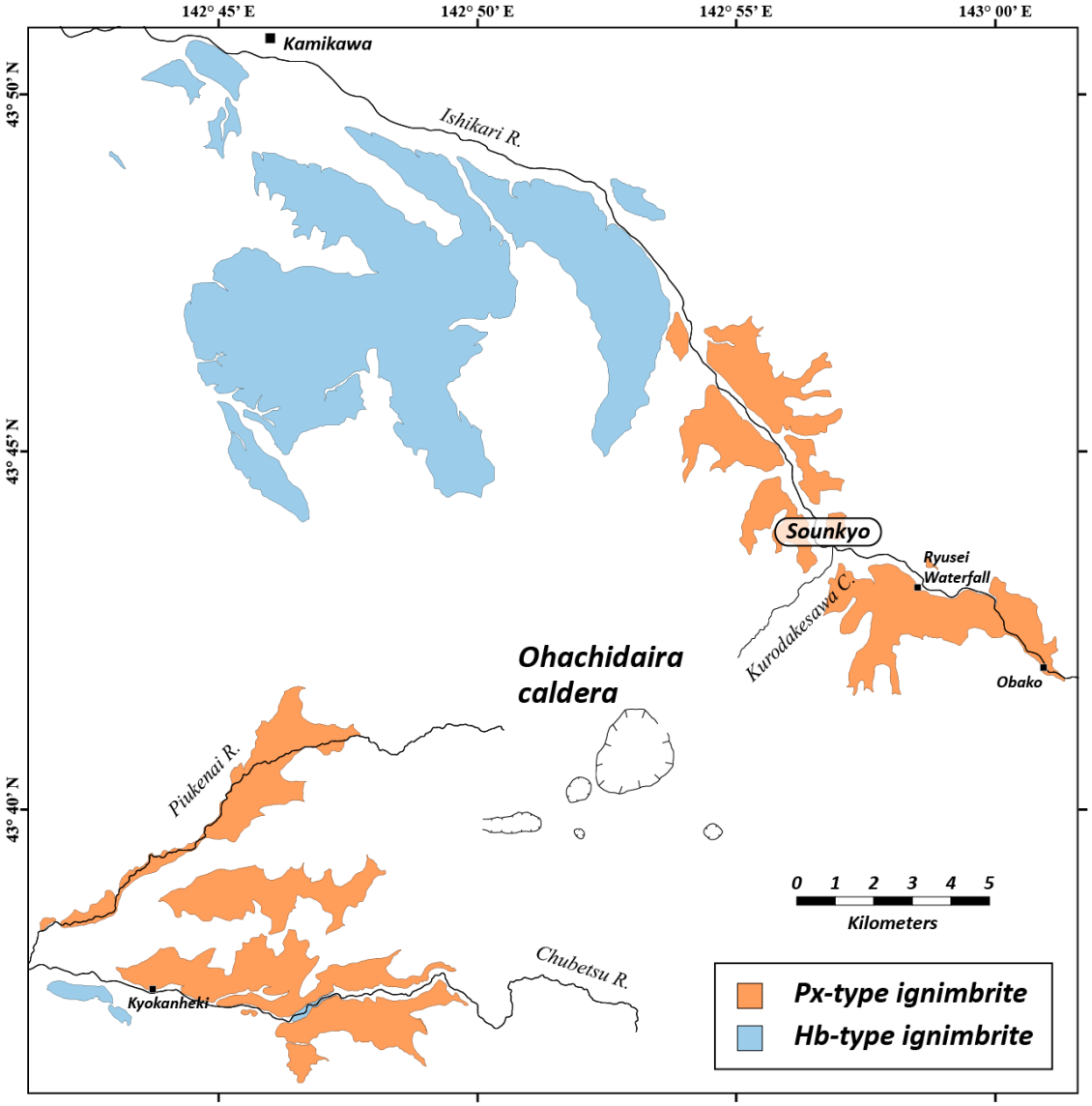


**Figure 2.4:** Map showing the distribution of Hb-type and Px-type ignimbrites at the foot of the Taisetsu volcano group (modified after Yasuda et al., 2015).

# Chapter 3

# Eruptive history of Ohachidaira volcano

## 3.1. Introduction

The summit caldera of Ohachidaira volcano may not have formed by a single eruption, but rather the caldera system may have evolved through several distinct eruptive events, as commonly observed elsewhere irrespective of the size of calderas (Vesuvius [3 km in diameter], Italy, Cioni et al., 1999, Latera [9 × 7 km], Italy, Palladino and Simei, 2005, Santorini [10 × 6 km], Greece, Druitt et al., 1989, Aso [25 × 18 km], Japan, Ono, 1965; Watanabe and Ono, 1969, Toba [100 × 30 km], Indonesia, Chesner and Rose, 1991). In general, eruptive events associated with caldera formation are recorded as relatively large-volume of ignimbrites occurring around and within calderas (Lipman, 1997). The Ohachidaira caldera has a record of several effusive and explosive events, as seen the volcanic succession in the caldera walls and ignimbrite sheets at the foot of the Taisetsu volcano group, some of which likely played a role in the caldera formation. Nevertheless, as I mentioned in Section 2.3, the eruption stratigraphy of Ohachidaira volcano reconstructed by some workers (Doi et al., 1962; Konoya et al., 1966; Katsui et al., 1979; Metsugi, 1987; Wakasa et al., 2006; Sato and Wada, 2012; Yasuda et al., 2015) is far from complete because of (1) the lack of accurate and detailed stratigraphy of the proximal deposits and (2) the lack of correlation between the proximal and distal deposits.

Conventional methods for determining the linkage between the spatially isolated eruptive products (e.g. proximal and distal deposits) are to detect lithological and petrological (e.g. chemical composition of juvenile materials) similarities between them. It should be, however, noted that the geological and petrological data are sometimes insufficient since (1) pyroclastic-fall and -flow deposits may show significant lateral

variations in composition (e.g. proportions of types of juvenile materials or juvenile/lithic ratios) and hence in lithofacies (Wright and Walker, 1977; Walker et al., 1981; Druitt and Bacon, 1986; Fierstein et al., 1997; Allen and Cas, 1998) and (2) chemical composition of juvenile materials of different eruptive events from a volcano could be indistinguishable. In such cases, paleomagnetic method is very useful to distinguish among deposits (Hayashida et al., 1996; Ort et al., 2013; Yasuda et al., 2015).

Paleomagnetic secular variations (PSV) are changes with periods between 10s and 1000s years in the components of the geomagnetic field (Butler, 1992). Variations in paleomagnetic directions of rocks from successive, different eruptions from a single volcano record a temporal change in geomagnetic field direction at the area. Therefore, determining the paleomagnetic directions of volcanic rocks can be a powerful tool for correlation and dating.

The aim of this chapter is to develop a better understanding of the eruptive styles, magnitudes, and history of Ohachidaira volcano on the basis of field mapping and paleomagnetic data. I identify the proximal deposits, assess whether they have originated from Ohachidaira volcano, and correlate them with the distal ignimbrites. I evaluate their contributions to the formation of the summit caldera. Note that the largest and latest ignimbrite-forming event (Sounkyo eruption) of Ohachidaira is discussed in detail in Chapter 4.

## 3.2. Ohachidaira volcano

Ohachidaira volcano, situated in the central Taisetsu volcano group, is truncated by a 2-km-diameter summit caldera. The Ohachidaira volcano is surrounded by the Taisetsu group consisting mainly of lava domes, such as Hokuchindake, Kurodake, Koizumidake, and Hakuundake, except for the southwestern section. A stratovolcanic complex, the Asahidake subgroup (Kumagatake, Ushiro-Asahidake, and Asahidake), was formed after caldera formation and developed on the southwestern flank of Ohachidaira volcano, concealing the eruptive sequence from Ohachidaira (Fig. 3.1; Ishige and Nakagawa, 2017).

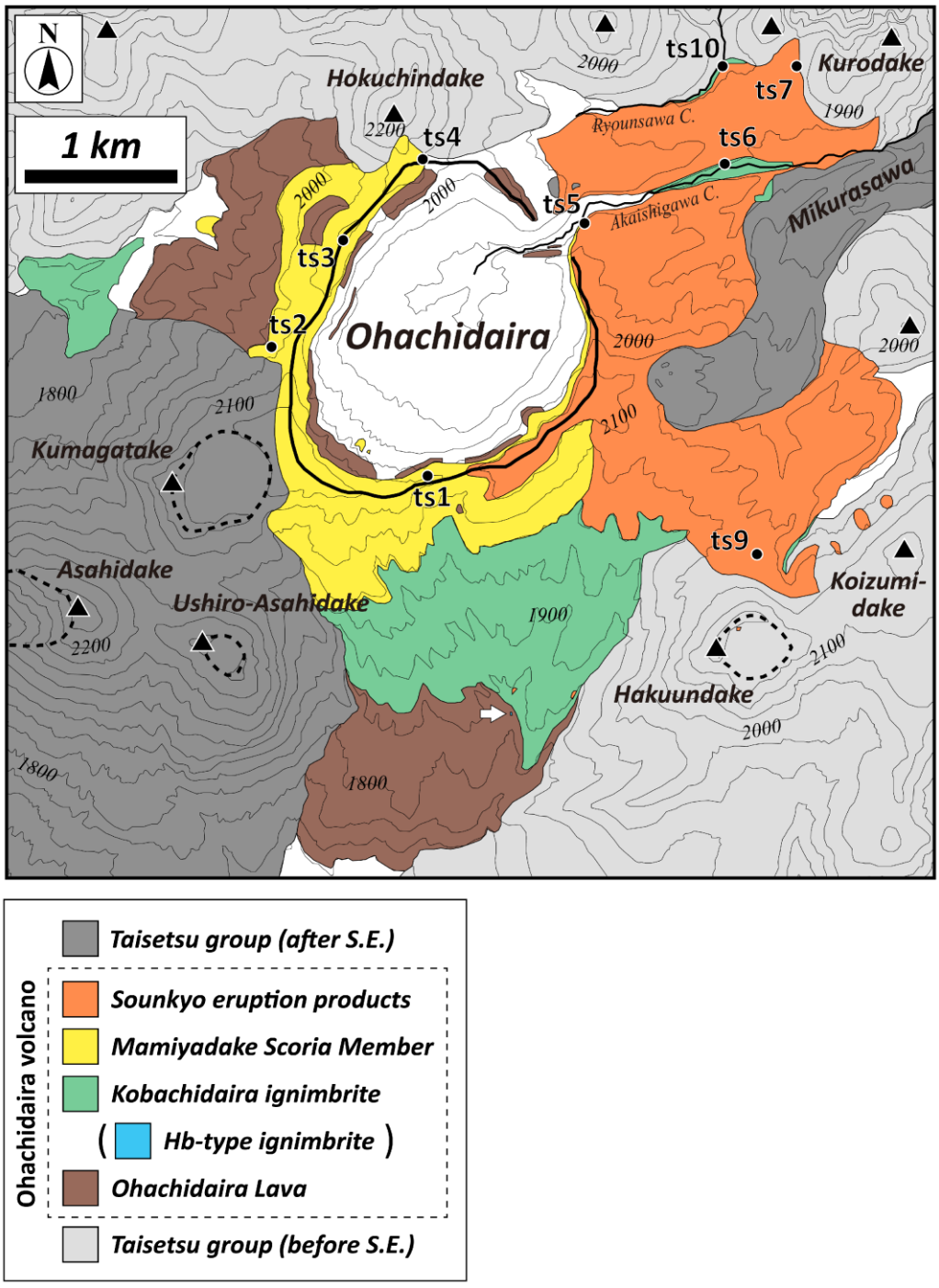


**Figure 3.1:** Simplified geologic map of Ohachidaira volcano. Black dots show locations where the samples for paleomagnetic analysis have been collected. The black ellipse marks the Ohachidaira caldera. The dotted ellipses mark craters or explosion crater. The white arrow marks the outcrop of the Hb-type ignimbrite. *S.E.* in the legend represents the Sounkyo eruption.

Early volcanism (600 ka–) at Ohachidaira was characterized by effusive and explosive activity, producing several lava flows (here named the Ohachidaira lava) and intermittent pyroclastic deposits. From ~60 ka, the Ohachidaira volcanism was dominated by explosive activity, including two small explosive eruptions (here named the Kobachidaira ignimbrite and Mamiyadake Scoria Member) and two major ignimbrite eruptions, the 40–80 ka Hb-type ignimbrite and 34 ka Px-type ignimbrite. Here I call the eruption of the Px-type ignimbrite and its associated products the "Sounkyo eruption."

### 3.2.1. Ohachidaira lava

The lower edifice of Ohachidaira is composed predominantly of lavas which are exposed in the lower part of the caldera wall and alternate with argillically altered pyroclastics. The lavas are traced as far as 3.6 km from the caldera center and overlain by the Hb-type ignimbrite. Each lava unit has a thickness of 10–50 m (30 m in average). The Ohachidaira lava is predominantly of hornblende-pyroxene andesite. Dacite, the minor component of the Ohachidaira lava, is characterized by abundant hornblende phenocrysts up to 10 mm in diameter. One bed of the lavas was K/Ar dated at ~0.6 Ma (NEDO, 1990).

### 3.2.2. Hb-type ignimbrite

The Hb-type ignimbrite is a widespread sheet of welded tuff (Yasuda et al., 2015; Figs. 2.4 and 3.2a). It can be traced for 22 km from the caldera center and attains at least 130 m thick on the foot of the Taisetsu volcano group. The Hb-type ignimbrite is massive or diffusely stratified and poorly sorted (Fig.3.2b). It is rich in pumice and scoria fragments scattered in an ash matrix. The proportion of pumice is generally roughly the same as that of scoria, but sometimes is higher or lower. Coarse pumice-rich or pumice- and scoria-rich lenses (up to 1 m thick; juvenile clasts up to 60 cm in diameter) are observed in some places. Sub-vertical fines-depleted pipes that are composed of pumice, scoria, and lithic clasts and a coarse ash matrix are sometimes

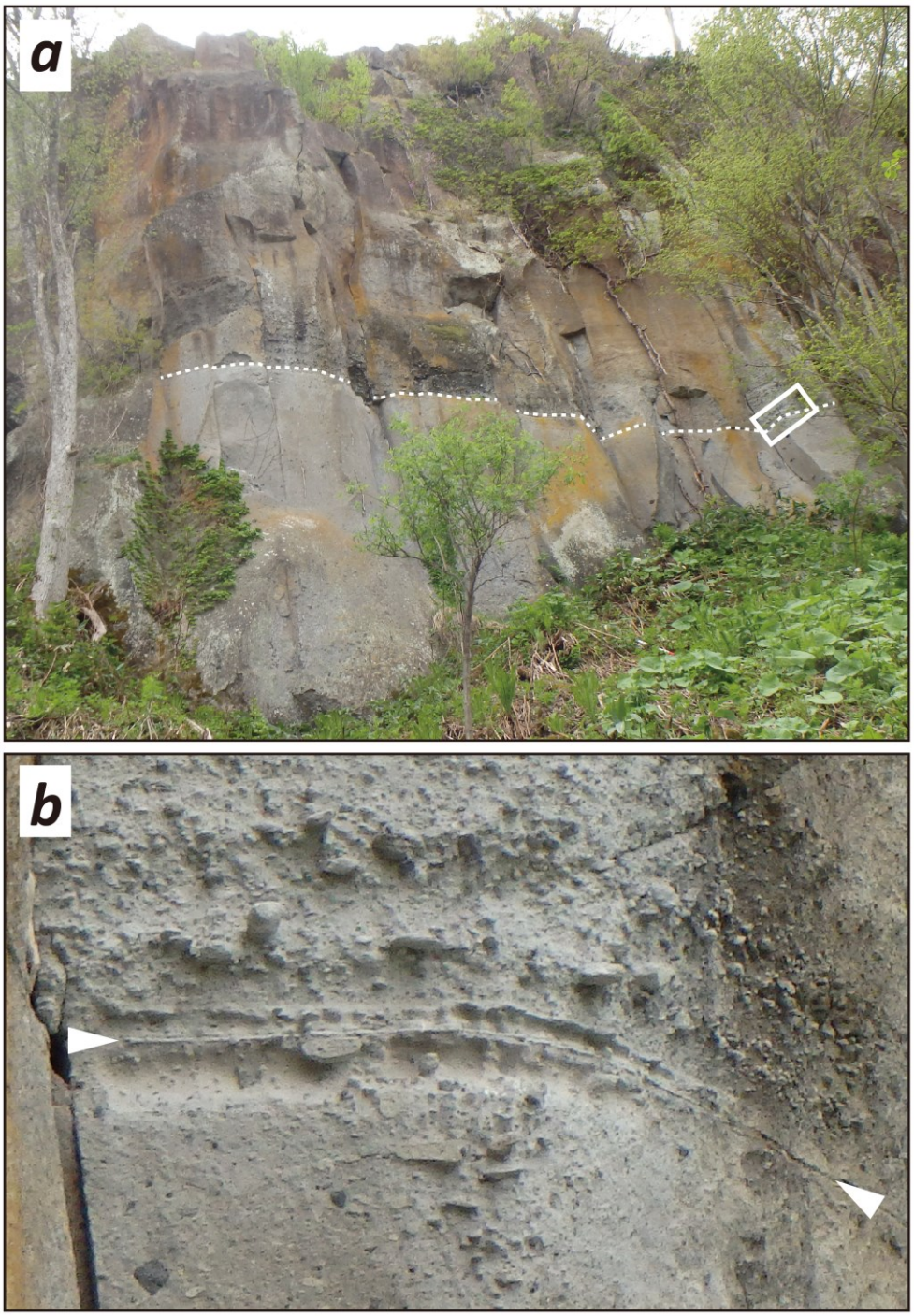


**Figure 3.2:** Section of Hb-type ignimbrite at the southwest of the town of Kamikawa. **a** The moderately welded, columnar-jointed Hb-type ignimbrite, intercalated by a thin fine ash horizon (*dashed line*). The *box* highlights the area shown in Fig. 3.2b. Note that the fine ash horizon does not disturb the columnar joints, suggesting a short hiatus in ignimbrite deposition. **b** Close-up view of a 5-mm-thick fine ash horizon (shown by *arrows*). Diffuse stratification above the fine ash horizon is marked by a variation in the grain size.

present. Lithic fragments are commonly minor and comprise variably altered lavas and welded tuff clasts.

In the summit area of the Taisetsu volcano group, there is only one outcrop of the Hb-type ignimbrite, 2.5 km south of the caldera center, where it overlies the Ohachidaira lava and appears to be overlain by the Kobachidaira ignimbrite via a >1.5-m-thick fluvial deposit. Here the Hb-type ignimbrite is 1.5 m thick and contains exceptionally large pumice and scoria blocks up to 1 m in size with few lithic fragments. Despite the thin nature of it, the coarseness of the clasts may indicate relative proximity to source.

### 3.2.3. Kobachidaira ignimbrite

The Kobachidaira ignimbrite (up to ~30 m thick) occurs only in the summit area, covering the middle to lower flanks of the Ohachidaira and overlain by the Mamiyadake Scoria Member or Sounkyo eruption products (Fig. 3.1). It is a non- to weakly welded, massive or diffusely bedded, extremely poorly sorted, matrix- to clast-supported, lithic and scoria-rich deposit. Individual beds are usually inversely graded and have a thickness of 20 cm to 6 m, most of which are >1 m thick. Meter-sized lithic blocks, up to 5.5 m in diameter, are common and tend to occur at the top of beds (Fig. 3.3). These beds dip at 7°–10° radially outwards from the Ohachidaira caldera. Such lithological character and distribution of the Kobachidaira ignimbrite may indicate that it corresponds to "lithic pyroclastic deposit" in Metsugi (1987).

**Figure 3.3:** A 5-m-thick bed of the Kobachidaira ignimbrite (KI1). Pale-colored coarse fragments are lithic debris. Note a 4-m-diameter lithic block lying at the top. The ruler is 1 m long.

The Kobachidaira ignimbrite is up to 30 m thick and can be divided into two subunits, in ascending order, KI1 and KI2. This division is based on variations in lithic component and grain size: (1) the lithic assemblage of KI1 is dominated by variably altered andesite and dacite with minor welded tuff clasts, whereas that of KI2 is dominated by welded tuff clasts with subordinate andesite and dacite; (2) the meter-sized lithic blocks are observed in KI1 (Fig. 3.3), but the lithic fragments in KI2 are usually less than 1 m in size; (3) an ash matrix of KI1 is generally fines-depleted while that of KI2 is fines-bearing. The boundary between KI1 and KI2 is gradational, with no intercalated ash falls. Localized gas-segregation pipes occur in KI2.

Near the headwaters of the Ryounsawa Creek, two >5-m-thick, massive, non- to weakly welded beds of KI1 are observed, and a low-angle cross-stratified tuff occurs at the top of lower bed of KI1. This tuff layer pinches and swells in thickness (15–30 cm) over distances of tens centimeters, composed of a sequence of ash tuff beds and fines-depleted coarse ash to fine pumice and scoria lapilli lenses. Above the tuff layer, the basal 1-m-thick part of the upper bed, exceptionally, contains abundant fiamme and is slightly more welded. The fiamme have the length of ~5 to 40 cm with variable flattening ratios. Above the basal zone, fiamme is scarce even though no sharp boundary is observed.

At intersection of the Akaishigawa Creek and the mountain trail, KI2 is diffusely stratified and totals >20 m thick, comprising the lower part of the left bank of the Akaishigawa Creek. Stratification is defined by coarse scoria- or lithic-rich horizons. Scoria and lithic fragments in the horizons are up to 1 m in size. A 30-cm-thick, stratified tuff divides KI2 into two units, which consists of ash tuff beds interlayered by fines-depleted coarse ash to fine pumice and scoria lapilli lenses.

### 3.2.4. Mamiyadake Scoria Member

The Mamiyadake Scoria Member forms a tephra ring as much as ~60 m thick, occurring all around the caldera but the northeast and comprising the upper part of the caldera wall (Fig. 3.4), which thins out and disappears within ~1 km from the caldera rim (Fig. 3.1). The succession of the tephra ring is clearly exposed in valley walls on the

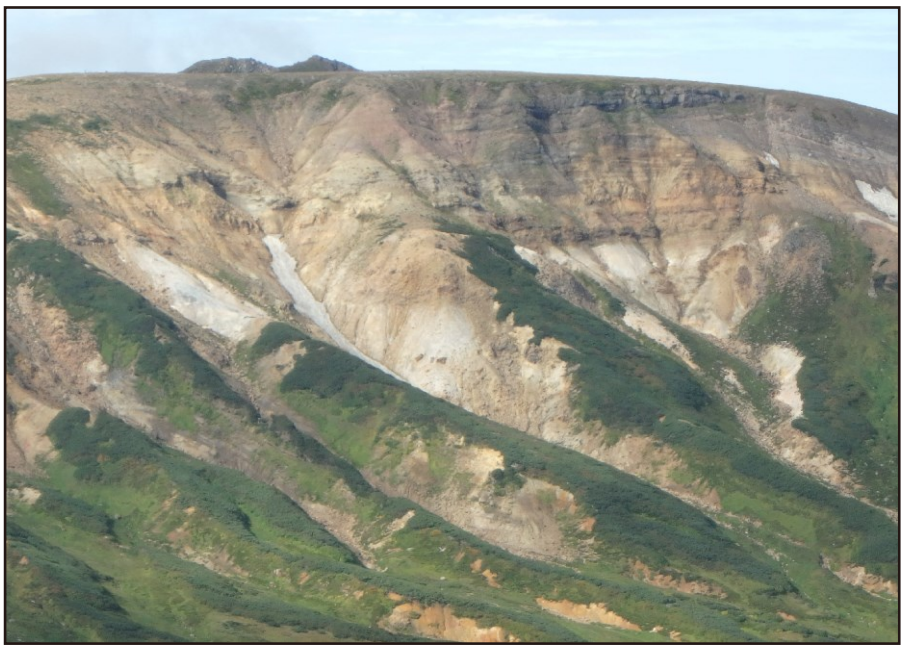

**Figure 3.4:** The well-stratified Mamiyadake Scoria Member forms the upper part of the southwestern caldera wall. The caldera wall is approximately 200 m high. The peak of the caldera rim is called "Mamiyadake."

**Figure 3.5:** Distribution of the Mamiyadake Scoria Member. The black ellipse marks the Ohachidaira caldera. Note that the strikes of the beds in the Mamiyadake Scoria Member roughly parallel to the caldera rim. The beds generally dip outward whereas some of them dip inward.

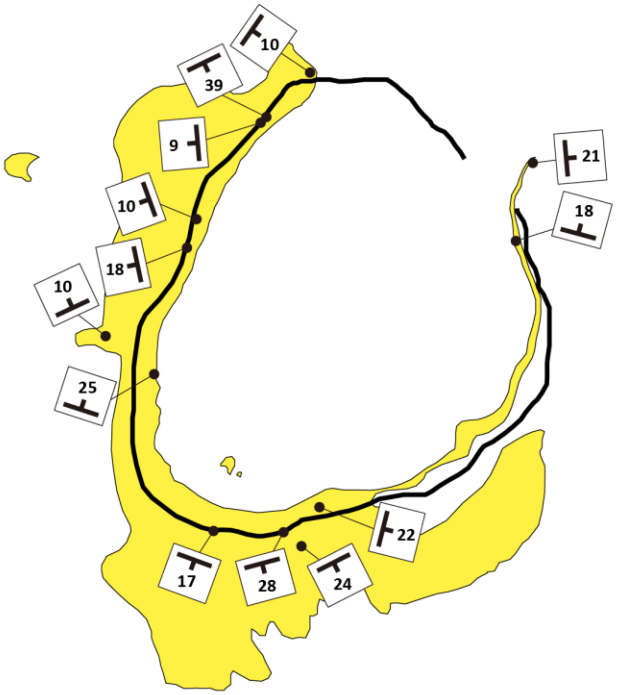

southern side of Ohachidaira volcano, where it overlies the Kobachidaira ignimbrite via a 1.5-m-thick reworked deposit, and is capped by the fallout of the Sounkyo eruption in the southeastern caldera wall. The tephra ring is dominated by pyroclastic breccia and stratified and cross-stratified lapilli-tuff beds with interstratified fine-ash beds. The strikes of the beds roughly parallel to the caldera rim (Fig. 3.5). Individual beds have a wide range of juvenile and lithic clast proportions. The juvenile components are generally dominated by scoria fragments although some beds contain pumice fragments of comparable or larger volume than scoria fragments. The lithic fragments consist mainly of andesite and dacite, with a smaller amount of volcanic breccia and welded tuff blocks.

At Nakadake peak, in the northwestern caldera wall, two spatter agglutinate units lie on the surface, mantling the caldera wall. Agglutinate units, each of which has a thickness of 6 m, are diffusely stratified, clast-supported, and spatter (flattened scoria clasts) rich. Spatters are welded each other, and locally, the remnant particles outlines are not preserved. Pumice and lithic fragments are scarce. A 30-cm-thick welded tuff is sandwiched between the two agglutinate units. It is diffusely stratified and consists of pumice lapilli dispersed in an ash matrix with minor pumice and lithic fragments. Below the agglutinate units, stratified to cross-stratified lapilli-tuff beds occur. Some beds pinch and swell and, in places, truncate previously deposited beds. Large lithic blocks rest within the lapilli-tuff beds without evidence of impact disturbance of underlying and enclosing strata.

On the basis of its distribution and lithology, the Mamiyadake Scoria Member should correspond to “base-surge deposit” in Metsugi (1987). I agree with his interpretation of the genesis of the deposit, but the Mamiyadake Scoria Member also includes fallout deposits and subordinate ignimbrites. Some lapilli-tuff beds (1) show low-angle cross-stratification, (2) pinch and swell, (3) truncate previously deposited beds, and (4) exhibit steep-dipping up to 39°, all of which are consistent with the interpretation that they are of base-surge origin. On the other hand, other coarse beds, for example those comprising the uppermost part of the northwestern caldera wall (Nakadake peak), apparently show evidence of fall deposition: (1) they are clast-supported and composed predominantly of scoria lapilli and blocks up to 80 cm in

diameter; (2) they decrease in thickness and the degree of welding as distance from the caldera increases. Although such scoria fall beds contain few lithic fragments, the lithic blocks reach up to 4 m in diameter in caldera rim exposures.

No age data is available for the Kobachidaira ignimbrite and the Mamiyadake Scoria Member, but the stratigraphic relationships indicate that they are younger than the 40–80 ka Hb-type ignimbrite and older than the 34 ka Px-type ignimbrite.

### 3.2.5. Sounkyo eruption products

The Sounkyo eruption is the latest and largest event at Ohachidaira. The eruption products are made up of five eruptive units (SK-A to -E) in proximal regions, corresponding to the distal deposits, a 1- to 2-m-thick pumice fallout and the Px-type ignimbrite up to 220 m thick. SK-A is a <60-m-thick, pumice-dominated fallout, which corresponds to the distal pumice fallout. SK-B is a massive valley-filling ignimbrite and is the proximal equivalent of the Px-type ignimbrite. SK-C is a >27-m-thick, unstratified and ungraded, coarse lithic breccia. SK-D is a <6-m-thick scoria fallout (SK-D). SK-E is a 5- to 15-m-thick ignimbrite.

## 3.3. Eruptive volume

A simple method for calculating the volume of ignimbrites is to multiply the area of distribution by the average thickness (e.g. Scarpati et al., 2014). However, the thickness of the Hb-type ignimbrite varies significantly place to place, due to its valley-filling nature and the underlying irregular topography, such that the simple method should not be applied to estimate its volume. Instead, I divide its distribution into several thickness-sectors and estimate the volume of each sector individually. The bulk volume of a particular sector can be estimated by multiplying the area by the half of the maximum thickness observed in that sector. The present-day volume of the Hb-type ignimbrite is estimated to be 4.61 $km^3$ (Table 3.1). Bulk volumes of the Ohachidaira lava, Kobachidaira ignimbrite, and Mamiyadake Scoria Member were estimated by multiplying the area of distribution by the average thickness, yielding 0.17

$km^3$, 0.04 $km^3$, and 0.08 $km^3$, respectively.

Lithic volumes contained in the deposits were calculated with the bulk volume and the mean lithic content, yielding the lithic volume of 0.02 $km^3$ for the Kobachidaira ignimbrite and that of 0.03 $km^3$ for the Mamiyadake Scoria Member. The Ohachidaira lava is virtually lithic free.

Magma (dense rock equivalent, DRE) volumes were calculated by subtracting the lithic volume from the deposits and assuming a magma density of 2.5 $g/cm^3$ and an average density of 1.5 $g/cm^3$ for the Kobachidaira ignimbrite and the Mamiyadake Scoria Member, yielding 0.01 $km^3$ and 0.03 $km^3$, respectively. The magma volume of the Ohachidaira lava is the same as the bulk volume of it.

**Table 3.1:** Volume considerations for the eruptive deposits from Ohachidaira, except for the Sounkyo eruption products.

| | Bulk volume ($km^3$) | Lithic* content (vol%) | Lithic volume ($km^3$) | DRE volume ($km^3$) |
|---|---|---|---|---|
| Mamiyadake Scoria Member | 0.08 | 40 | 0.03 | 0.03 |
| Kobachidaira ignimbrite | 0.04 | 40 | 0.02 | 0.01 |
| Hb-type ignimbrite | 4.61 | ? | ? | ? |
| Ohachidaira lava | 0.17 | - | - | 0.17 |

* Lithic content is the mean content of lithic fragments in each unit. Lithic contents in the deposits were semi-quantitatively estimated by comparing, at outcrops, a color index and lithic clasts dispersed in an ash matrix, and the finer (less than a few mm) lithic fragments comprising the ash matrix were ignored. Therefore our estimates of lithic contents will be a minimum.

## 3.4. Eruptive source

The eruptive source of tephra can be determined by lateral variations in thickness, grain-size, and the degree of welding for fallout deposits, or by flow direction indicators and lithological characteristics for flow-origin deposits (e.g. Wright and Walker, 1977; Self et al., 1986; Schumacher and Mues-Schumacher, 1996; Cagnoli and Tarling, 1997; Palmer and MacDonald, 1999).

The lavas exposed in the caldera walls extend radially down the flanks of Ohachidaira volcano, indicating that the source of the Ohachidaira lava was within the Ohachidaira caldera. For the Kobachidaira ignimbrite, its distribution is confined near the caldera (<2.9 km from the caldera center) but inside it, suggesting its source at the Ohachidaira caldera. The Mamiyadake Scoria Member was also sourced from the Ohachidaira caldera, as evidenced by: (1) its occurrence along the periphery of the caldera; (2) the strikes of the beds roughly parallel to the caldera rim (Fig. 3.5); and (3) the rapid decrease in thickness, grain-size, and the number of beds outward from the caldera rim. The source of the Sounkyo eruption would have been within the Ohachidaira caldera, because (1) its proximal products crop out extensively northeast and southeast of the Ohachidaira caldera and (2) the initial fallout unit (SK-A) shows a decrease in grain-size, in the degree of welding, and in the thickness and number of beds, as distance from the Ohachidaira caldera increases, indicating that SK-A was erupted from a vent within the caldera (see Chapter 4).

For the Hb-type ignimbrite, there is no proof for or against its source to be the Ohachidaira caldera. Sato and Wada (2012) correlated the ignimbrite with the Ohachidaira caldera based on its distribution. Nevertheless, the distribution they mentioned is confined to the foot of the Taisetsu volcano group, which in fact supports the inference that the ignimbrite was vented from somewhere in the Taisetsu volcano group rather than the Ohachidaira caldera. Its proximal outcrop located 2.5 km south of the caldera center is not decisive evidence to identify its source. The vent (or caldera) that fed the Hb-type ignimbrite was possibly concealed by younger eruptive deposits. No structural evidence for an eruptive source of the Hb-type ignimbrite has otherwise been found. One way to assess whether its source was the Ohachidaira caldera is to

make petrological and geochemical comparisons between the welded tuffs included in deposits from the Ohachidaira caldera (i.e. the Kobachidaira ignimbrite, Mamiyadake Scoria Member, and Sounkyo eruption products) and the Hb-type ignimbrite.

## 3.5. Paleomagnetic analysis

The proximal products I analyzed include the Kobachidaira ignimbrite, Mamiyadake Scoria Member, and Sounkyo Member, whose paleomagnetic directions were compared with those in the distal products, the Hb-type and Px-type ignimbrites, estimated by Yasuda et al. (2015).

### 3.5.1. Sampling and measurement

Location of sampling sites is shown in Fig. 3.1. Twenty scoria clasts were collected at two sites (ts6, 10) from the Kobachidaira ignimbrite. The Mamiyadake Scoria Member was sampled at four sites (ts1–4) with a total of thirty-two scoria clasts and eight matrix samples. Twenty-eight juvenile clasts collected at three sites (ts5,7,9) from the Sounkyo Member, SK-A, -B, and -E, are predominantly scoria with subordinate pumice clasts. Clasts and matrix samples were collected as hand samples oriented by magnetic compass. In the laboratory, the oriented samples were cut into 24-mm-tall, 24-mm-diameter cylinder cores (specimens) for analysis. The natural remanent magnetization (NRM) of the specimens was measured using a Natsuhara SMD-88 spinner magnetometer. All specimens were subjected to thermal demagnetization using a Natsuhara TDS-1 thermal demagnetizer with residual fields <10 nT. The specimens were demagnetized in steps of 50°C at low temperatures up to 500°C and of 30°C at higher temperatures up to 560, 590, or 620°C. Principal component analysis (Kirschvink, 1980) was carried out to obtain the best fit demagnetization lines for linear demagnetization trajectories. Only characteristic components of NRM (ChRM) determined by results of ≥3 successive thermal demagnetization steps with maximum angular deviation (MAD) <10° are considered

reliable. Site-mean ChRM directions were then combined for each eruptive episode (between-site) ChRM direction. Mean directions were calculated according to standard Fisher (1953) statistics.

## 3.5.2. Results

### 3.5.2.1. Magnetic characteristics

Figure 3.6 shows the change in direction and intensity of the NRM of representative specimens with progressive demagnetization. In nearly all specimens, the remanence at low–intermediate temperatures displayed a random direction. Only at site ts03, thermal demagnetization up to 400°–560°C removes one or two low-stability components of NRM. For all sites ChRM was isolated after elimination of the low-stability component, which decays univectorally toward the origin. Typically, specimens show a range of unblocking of remanence between 590°C and 620°C, suggesting magnetite as the dominant carrier of NRM with a contribution by hematite in some samples.

### 3.5.2.2. Characteristic remanent magnetization

ChRM directions are well clustered within each site and yield site-mean directions with $k$ >24 and $\alpha_{95} \leq 10°$, most of which with $k$ >100 and $\alpha_{95} \leq 5°$ (Fig. 3.7 and Table 3.2). Even though the ChRM directions for the site ts06 have relatively high dispersion ($k$ = 24.2, $\alpha_{95}$ = 10°), if I discarded a specimen direction with exceptionally shallow inclination, they would become well grouped ($k$ = 474.3, $\alpha_{95}$ = 2.4°) close to the site-mean direction from another Kobachidaira ignimbrite site. The sample that has a remanent magnetization with a peculiar direction has been likely reworked after emplacement, so it was not used to for determining the between-site mean direction.

The between-site dispersion of ChRM directions for the Sounkyo Member is low ($k$ = 1682.8, $\alpha_{95}$ = 3°), while that for the Mamiyadake Scoria Member is greater ($k$ = 58.6, $\alpha_{95}$ = 12.1°) due to site ts1 with an anomalous site mean direction (Table 3.2). If the site direction from ts1 was not used, the ChRM value for the Mamiyadake Scoria Member would show less dispersion ($k$ = 234.8, $\alpha_{95}$ = 8.1°; Table 3.3).

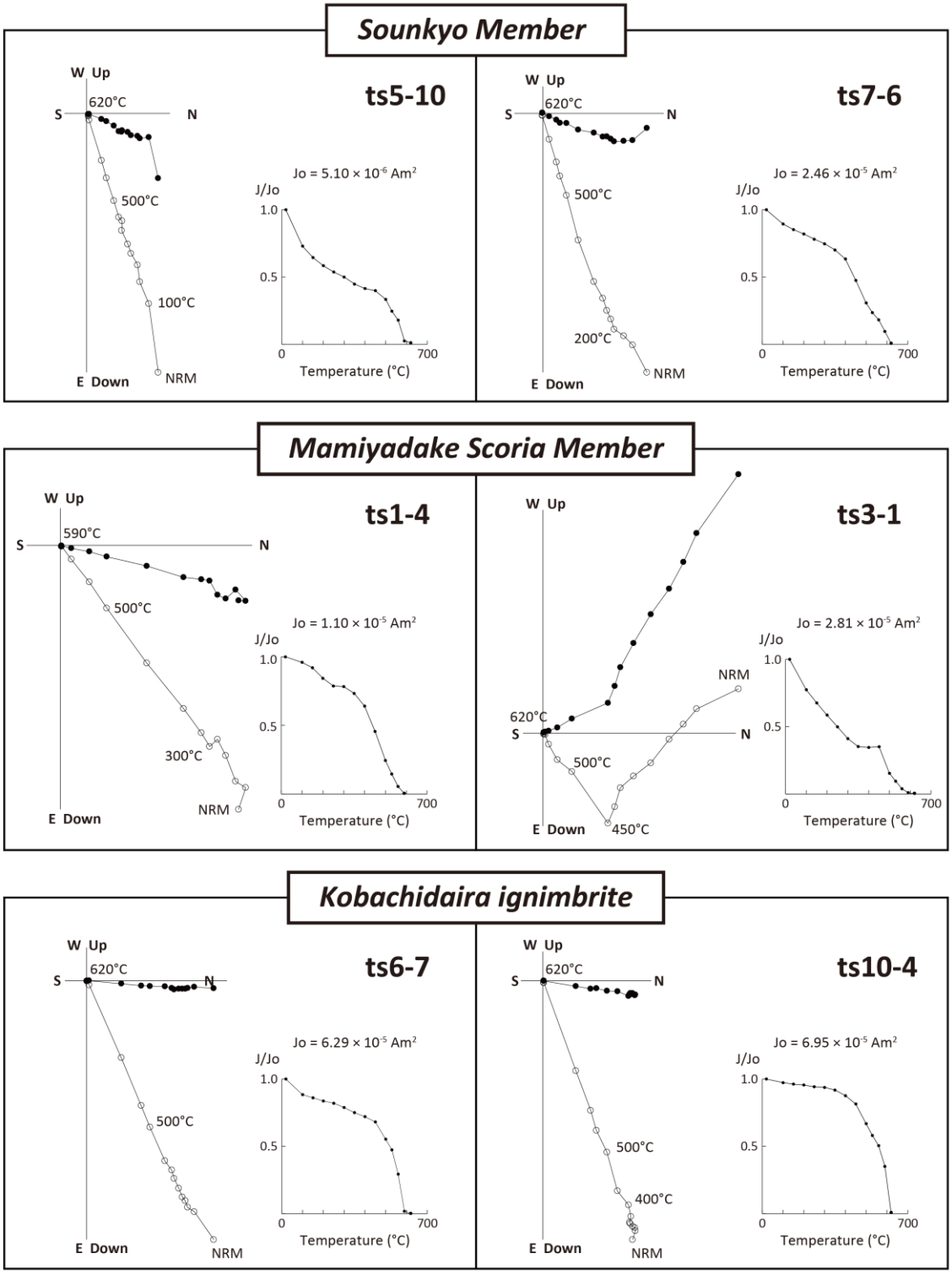


**Figure 3.6:** Thermal demagnetization data for representative specimens from the Kobachidaira ignimbrite, Mamiyadake Scoria Member, and Sounkyo Member. For each specimen, the left is an orthogonal plot, and the right is a normalized intensity decay curve. *Solid* and *open circles* are the projection on the horizontal and vertical planes, respectively.

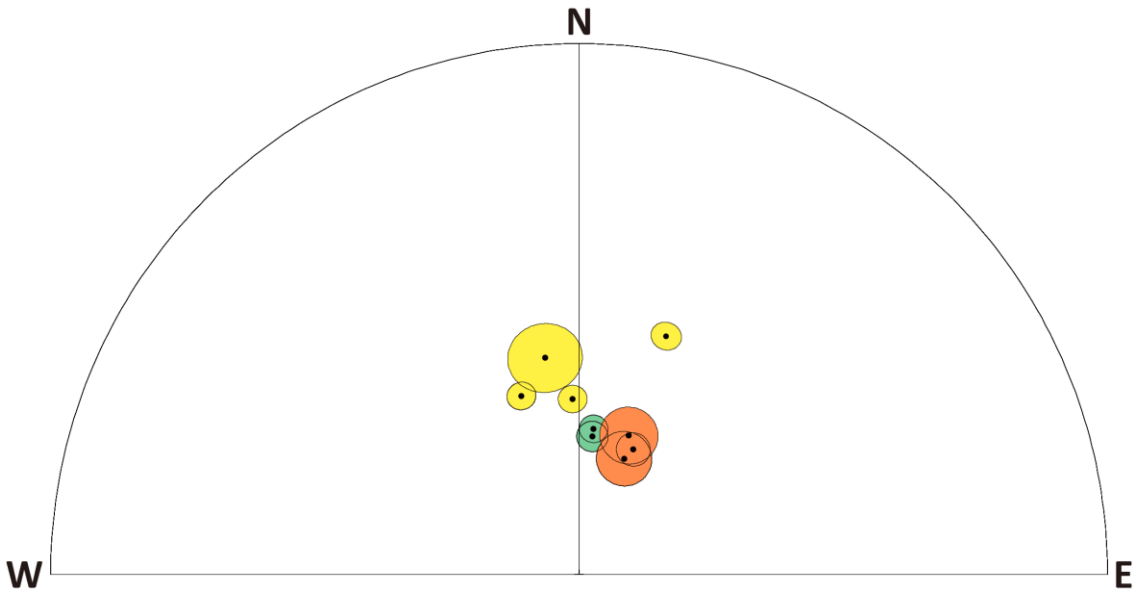


**Figure 3.7:** Equal-area lower hemisphere projection of within-site mean ChRM directions and 95% confidence circles for the Kobachidaira ignimbrite (*green*), Mamiyadake Scoria Member (*yellow*), and Sounkyo Member (*orange*). The ChRM directions are well grouped in each eruptive episode, except for one site (ts1) of the Mamiyadake Scoria Member.

**Table 3.2:** Summary of paleomagnetic results.

| | Site | *N* | *D*(°) | *I*(°) | $\alpha_{95}$(°) | *k* |
|---|---|---|---|---|---|---|
| *Sounkyo M.* | | | | | | |
| | ts5 | 10 | 23.6 | 69.1 | 2.6 | 354.3 |
| | ts7 | 8 | 21.4 | 71 | 4.2 | 174.1 |
| | ts9 | 10 | 19.8 | 67.3 | 4.4 | 120.7 |
| *Mamiyadake S.M.* | | | | | | |
| | ts1 | 10 | 20.2 | 50.5 | 2.2 | 471.3 |
| | ts2 | 11 | -18 | 61.1 | 2.2 | 444.3 |
| | ts3 | 8 | -9 | 56 | 5.5 | 102.6 |
| | ts4 | 11 | -2.1 | 63 | 2.2 | 448.7 |
| *Kobachidaira Ig* | | | | | | |
| | ts6 | 10 | 16.1 | 66.3 | 10 | 24.2 |
| | ts10 | 10 | 5.7 | 67.5 | 2.1 | 508.3 |

*N*, number of samples from which ChRM are obtained; *D*, mean declination (in situ); *I*, mean inclination (in situ); $\alpha_{95}$, radius of 95% confidence circle; *k*, precision parameter.

### 3.5.3. Implications for the reconstruction of eruptive history

The within-site data are generally of good quality, suggesting that the estimated site mean directions are representative of the ChRM for the deposits of that location. Moreover, in spite of a low number of sites used in the calculation of the eruptive episode ChRM, the between-site mean direction for each eruptive episodes has moderate to low dispersion and is significantly distinct each other. These indicate that the estimated ChRM may record the direction of the Earth's magnetic field at the time of emplacement and thus allows correlation of deposits.

ChRM directions for the Px-type ignimbrite and Sounkyo Member are statistically indistinguishable (Fig. 3.8), together with their lithological and petrological characteristics, confirms a correlation between them (see Chapter 4). The ChRM values for the Hb-type ignimbrite, Kobachidaira ignimbrite, Mamiyadake Scoria Member, and Sounkyo Member are distinguishable each other (Fig. 3.8), which is consistent with the field evidence suggesting that each eruptive episodes are temporally distinct.

Further work in the Mamiyadake Scoria Member would allow for a better defined estimate of the ChRM direction. Apparently, it is necessary to estimate a ChRM direction for the Hb-type ignimbrite in proximal regions to make sure if its ChRM directed toward that for the Hb-type ignimbrite in distal regions.

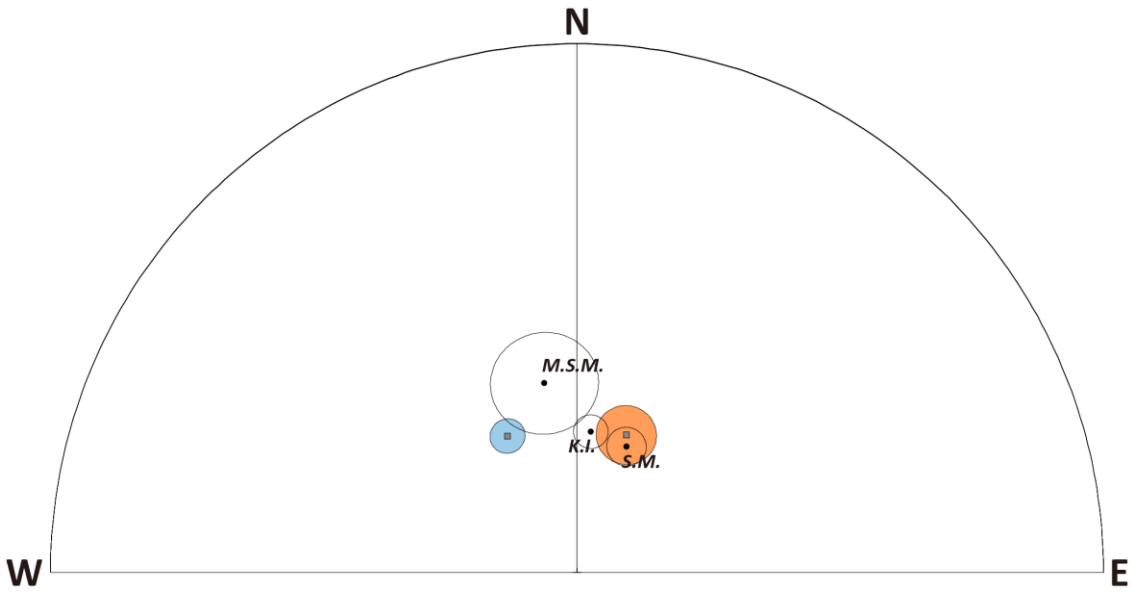


**Figure 3.8:** Equal-area lower hemisphere projection of between-site mean ChRM directions and 95% confidence circles for the Kobachidaira ignimbrite (*K.I.*), Mamiyadake Scoria Member (*M.S.M.*), and Sounkyo Member (*S.M.*). ChRM directions for the Hb-type and Px-type ignimbrites are shown as blue and orange circles, respectively (modified after Yasuda et al., 2015).

**Table 3.3:** Between-site mean ChRM directions for three eruptive episodes.

| | Site | *N* | *D* (°) | *I* (°) | $\alpha_{95}$ (°) | *k* |
|---|---|---|---|---|---|---|
| *Sounkyo M.* | | | | | | |
| | ts5, ts7, ts9 | 3 | 21.6 | 69.1 | 3 | 1682.8 |
| *Mamiyadake S.M.* | | | | | | |
| | ts2, ts3, ts4 | 3 | -9.8 | 60.2 | 8.1 | 234.8 |
| *Kobachidaira Ig* | | | | | | |
| | ts6, ts10 | 2 | 5.6 | 68.1 | 2.6 | 9083.9 |

*N*, number of sites; *D*, declination; *I*, inclination; $\alpha_{95}$, radius of 95% confidence circle; *k*, precision parameter.

## 3.6. Contributions to the caldera development

Collapse calderas can be formed by during effusive explosive (lava flows and domes) or non-explosive (intrusions) events. Calderas in Hawaii have developed in association with mafic effusive activities over broad time ranges (days to weeks; Newhall and Dzurisin, 1988). At Fernandina and Miyakejima, caldera collapse progressed over several days as magma displacement occurred beneath the surface with a minor amount erupted (Filson et al., 1973; Geshi et al., 2002). The early activity of Ohachidaira volcano was dominated by the eruption of lava flows, the total volume of which is 0.17 $km^3$. I consider that it is very unlikely that caldera collapse occurred during the eruption of such lavas. The magma eruption rate for the Ohachidaira lava eruption may be significantly smaller for caldera collapse. In general, the formation of calderas by caldera collapse requires rapid drainage rates for collapse to occur (Scandone, 1990). Moderate to large ignimbrite eruptions that led to caldera collapse have an eruption rate of $10^7$–$10^8$ kg/s or more (Scott et al., 1996; Hildreth and Fierstein, 2000; Houghton et al., 2010; Simmons et al., 2017ab). Even at Fernandina and Miyakejima, the magma evacuation rate of $10^5$–$10^6$ kg/s was estimated (Stix and Kobayashi, 2008). The eruption of the Ohachidaira lava, however, may have had an eruption rate of $10^3$ kg/s or less (assuming the eruption duration, years or more). The low magma evacuation rate may not facilitate caldera collapse because of the decrease in rates of chamber decompression due to elastic deformation of chamber walls.

The original bulk volume of the Hb-type ignimbrite is apparently greater than 4.61 $km^3$, which seems likely to be accompanied by caldera formation. Nevertheless, its source vent or caldera is unknown.

The Kobachidaira ignimbrite eruption was characterized by an initial vent widening/clearing episode of Ohachidaira volcano. The variably altered andesite and dacite lava blocks, the predominant type in the lithic fraction of KI1, were essentially derived by vent or subsurface conduit erosion. Its coarseness (<5.5 m) and abundance (~50 vol%) of lithic fragments throughout KI1 reflects a vent opening and development. It should be noted that the underling Hb-type ignimbrite does not show such evidence for a vent opening as suggested by its lithic-poor nature, though the last phase of the

early effusive episode of Ohachidaira might have filled the vent and conduit with lavas. Although KI2 are similar to KI1 in the abundance of lithic fragments, the dominant lithic type in KI2 is welded tuff clasts. The welded tuff clasts consist of scoria and lithic fragments with minor pumice clasts, which have similar appearance to the host ignimbrite. The welded tuff clasts may appear to consist mostly of vent-filling ignimbrite that has become moderately welded before incorporation into the subsequently erupted host ignimbrite.

The Mamiyadake Scoria Member is a thick succession formed by phreatomagmatic and magmatic activities. In general it is enriched in lithic clasts (the mean lithic content, ~40 vol%), whose assemblage is dominated by shallow-origin volcanic rocks, indicating that the shallow conduit and vent were progressively widened as the eruption proceeded.

The Sounkyo eruption is considered to play a significant role in the formation of the Ohachidaira caldera because it vented the most abundant magma and lithic fragments among the eruptive episodes of Ohachidaira volcano (see Chapter 4 for detail).

## 3.7. Conclusions

Based on field and paleomagnetic data, I recognize five eruptive episodes from Ohachidaira stratovolcano. The ChRM directions from the pyroclastic deposits of four to five episodes are distinguishable each other, indicating that the paleomagnetic data provides a useful tool to help identifying and evaluating the tentative stratigraphy of the eruptive products constructed by field observations. The proximal Sounkyo member and the distal Px-type ignimbrite, which are separated in space, have ChRM directions statistically indistinguishable, suggesting their simultaneous emplacement. From 0.6 Ma, Ohachidaira produced andesitic to dacitic lavas and pyroclastics, forming the lower edifice. Between 60 ka and 34 ka, Ohachidaira volcano has had two (or possibly one) major (VEI 5) and two minor (VEI 3) explosive eruptive episodes, which were associated with the construction of the upper edifice and the formation of the summit caldera. Deposits from these eruptions occur in caldera walls, valleys extending outward

from the caldera rim, and at the foot of the Taisetsu volcano group. While the last largest explosive episode (Sounkyo eruption) made a major contribution to the caldera development, the earlier explosive events (Kobachidaira ignimbrite and Mamiyadake Scoria Member) must have corresponded to vent enlargement to some extent. I revealed the eruptive styles, magnitudes (i.e. distribution and volume), and history of Ohachidaira volcano. Such basic geological data contributes to predict and mitigate the hazards and risk associated with future eruptions from the volcano.

# Chapter 4

# The origin of a coarse lithic breccia in the 34 ka caldera-forming Sounkyo eruption

## 4.1. Introduction

Moderate to large (VEI >5) explosive eruptions produce ignimbrites and/or plinian fallouts, often associated with formation of calderas at their source areas (Lipman, 1997). Caldera depressions can be formed either by collapse of the roof of a magma chamber due to magma withdrawal (e.g. 0.73 Ma Bishop Tuff, Long Valley, Hildreth and Mahood, 1986, Crater Lake, Bacon, 1983; Suzuki-Kamata et al., 1993) or by vent widening (e.g. Nigorikawa, Ando, 1983; Kurozumi and Doi, 2003). Field-based studies addressing large calderas have reported some evidence for caldera collapse during magma withdrawal, such as (1) thick intracaldera ignimbrite fill intercalated with caldera-wall slide breccias (Lipman, 1976, 1997; Hildreth, 1996), (2) the similarity between the caldera volume and the erupted magma volume (Bacon, 1983; Hildreth and Mahood, 1986), and (3) coarse lithic breccias associated with outflow ignimbrites (co-ignimbrite lag breccias, Druitt and Sparks, 1984; Walker, 1985).

Why are the coarse lithic breccias an evidence for caldera collapse? For large caldera-forming eruptions, the lithic breccias are commonly interbedded with or overlain by a climactic ignimbrite (e.g. Druitt and Sparks, 1982; Aramaki, 1984; Druitt and Bacon, 1986; Nairn et al., 1994; Allen and Cas, 1998; Allen, 2001; Lindsay et al., 2001; Palladino and Simei, 2005; Bear et al., 2009). The great diversity of lithic component of the lithic breccias, such as at Crater Lake, Phlegraean Fields, and Santorini may record the opening of multiple vents (Suzuki-Kamata et al., 1993; Rosi et al., 1996; Druitt, 2014). Azimuthal differences in lithic component proportions in the

lithic breccia, associated with the climactic eruption of Mount Mazama (Crater Lake caldera), correlate well with the geology of the caldera walls, suggesting multiple vents along a ring fracture system (Suzuki-Kamata et al., 1993). The lithic breccias have been widely interpreted as reflecting the opening of new vents and conduit enlargement associated with caldera collapse, followed by a rapid increase in magma discharge rate (Druitt and Sparks, 1984; Walker, 1985).

For small caldera-forming eruptions, on the other hand, the lithic breccias overlie a climactic ignimbrite or plinian fallout, and their lithic assemblages do not show a great diversity as well as those in large caldera-forming eruptions (e.g. Browne and Gardner, 2004; Andrews et al., 2007). Despite differences in stratigraphic position and in lithic assemblages, it is generally considered that the lithic breccias in small caldera-forming eruptions also mark the onset of caldera collapse and that the caldera collapse happened after the eruption climax (e.g. Pinatubo, Scott et al., 1996; Ceboruco, Gardner and Tait, 2000; Browne and Gardner, 2004, Ksudach, Andrews et al., 2007; Andrews and Gardner, 2010). In order to investigate formation mechanisms of small calderas, it is important to interpret the origin of lithic breccias with evaluation of lithic componentry data, together with an assessment of whether caldera collapse occurs.

In this Chapter, I describe the case of the 34 ka Sounkyo eruption, which is the latest and largest event at a 2-km-diameter summit caldera in the Taisetsu volcano group, Japan. The Sounkyo eruption products comprise fallout and pyroclastic-flow deposits of basaltic andesitic to dacitic composition, with a coarse lithic breccia generated after an eruption climax. I present the detailed stratigraphy based on field mapping (Fig. 4.1) and correlation. I estimate the volume of the eruption products and determine the componentry of lithic fragments to assess the origin of the caldera and the lithic breccia. Finally, I compare my results with other small caldera-forming eruptions, proposing an alternative model for the formation of lithic breccias.

## 4.2. Stratigraphy of the Sounkyo eruption products

The Sounkyo eruption products occur at the foot of the Taisetsu volcano group (distal) and around the Ohachidaira caldera (proximal). The distal and proximal products of the eruption show apparently distinctive lithofacies (Fig. 4.2), the latter of which is more complex, and do not overlap in distribution. Both of pumice, scoria, and banded pumice fragments are ubiquitously present in the eruption products as juvenile materials.

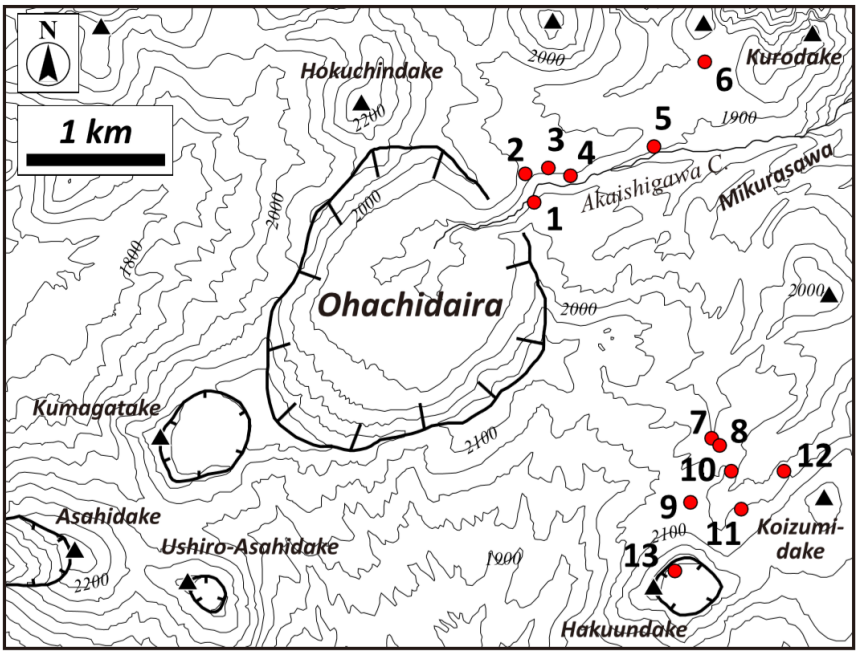


**Figure 4.1:** Location map of the proximal area around the Ohachidaira caldera. Locality numbers referred in text are shown. Contour interval, 50 m.

### 4.2.1. Distal products

The Sounkyo eruption products comprise a pumice-fall deposit and the overlying Px-type ignimbrite at the foot of the Taisetsu volcano group (Sato and Wada, 2010).

#### 4.2.1.1. Distal pumice-fall deposit

At the eastern foot of the Taisetsu volcano group a pumice-fall deposit is conformably overlain by the Px-type ignimbrite (Katsui et al., 1979; Sato and Wada, 2010). The pumice-fall deposit is best exposed at Obako 11 km east of the caldera, where it comprises a lower, 40-cm-thick, thin-bedded part and an upper, 160-cm-thick,

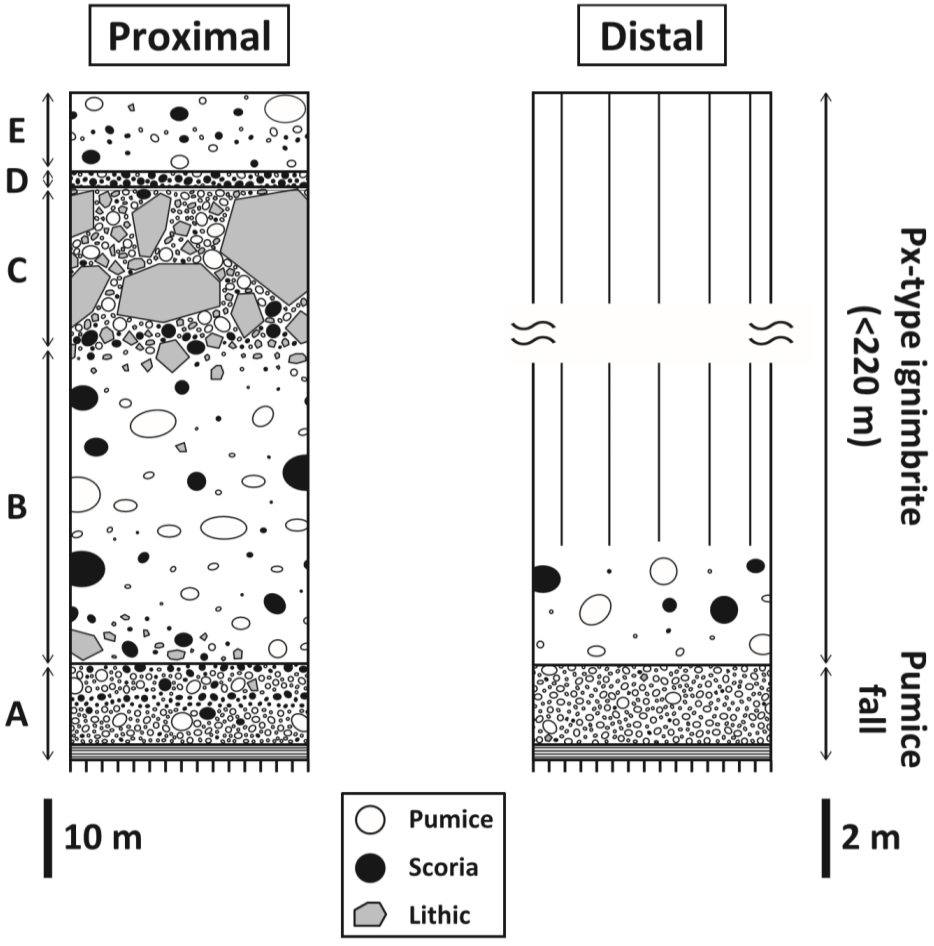


**Figure 4.2:** Generalized stratigraphic sections through the Sounkyo eruption products in proximal and distal regions. Note the difference in scales for individual sections.

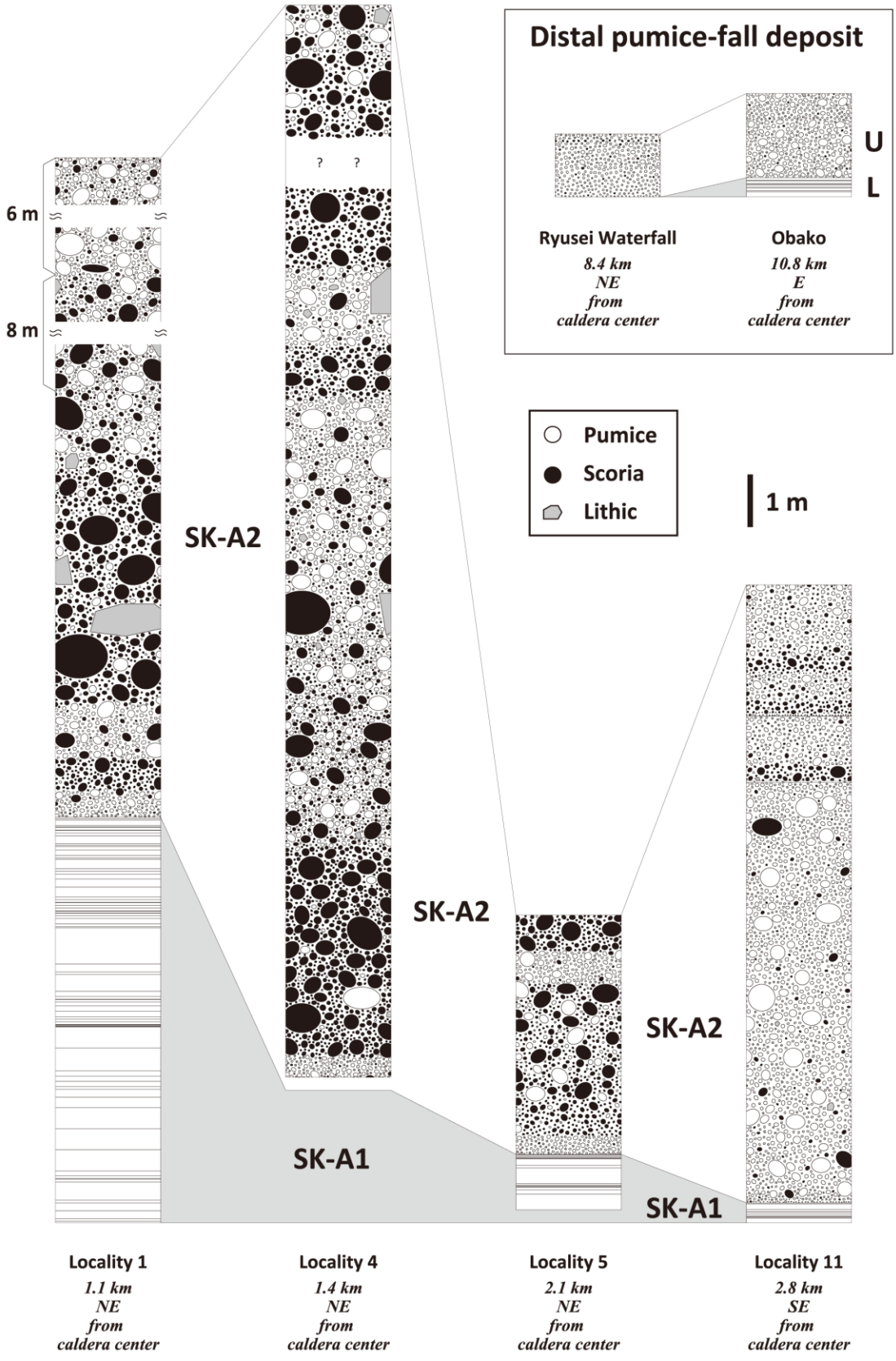
Distal pumice-fall deposit
U
L
Ryusei Waterfall
8.4 km
NE
from
caldera center
Obako
10.8 km
E
from
caldera center
Pumice
Scoria
Lithic
1 m
6 m
8 m
? ?
SK-A2
SK-A2
SK-A2
SK-A1
SK-A1
Locality 1
1.1 km
NE
from
caldera center
Locality 4
1.4 km
NE
from
caldera center
Locality 5
2.1 km
NE
from
caldera center
Locality 11
2.8 km
SE
from
caldera center

coarser-grained part (Fig. 4.3). Here, the lower part is sequences of alternating fine to coarse ash and fine-lapilli fall layers, and unconformably overlies the basement siltstone. The fine-lapilli layers consist of both pumice and scoria with few lithic fragments. The upper part consists predominantly of pumice lapilli and blocks up to 10 cm in diameter, and is diffusely stratified into at least three layers. Scoria and lithic clasts are subordinate in the upper part of the fallout, but a one-clast-thick scoria horizon is present at Ryusei Waterfall (Fig. 4.3). Note that the pumice-fall deposit is absent beneath the Px-type ignimbrite at the north-northeastern and southwestern foot of the Taisetsu volcano group (Fig. 4.4).

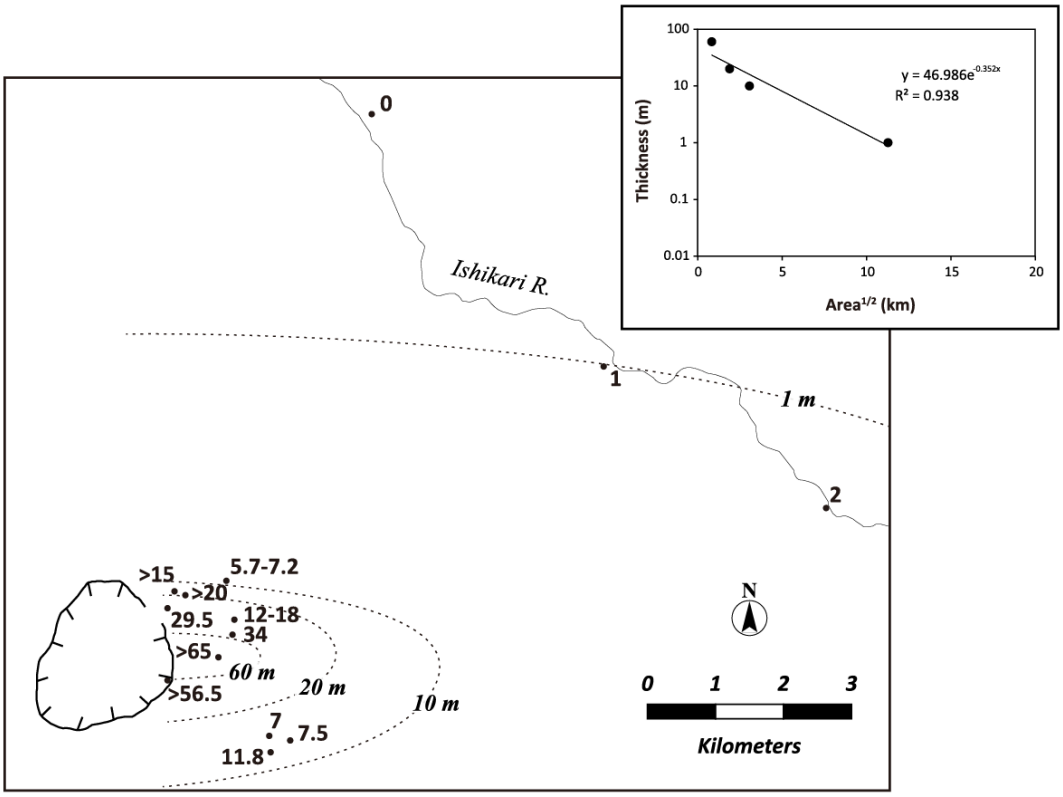


**Figure 4.4:** Isopach map of SK-A fallout and the distal pumice-fall deposit (thicknesses in meters). > indicates that the base of the fallout is unexposed or the top is unpreserved. Note that SK-A2 or the upper part of the distal pumice-fall deposit makes up most of the thickness. *Inset* shows the log of thickness vs. square root of area diagram.

---

**Figure 4.3:** Stratigraphic sections for SK-A fallout and the distal pumice-fall deposit. Gray zone traces SK-A1 and the lower part of the distal pumice-fall deposit (*L*). Thicknesses of individual beds are only described for SK-A1 and the lower part of the distal pumice-fall deposit because of their thinness and the difficulty of distinguishing between pumice and scoria clasts (see section 4.2.2.1). Question-marks indicate the areas which are obscured by talus. Locations of these sections are shown in Figs. 2.4 and 4.1.

#### 4.2.1.2. Px-type ignimbrite

The Px-type ignimbrite (<220 m thick) is widespread and outcrops to a maximum distance of 16 km from source. It mainly exists at the eastern to northeastern and western to southwestern foot of the Taisetsu volcano group, occurring along valleys of the Ishikari, Piukenai, and Chubetsu rivers (Fig. 2.4). It can be traced in near-continuous exposure for 10 km along the Ishikari River valley, Sounkyo Gorge. The Px-type ignimbrite is a moderately to intensely welded, columnar-jointed tuff except for the non-welded base. The Px-type ignimbrite is usually composed of a single cooling unit although two cooling units can be recognized at Kyokanheki, 14 km southwest of the caldera (Yasuda et al., 2015). The Px-type ignimbrite is massive and contains predominantly pumice and scoria lapilli and blocks supported by a gray ash matrix. Lithic fragments are rare (2–5 vol%) and are dominantly andesite lava clasts at the non-welded base. Pumice concentration zones and gas segregation pipes are locally present.

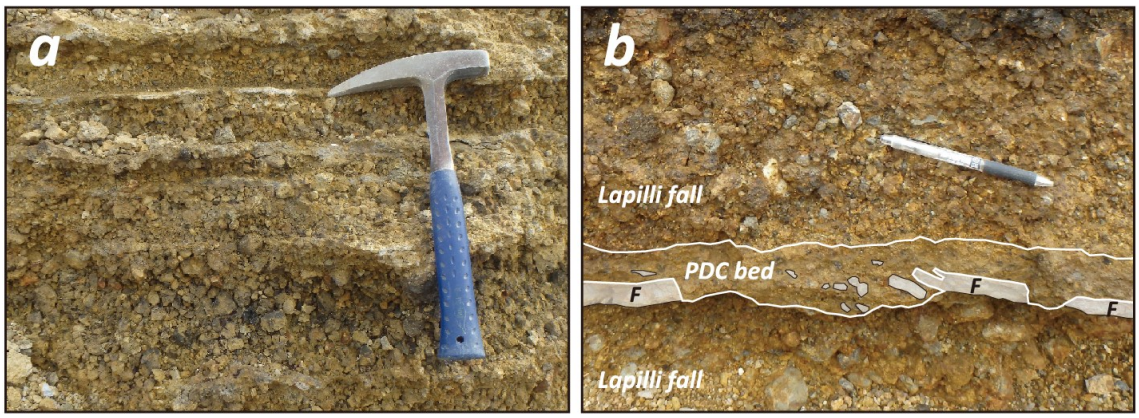


**Figure 4.5:** SK-A1 fallout at locality 1. **a** Stratification marked by variations in grain size. The uppermost bed (the head of the hammer) clearly shows inverse grading. Hammer is 33 cm long. **b** The PDC bed includes slabs of the fine-ash deposit eroded from the underlying fine-ash layer (*F*). Pen for scale is 14 cm long.

### 4.2.2. Proximal products

The Sounkyo eruption products crop out extensively northeast and southeast of the Ohachidaira caldera in proximal regions (Fig. 3.1). The proximal products consist of five units (Fig. 4.2), from base to top: pumice- and scoria-fall deposit (SK-A), climactic ignimbrite (SK-B), lithic breccia (SK-C), scoria-fall deposit (SK-D), and smaller-volume ignimbrite (SK-E). All are interpreted as the products of a single eruption on account of the absence of paleosols and significant disconformities among these units.

#### 4.2.2.1. SK-A

SK-A mantles the underlying topography with a dispersal axis directed to the east (Fig. 4.4) and can be sub-divided into SK-A1 and SK-A2 (Fig. 4.3): a basal thin-bedded part (A1) and an overlying, thick, coarser-grained, diffusely stratified part (A2). SK-A1 consists of >60 fall layers at locality 1 where it is best exposed and shows its maximum thickness of 7 m. Here, SK-A1 is non- to weakly welded, and consists mainly of pumice and scoria lapilli-fall layers, intercalating with fine- to coarse-ash layers (Fig. 4.5a). The lapilli and coarse ash-fall layers often exhibit inverse grading, along with occasional inverse-normal grading (Fig. 4.5a). Many of juvenile clasts in SK-A1 have been weathered and altered to dull yellow, dark yellow-brown color, which makes it difficult to recognize whether they are pumice or scoria (Fig. 4.5). Lithic fragments are generally rare (<10 vol%). SK-A1 fallout is characteristically interrupted by several thin, non- to weakly welded, pyroclastic density-current (PDC) beds with erosive bases (Fig. 4.5b). SK-A1 shows a decrease in grain-size, and in the thickness and number of beds, as distance from the caldera increases.

SK-A2 has a maximum thickness of ~60 m near the caldera rim and thins rapidly to several meters within the first 2 km outward from the caldera (Fig. 4.4). In caldera rim exposures, while the upper half of SK-A2 is diffusely stratified and rich in pumice lapilli and blocks up to 66 cm in diameter, the lower half of it is stratified and extremely rich in scoria fragments. The scoria-rich lower half is intensely agglutinated and welded that the remnant particles outlines are occasionally obliterated. Downwind distally, the

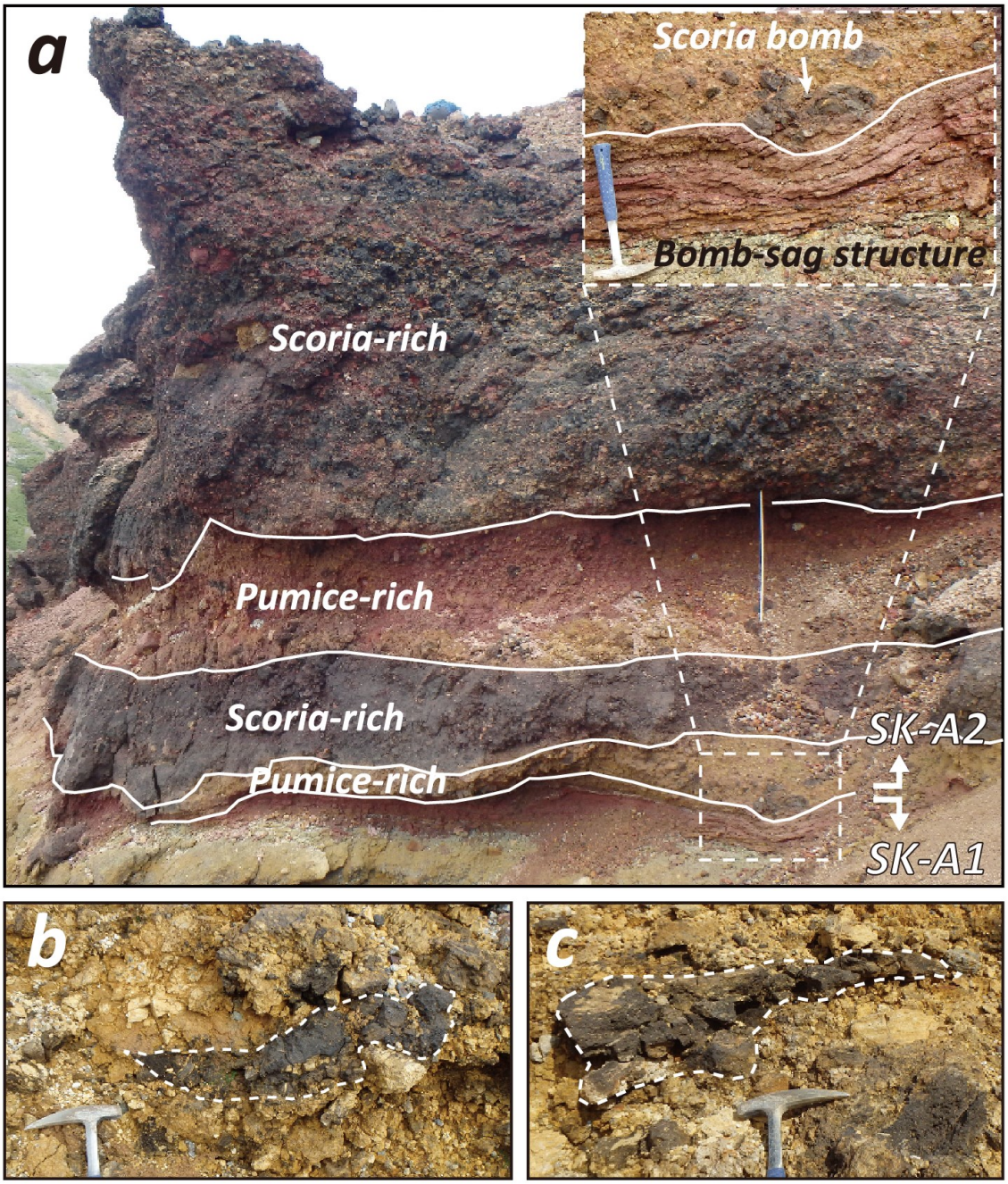


**Figure 4.6:** SK-A2 fallout at locality 1. **a** The lower part of SK-A2. Scoria-rich, welded layers are intercalated with pumice-rich, non-welded layers. Note the sag structure caused by a scoria bomb at the bottom of SK-A2. The Ohachidaira caldera is to the right. The ruler (center right) is 1 m long. Hammer is 33 cm long. **bc** Flattened scoria clasts (spatters) in the pumice-rich layers.

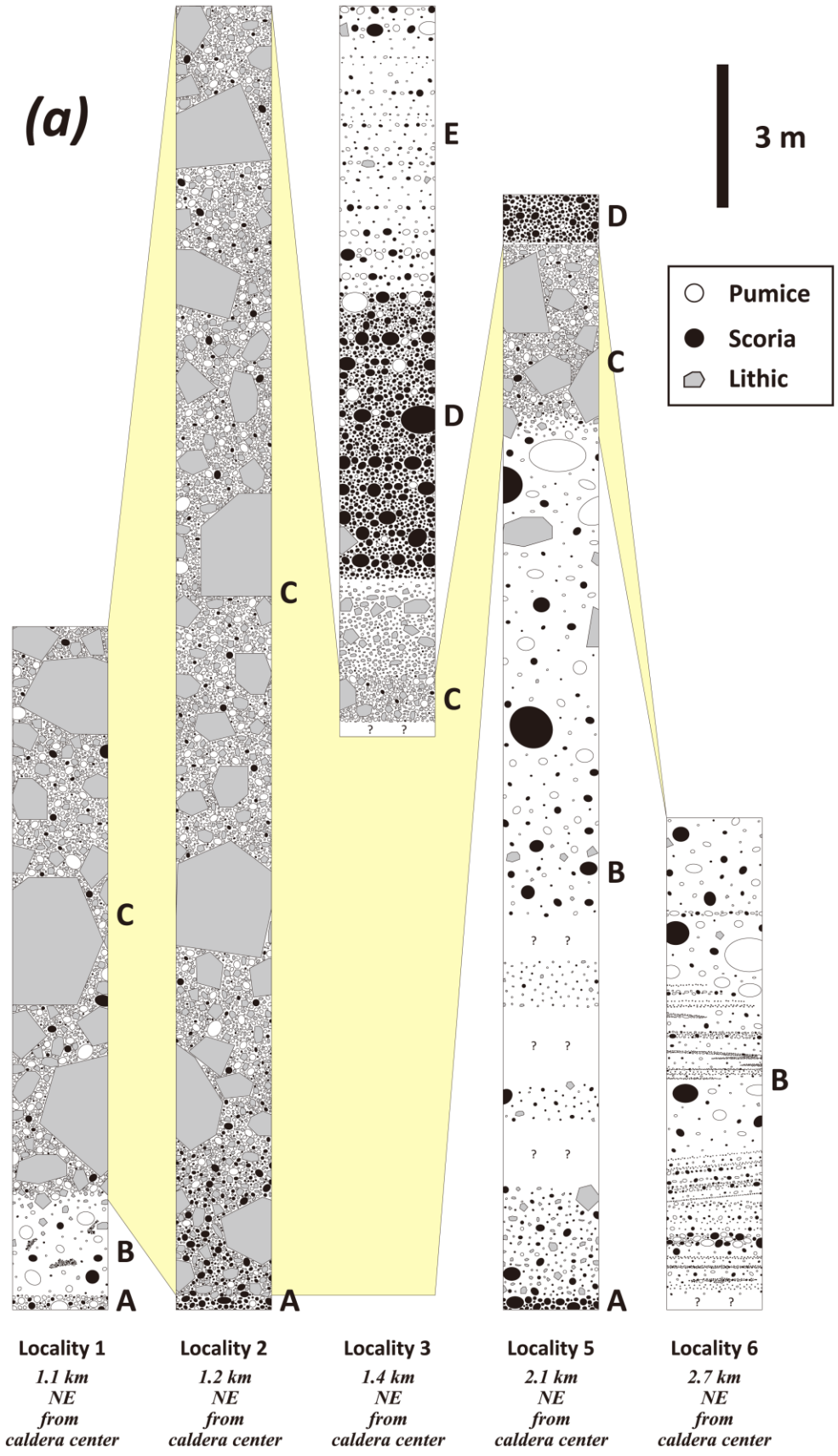
(a)
3 m
Pumice
Scoria
Lithic
E
D
C
D
C
C
B
A
B
A
A
B
Locality 1
1.1 km NE from caldera center
Locality 2
1.2 km NE from caldera center
Locality 3
1.4 km NE from caldera center
Locality 5
2.1 km NE from caldera center
Locality 6
2.7 km NE from caldera center

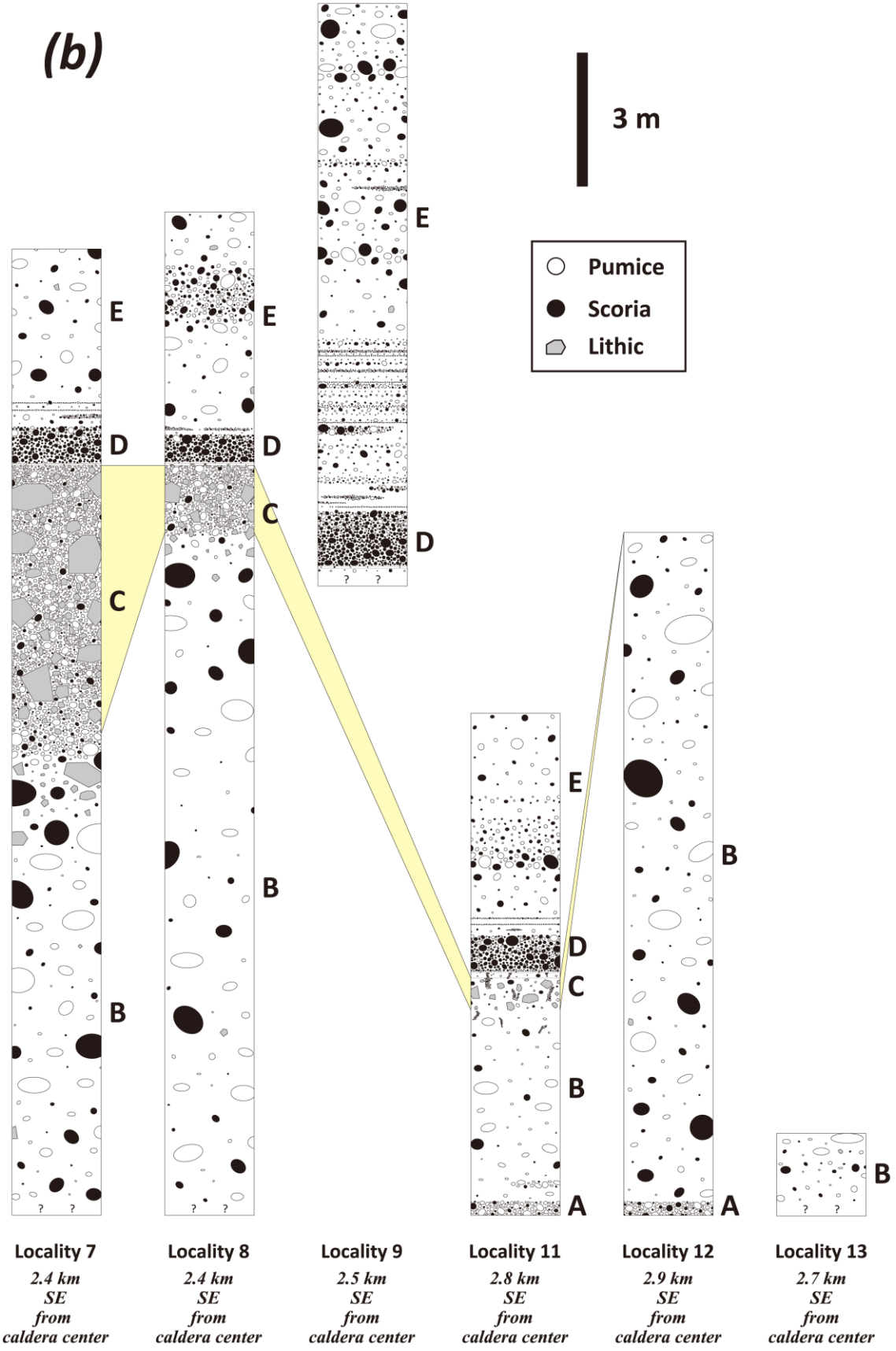
(b)
3 m
Pumice
Scoria
Lithic
E
D
C
B
A
Locality 7
2.4 km SE from caldera center
Locality 8
2.4 km SE from caldera center
Locality 9
2.5 km SE from caldera center
Locality 11
2.8 km SE from caldera center
Locality 12
2.9 km SE from caldera center
Locality 13
2.7 km SE from caldera center

scoria-rich zone appears to be separated and intercalated with pumice-rich layers throughout the fallout, and the total pumice/scoria ratio within SK-A2 increases (Figs. 4.3 and 4.6a). The degree of welding of the scoria-rich zone decreases as distance from the caldera increases. At locality 1, a sag structure caused by impact of a scoria bomb occurs at the base of SK-A2 (Fig. 4.6a), and flattened scoria clasts (spatters) are sometimes found in the pumice-rich layers (Figs. 4.6b and 4.6c). Lithic fragments are scarce throughout SK-A2 (2 vol%). The upper contact with the overlying ignimbrite (SK-B) is usually sharp.

#### 4.2.2.2. SK-B

SK-B is a >50-m-thick valley-filling ignimbrite that is non- to weakly welded and locally columnar-jointed. SK-B is partly massive and partly diffusely stratified or cross-stratified. The stratification is marked by variations in clast size and concentration. SK-B is largely composed of pumice and scoria clasts up to 70 cm in diameter supported by a gray ash matrix. Lithic fragments are generally minor (2–5 vol%), but a lithic-rich horizon locally occurs at its base (e.g. locality 5; Fig. 4.7a). Gas-segregation pipes are occasionally present. The contact between SK-B and -C are commonly planar and gradational.

#### 4.2.2.3. SK-C

SK-C is the most conspicuous and coarsest deposit in the proximal products. SK-C lithic breccia is non-welded and consists dominantly of angular to subangular, lapilli to block size lithic fragments (50–70 vol%) up to 2.6 m in diameter with subordinate pumice and scoria lapilli. The lithic breccia varies from clast-supported to matrix-supported with a fines-depleted coarse ash matrix (Fig. 4.8a). The juvenile clasts rarely exceed 20 cm in diameter. Despite the lithic breccia attains a maximum thickness of >27 m, it is unstratified and ungraded. The maximum lithic size in the lithic breccia

---

**Figure 4.7:** Stratigraphic unit correlations for the proximal units SK-B to -E. Yellow zone traces SK-C lithic breccia. The uppermost part of SK-A is only described when the boundary between SK-A and -B is visible. Question-marks indicate the areas which are obscured by talus. Note that both the maximum lithic size and the thickness of SK-C lithic breccia rapidly decrease outward from the caldera. (**a**) is for the northeast sections, and (**b**) for the southeast sections. Locations of these sections are shown in Fig. 4.1.

steadily decreases outwards from ~2 m at locality 1, 1.1 km from the caldera center, to 20 cm at locality 11, 2.8 km from the caldera center (Fig. 4.9). Although the lithic breccia thickens into topographic depressions, it thins rapidly away from the caldera (Fig. 4.7). The lithic breccia is usually overlain by a 3- to 12-cm-thick, fine to coarse, massive ash tuff, which in turn is overlain by a 2- to 5-cm-thick massive fine-ash layer. The boundaries between these three deposits are sharp.

A fines-bearing facies of SK-C lithic breccia occurs only in the furthest section in proximal regions, locality 11 (Fig. 4.8b). In this section the lithic breccia is 70 cm thick and contains gas-segregation pipes, emanating from the lithic breccia, rising through the overlying ash tuff, ending at the bottom of the fine-ash layer (Fig. 4.10). This indicates that the ash tuff was emplaced immediately after deposition of the lithic breccia during which gas was still being released from the lithic breccia, and the fine ash settled on the tuff afterwards. This fine ash may represent a co-ignimbrite ash-fall deposit, and/or it may represent elutriation of fine ash from the underlying lithic breccia deposit by the escape of fluidizing gas.

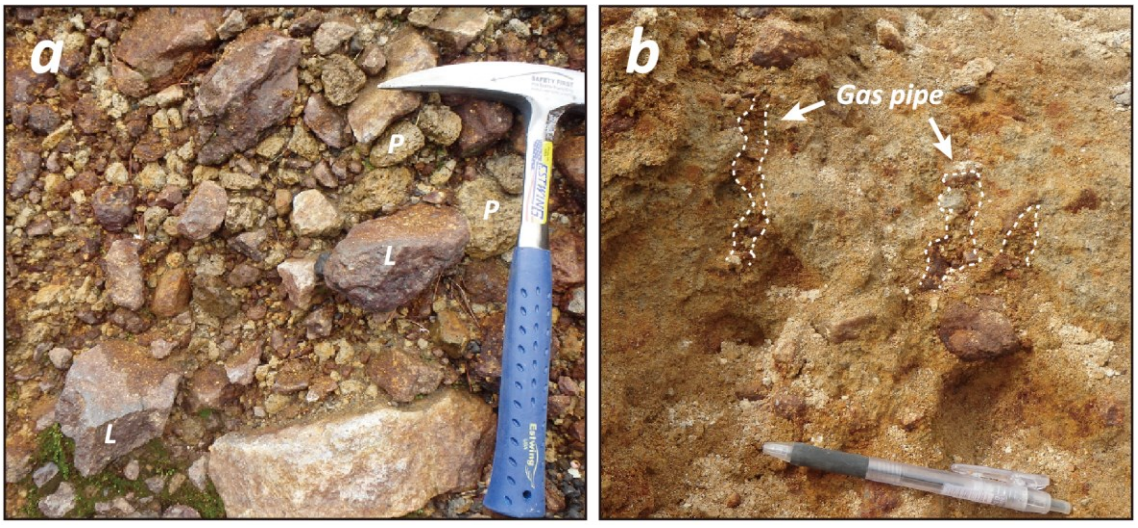


**Figure 4.8:** SK-C lithic breccia. **a** A fines-depleted, clast-supported, lithic-rich breccia at locality 2. Lithic clasts (*L*, dark reddish brown) are angular to subangular while pumice clasts (*P*, grayish yellow) are subrounded. Hammer is 33 cm long. **b** A fines-bearing, matrix-supported, lithic-rich breccia with fines-depleted pipes (gas-segregation pipes) at locality 11. Pen is 14 cm long.

Although SK-C lithic breccia superficially resembles a lithic-rich fall deposit, I interpret it a flow origin instead as the following reasons: the lithic breccia (1) lacks internal stratification even where it is >27 m thick, (2) thickens into topographic depressions, (3) contains subrounded juvenile clasts (Fig. 4.8a), (4) lacks impact structures even beneath meter-sized lithic blocks, (5) consists of abundant coarse lithic blocks significantly larger than accompanying pumice and scoria clasts, suggesting a lack of hydraulic equivalence, and (6) grades laterally outward into a fines-bearing, matrix-supported facies with gas-segregation pipes.

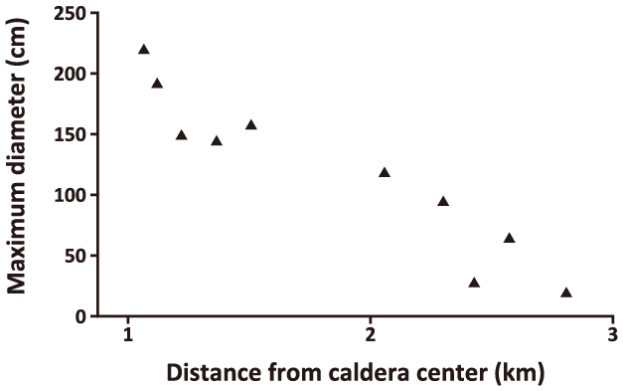


**Figure 4.9:** Average of maximum diameter of five largest lithic clasts plotted against distance from the caldera center for SK-C lithic breccia. Lithic-clast size clearly decreases away from source.

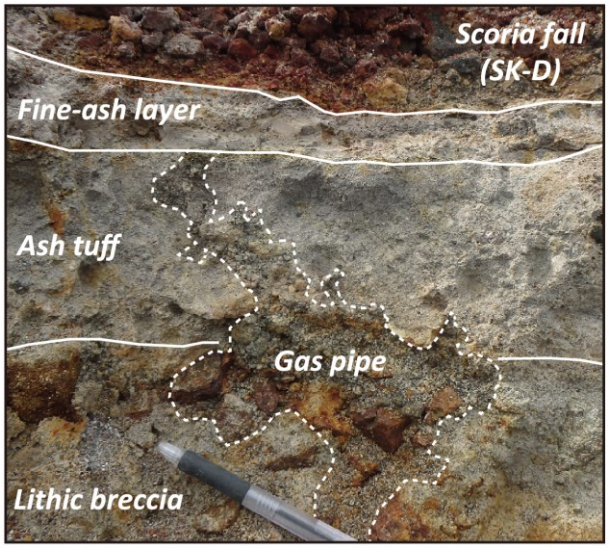


**Figure 4.10:** Boundary between SK-C lithic breccia and SK-D fallout at locality 11. The lithic breccia is overlain by an ash tuff, which in turn is overlain by a fine-ash layer. Note that the gas pipe in the lithic breccia passes up into the overlying ash tuff and terminates at the bottom of the fine-ash layer.

#### 4.2.2.4. SK-D

SK-D mantles the underlying topography, and, like SK-A fallout, its dispersal was eastward (Fig. 4.11). At the most proximal outcrop of SK-D (1.4 km from the caldera center), locality 3, it attains a maximum thickness of 6 m and overlies a 2-m-thick reworked deposit of SK-C lithic breccia, which in turn rests on the primary lithic breccia. Here SK-D is composed predominantly of scoria lapilli and blocks up to 56 cm in diameter with diffuse stratification, in which individual layers, generally 30–50 cm thick, exhibit inverse grading. Bread-crusted bombs are present in SK-D. Downwind distally, SK-D has an average thickness of 1 m (Fig. 4.11) and is a non-welded, massive scoria-lapilli fallout. Although being minor at the bottom of SK-D, the proportion of pumice fragments gradually increases in the middle and sharply increases at the top. Lithic fragments are scarce (2 vol%). The upper contact with the ignimbrite (SK-E) is generally distinct.

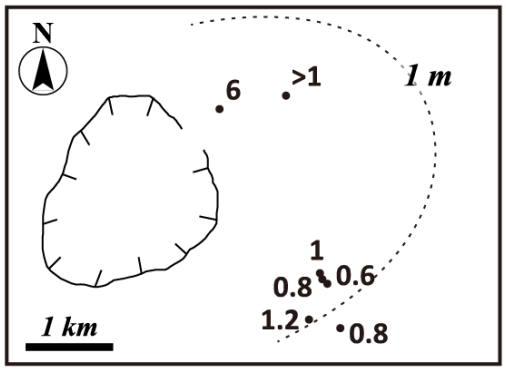


**Figure 4.11:** Isopach map of SK-D fallout (thicknesses in meters). > indicates that the top of the fallout is unpreserved.

#### 4.2.2.5. SK-E

SK-E is a non- to weakly welded, locally columnar-jointed, massive to stratified, poorly sorted, ignimbrite. SK-E is generally 5–15 m thick and commonly present at the surface of the northeast and southeast of the Ohachidaira caldera. Although superficially similar in appearance to SK-B, two key differences between SK-B and -E preclude a correlation: (1) SK-B contains significant amount of plutonic lithic fragments whereas SK-E contains a few (see section 4.4.3); (2) bread-crusted bombs are abundant in SK-E, but they are rarely observed in SK-B. At locality 3, SK-E and the uppermost part of SK-D are comparable in terms of the ratio of pumice to scoria, lithic component, and the presence of bread-crusted bombs, suggesting continuous deposition from SK-D to -E.

## 4.3. Correlation between the distal and proximal products of the Sounkyo eruption

Although the distal products (the pumice-fall deposit and Px-type ignimbrite) and proximal products (SK-A to -E) are separated in space as there exists no information about the medial products due to difficulties in access, I deduce that the distal and proximal products were generated in the same eruption for two reasons. First, paleomagnetic data suggests that the proximal units SK-A to -E were emplaced contemporaneously with the Px-type ignimbrite (see Chapter 3 for detail). Second, the whole-rock chemical composition of juvenile clasts from the proximal ignimbrite units SK-B and -E are similar with those from the Px-type ignimbrite, as described below.

### 4.3.1. Distal pumice-fall deposit

The distal pumice-fall deposit is interpreted to be a lateral counterpart of SK-A, since (1) SK-A is the only fall deposit observed in proximal regions that has significant thickness and coarseness to correlate with the distal pumice-fall deposit, (2) both of the distal pumice-fall deposit and SK-A are composed of a lower, thin-bedded part and an upper, thick, coarser-grained, diffusely stratified part, and (3) although the upper part of the distal pumice-fall deposit contains less scoria in the juvenile fraction than the upper part of SK-A (A2), a total pumice/scoria ratio within SK-A2 increases distally even within the proximal area so that consistency is maintained (Fig. 4.3).

### 4.3.2. Px-type ignimbrite

Possible candidates for the proximal equivalent of the Px-type ignimbrite are the three flow-origin units: SK-B ignimbrite, SK-C lithic breccia, and SK-E ignimbrite. In order to correlate between the Px-type ignimbrite and the three proximal units, whole-rock chemical analysis was carried out on fifty-five scoria and pumice samples. Fifteen samples of the Px-type ignimbrite were taken from the lower to middle levels of

it. Twenty-one samples of SK-B, eleven of SK-C, and eight of SK-E were taken from the bottom to the top of each unit.

Whole rock major- and trace-element compositions were determined with a Rigaku ZSX Primus II X-ray fluorescence spectrometer at Kobe University, using the glass bead method. Scoria and pumice samples were crushed in a Fritsch tungsten carbide swing mill. One point eight grams of the powdered sample was mixed with 3.6 g of Johnson Matthey Spectroflux 100B (lithium metaborate and lithium tetraborate, 80:20 w/w%) and fused in a platinum crucible for 7 minutes at 1200 °C, producing a homogeneous glass bead 35 mm in diameter. Representative compositions are shown in Table 4.1.

Scoria samples are basaltic andesite to andesite, with 55.8–59.3 wt% $SiO_2$, whereas pumice samples are dacite, with 64.0–67.2 wt% $SiO_2$ (Fig. 4.12). Most of the major element compositions of scoria and pumice samples cluster together, but those of SK-C lithic breccia tend to have lower CaO than those of the Px-type ignimbrite. In addition to this, scoria samples of SK-C lithic breccia are generally depleted in Sr and enriched in Ba relative to those of the Px-type ignimbrite, indicating that the Px-type ignimbrite does not correlate with SK-C lithic breccia. The compositional affinity between the Px-type and SK-B ignimbrites, together with their stratigraphic position with respect to the initial fallout, confirms their correlation. The Px-type ignimbrite is composed of two cooling units at Kyokanheki, which implies depositional hiatus between them. It is possible that the two cooling units are the distal equivalent of SK-B and -E ignimbrites, respectively.

Although there is still a possibility that the upper level of the Px-type ignimbrite is the distal equivalent of SK-C lithic breccia, it is conceivable that SK-C PDCs hardly traveled down to the foot of the Taisetsu volcano group to accumulate the Px-type ignimbrite for the following reasons. First, SK-C lithic breccia grades from a clast- to matrix-supported, fines-depleted facies into a matrix-supported, fines-bearing facies at the farthest section (locality 11). The abundance of lithic component, however, remains almost constant with distance from source. It implies that the lithic breccia was formed from lithic-rich PDCs fed by an extremely lithic-rich pyroclastic fountain, which seem to have low mobility. Second, the lithic breccia becomes thinner and less coarse and

finally disappears within 3 km from the caldera center, suggesting that the capacity (Hiscott, 1994) of SK-C PDCs sharply decreased even within the proximal area.

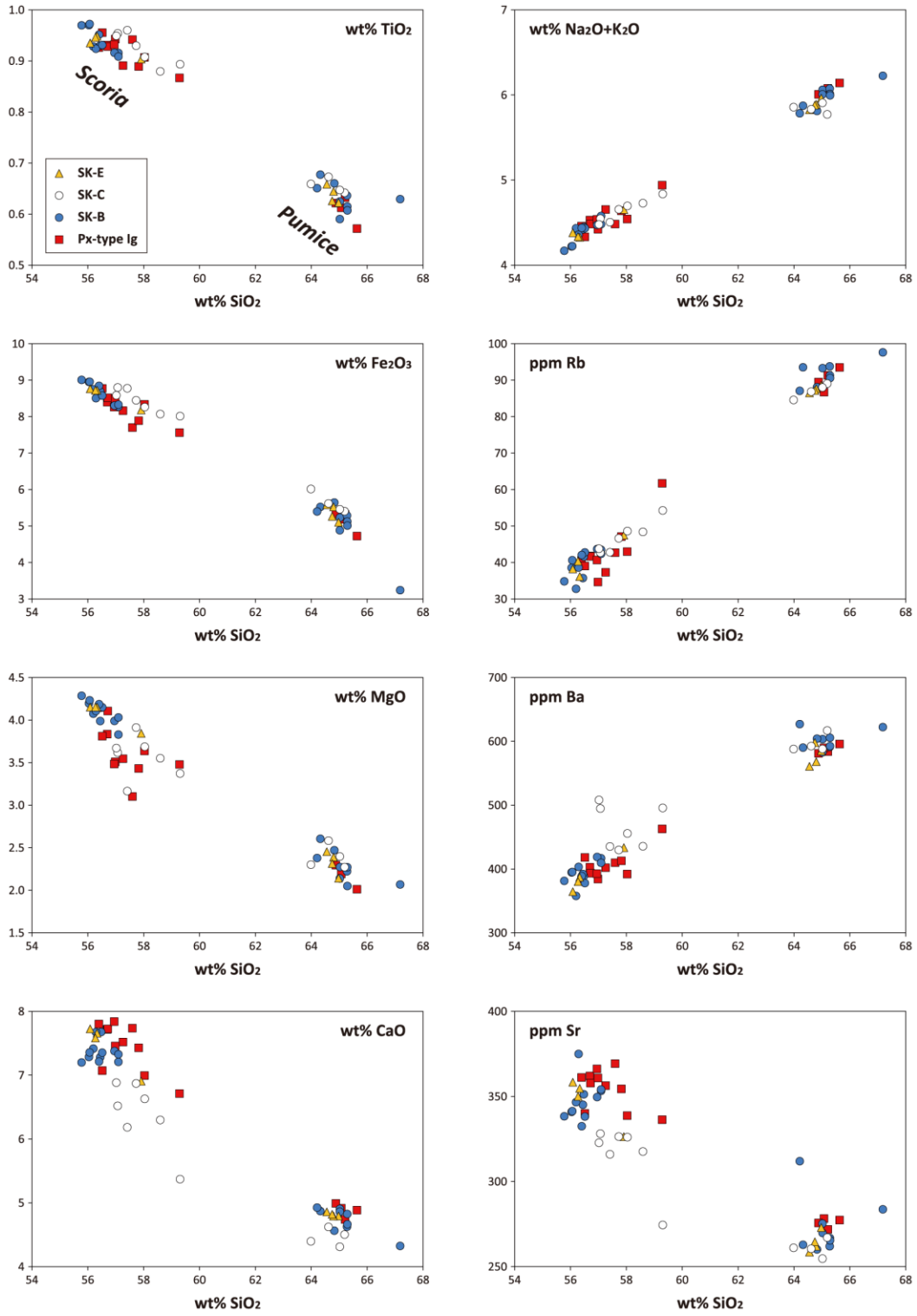


**Figure 4.12:** Selected whole-rock variation diagrams for the pumice and scoria components.

**Table 4.1:** Whole rock major- and trace-element compositions of representative samples from the Sounkyo eruption products.

| | Scoria | | | | | | | | | | | |
|---|---|---|---|---|---|---|---|---|---|---|---|---|
| | Px-type Ig | Px-type Ig | Px-type Ig | SK-B | SK-B | SK-B | SK-C | SK-C | SK-C | SK-E | SK-E | SK-E |
| | 052 | 059 | 060 | 027 | 037 | 050 | 008 | 010 | 020 | 102 | 104 | 107 |
| *Major elements (wt%)* | | | | | | | | | | | | |
| $SiO_2$ | 56.06 | 57.18 | 55.74 | 54.51 | 56.54 | 55.58 | 58.00 | 56.28 | 56.10 | 55.82 | 56.16 | 57.42 |
| $TiO_2$ | 0.92 | 0.89 | 0.87 | 0.95 | 0.90 | 0.92 | 0.87 | 0.94 | 0.93 | 0.93 | 0.95 | 0.90 |
| $Al_2O_3$ | 17.25 | 17.08 | 17.19 | 17.82 | 17.24 | 17.42 | 17.51 | 17.91 | 17.80 | 17.55 | 17.49 | 17.14 |
| $Fe_2O_3$ | 8.55 | 8.21 | 7.95 | 8.80 | 8.25 | 8.43 | 7.84 | 8.68 | 8.45 | 8.72 | 8.69 | 8.11 |
| MnO | 0.16 | 0.15 | 0.15 | 0.18 | 0.15 | 0.16 | 0.14 | 0.15 | 0.15 | 0.16 | 0.16 | 0.15 |
| MgO | 4.12 | 3.58 | 3.45 | 4.19 | 3.99 | 4.08 | 3.30 | 3.57 | 3.61 | 4.13 | 4.14 | 3.81 |
| CaO | 7.75 | 6.89 | 7.32 | 7.04 | 7.26 | 7.23 | 5.25 | 6.43 | 6.77 | 7.69 | 7.63 | 6.85 |
| $Na_2O$ | 3.09 | 3.07 | 3.17 | 2.97 | 3.10 | 3.01 | 2.98 | 3.04 | 2.99 | 3.15 | 3.16 | 3.08 |
| $K_2O$ | 1.34 | 1.40 | 1.36 | 1.11 | 1.43 | 1.35 | 1.75 | 1.44 | 1.41 | 1.21 | 1.16 | 1.53 |
| $P_2O_5$ | 0.17 | 0.06 | 0.16 | 0.17 | 0.17 | 0.17 | 0.17 | 0.18 | 0.17 | 0.17 | 0.17 | 0.17 |
| Total | 99.41 | 98.53 | 97.34 | 97.73 | 99.03 | 98.34 | 97.80 | 98.61 | 98.38 | 99.54 | 99.71 | 99.16 |
| *Trace elements (ppm)* | | | | | | | | | | | | |
| Cr | 15 | 13 | 13 | 15 | 15 | 14 | 15 | 15 | 14 | 13 | 14 | 14 |
| Co | 27 | 21 | 22 | 23 | 27 | 24 | 24 | 21 | 24 | 26 | 25 | 24 |
| Ni | 1 | 3 | 4 | 7 | 4 | 4 | 8 | 3 | 4 | 3 | 1 | 4 |
| Cu | 14 | 21 | 25 | 5 | 5 | 15 | 5 | 12 | 7 | 17 | 15 | 11 |
| Zn | 80 | 84 | 82 | 91 | 75 | 79 | 74 | 80 | 82 | 81 | 85 | 77 |
| Rb | 40 | 42 | 36 | 34 | 43 | 42 | 53 | 42 | 43 | 38 | 36 | 47 |
| Sr | 359 | 334 | 347 | 331 | 351 | 333 | 268 | 324 | 318 | 357 | 354 | 324 |
| Y | 25 | 20 | 22 | 23 | 24 | 23 | 23 | 23 | 24 | 23 | 24 | 24 |
| Zr | 111 | 112 | 110 | 111 | 115 | 114 | 117 | 123 | 115 | 111 | 114 | 116 |
| Nb | 4 | 4 | 4 | 4 | 4 | 4 | 5 | 5 | 4 | 5 | 4 | 4 |
| Pb | 8 | 9 | 12 | 7 | 9 | 7 | 6 | 9 | 5 | 9 | 6 | 6 |
| Ba | 381 | 386 | 391 | 373 | 406 | 372 | 485 | 488 | 500 | 363 | 386 | 430 |

| | Pumice | | | | | | | | | | | |
|---|---|---|---|---|---|---|---|---|---|---|---|---|
| | Px-type Ig | Px-type Ig | Px-type Ig | SK-B | SK-B | SK-B | SK-C | SK-C | SK-C | SK-E | SK-E | SK-E |
| | 057 | 063 | 067 | 032 | 048 | 049 | 015 | 017 | 019 | 001 | 101 | 103 |
| *Major elements (wt%)* | | | | | | | | | | | | |
| $SiO_2$ | 63.65 | 64.64 | 63.17 | 62.82 | 63.74 | 63.64 | 63.90 | 63.73 | 63.42 | 63.56 | 63.92 | 63.32 |
| $TiO_2$ | 0.62 | 0.61 | 0.61 | 0.66 | 0.58 | 0.59 | 0.63 | 0.63 | 0.66 | 0.61 | 0.65 | 0.63 |
| $Al_2O_3$ | 15.15 | 15.66 | 15.23 | 15.50 | 15.95 | 15.74 | 15.69 | 15.73 | 15.54 | 15.82 | 15.66 | 15.36 |
| $Fe_2O_3$ | 5.19 | 5.15 | 5.19 | 5.39 | 4.79 | 4.88 | 5.30 | 5.35 | 5.52 | 4.99 | 5.53 | 5.40 |
| MnO | 0.11 | 0.11 | 0.11 | 0.12 | 0.10 | 0.10 | 0.11 | 0.11 | 0.12 | 0.10 | 0.11 | 0.11 |
| MgO | 2.21 | 2.18 | 2.23 | 2.54 | 2.10 | 2.00 | 2.23 | 2.35 | 2.53 | 2.09 | 2.43 | 2.33 |
| CaO | 4.63 | 4.88 | 4.86 | 4.76 | 4.77 | 4.55 | 4.41 | 4.23 | 4.54 | 4.69 | 4.81 | 4.68 |
| $Na_2O$ | 3.24 | 3.36 | 3.22 | 2.95 | 3.33 | 3.23 | 3.01 | 3.03 | 3.13 | 3.29 | 3.17 | 3.20 |
| $K_2O$ | 2.69 | 2.63 | 2.63 | 2.79 | 2.56 | 2.62 | 2.65 | 2.76 | 2.59 | 2.54 | 2.60 | 2.56 |
| $P_2O_5$ | 0.12 | 0.12 | 0.13 | 0.14 | 0.12 | 0.12 | 0.09 | 0.09 | 0.10 | 0.12 | 0.13 | 0.13 |
| Total | 97.61 | 99.34 | 97.37 | 97.67 | 98.03 | 97.47 | 98.02 | 98.02 | 98.14 | 97.82 | 99.02 | 97.73 |
| *Trace elements (ppm)* | | | | | | | | | | | | |
| Cr | 16 | 17 | 16 | 15 | 14 | 14 | 15 | 16 | 17 | 15 | 18 | 18 |
| Co | 15 | 13 | 12 | 16 | 12 | 12 | 14 | 12 | 15 | 13 | 13 | 13 |
| Ni | 6 | 7 | 6 | 8 | 7 | 6 | 5 | 7 | 7 | 7 | 6 | 6 |
| Cu | 6 | 9 | 7 | 11 | 8 | 12 | 4 | 3 | 4 | 13 | 14 | 14 |
| Zn | 57 | 53 | 54 | 51 | 50 | 50 | 54 | 55 | 58 | 46 | 53 | 53 |
| Rb | 89 | 86 | 87 | 91 | 86 | 88 | 87 | 86 | 85 | 87 | 86 | 86 |
| Sr | 265 | 276 | 268 | 257 | 270 | 259 | 262 | 250 | 256 | 267 | 256 | 256 |
| Y | 21 | 21 | 22 | 24 | 21 | 21 | 20 | 20 | 20 | 21 | 22 | 22 |
| Zr | 134 | 136 | 129 | 141 | 137 | 146 | 133 | 133 | 142 | 130 | 131 | 131 |
| Nb | 5 | 5 | 5 | 6 | 5 | 6 | 5 | 6 | 5 | 4 | 5 | 5 |
| Pb | 11 | 12 | 11 | 13 | 10 | 10 | 6 | 5 | 6 | 11 | 11 | 11 |
| Ba | 570 | 586 | 566 | 576 | 571 | 577 | 605 | 576 | 581 | 572 | 555 | 555 |

## 4.4. Lithic component analysis

Lithic fragments ejected during an eruption are generated by erosion and failure of walls of the conduit and magma chamber, as well as by major wall slumping and explosive excavation along the slipping caldera faults accompanying caldera collapse (Lipman, 1976; Varekamp, 1993; Macedonio et al., 1994; Rosi et al., 1996; Valentine and Groves, 1996; Kokelaar, 2007; Del Gaudio and Ventura, 2008). Thus, the variations in lithic concentration and lithic types up through the stratigraphy can reflect the evolution of the conduit and vent during the eruption, along with the timing and dynamics of caldera formation (Suzuki-Kamata et al., 1993; Brown and Branney, 2004; Browne and Gardner, 2004; Pittari et al., 2008; Druitt, 2014; Simmons et al., 2016; Edgar et al., 2017).

### 4.4.1. Method

Lithic component analysis was conducted for the proximal products of the Sounkyo eruption at eight localities (16 horizons). Lithic clasts in SK-A were collected at three horizons, in SK-B at six, in SK-C at five, in SK-D at one, and in SK-E at one. I collected lithic fragments larger than 2 cm (most of them are block-sized) and classified them into three types in the field: (1) volcanic rocks; (2) sedimentary rocks; (3) plutonic rocks. I collected ~150 lithic clasts from each horizon in SK-C, but ~50 lithic clasts from each horizon in other units on account of the scarceness of lithic clasts in all units but SK-C.

### 4.4.2. Lithic clast types and their provenance

Even though lithic fragments in pyroclastic deposits include vent-derived accessory ones and substrate-derived accidental ones, those in the proximal products of the Sounkyo eruption are interpreted to be essentially vent-derived. This is because (1) the basement rocks that formed before the Sounkyo eruption are not exposed on the slopes between the caldera rim and the outcrops where I collected the lithic samples,

and (2) the flow-origin units SK-B, -C, and -E always overlie the initial fallout (SK-A) and never directly overlie the basement in the studied area.

The volcanic lithic fragments are the dominant lithic type (Fig. 4.13) and consist mostly of lava clasts, along with a low content of volcanic breccia blocks and welded tuff clasts. The lava clasts consist predominantly of variably altered andesites with subordinate dacites. The volcanic breccia blocks consist of angular fragments of andesitic lavas scattered in a light gray to yellowish brown, coarse ash matrix. All lava lithic types exist in the caldera walls, and the volcanic breccia blocks are similar in appearance to the pyroclastics exposed in the caldera walls. The welded tuff clasts occur especially in SK-D and -E, and are dominated by fragments that closely resemble ignimbrites of the Sounkyo eruption compared to the ~1–2 Ma rhyolitic basement ignimbrites. The welded tuff clasts in SK-D and -E could have been recycled from SK-B welded vent fill. The volcanic lithic fragments are therefore considered to be shallow-origin, eroded from the uppermost level of the conduit and vent, as deep as 900 m below the caldera floor where the boundary between the Neogene volcanic rocks and the Hidaka Supergroup may be situated (see Chapter 2).

The sedimentary lithic fragments are always subordinate in abundance (Fig. 4.13) and include sandstones, mudstones, and cherts. They were essentially derived from the Hidaka Supergroup. Although the base of the Supergroup is not exposed in the study area, two lines of evidence imply that it has a few km thick: (1) the Supergroup is >1500 m thick in a drill hole on the northeast slope of the Taisetsu volcano group (NEDO, 1989); (2) the total thickness of the Supergroup is ~3400 m in Tomuraushi region (Watanabe and Iwata, 1987) situated in the southern side of the Taisetsu volcano group. The sedimentary lithic fragments are thus inferred to originate at mid-depth, deeper than 900 m from the caldera floor.

The plutonic lithic fragments are significantly variable in abundance up through the proximal products (Fig. 4.13) and are fine-grained granodiorites. They are often coated with scoria and rarely with banded pumice, suggesting that they were incorporated in magma below the magma fragmentation level. The lithic granodiorite probably formed the deepest part of the conduit walls.

### 4.4.3. Result

Throughout the eruption, the volcanic rocks are the major lithic type while the sedimentary rocks are always scarce (Fig. 4.13). No lateral variation of lithic clast populations between the localities northeast and southeast of the Ohachidaira caldera was observed, whereas there is a vertical variation due to the abundance of the plutonic rocks (Fig. 4.13). During the eruption of SK-A and the lower part of SK-B, the lithic fragments consist predominantly of the volcanic rocks (98–100%) with the minor sedimentary (0–2%) and plutonic rocks (0–2%). From the lower to middle and upper parts of SK-B, there is an increase in the plutonic rocks (from 2% to 24–50%) at the expense of the volcanic rocks (from 98% to 50–74%). Into SK-C, the lithic component is dominated again by the volcanic rocks (92–99%) with the few plutonic rocks (1–3%). SK-D and -E are rich in volcanic rocks (90–96%), while containing the few sedimentary (0–7%) and plutonic rocks (3–4%).

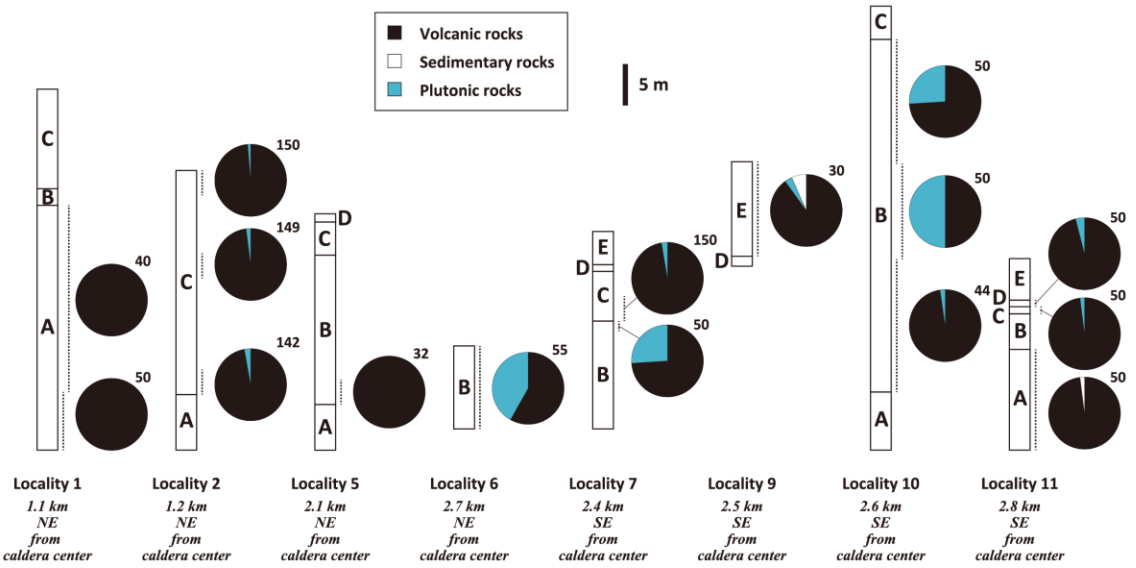


**Figure 4.13:** Pie diagrams of proportions of lithic-type for the proximal products of the Sounkyo eruption (SK-A to -E). Vertical dotted lines beside columns show the height where lithic clasts were collected for analysis. The number of lithic clasts collected in each horizon is shown in the upper right of each pie diagram. Locations of these sections are shown in Fig. 4.1.

## 4.5. Discussion

### 4.5.1. Nature of the initial fallout phase

The main upper part of the initial fallout (SK-A2 and the upper part of the distal pumice-fall deposit) shows the considerable vertical and lateral variations in juvenile component. In caldera rim exposures, the lower part of SK-A2 is very scoria-rich while the upper part of it is pumice-rich. Farther downwind, SK-A2 comprises scoria-rich layers intercalated with relatively pumice-rich layers (e.g. locality 1; Fig. 4.6a). More distally, SK-A2 becomes strongly enriched in pumice at locality 11 as well as at the distal outcrops (Fig. 4.3). Several lines of evidence suggest ballistic emplacement of scoria fragments during the eruption of SK-A2, explaining these complex variations: (1) the total thickness and the degree of welding of the scoria-rich layers are greatest at the caldera rim and decrease rapidly away from the source; (2) the scoria bomb with impact sag occurs at the base of SK-A2 (Fig. 4.6a); and (3) flattened scoria clasts (spatters) are sometimes found even within the pumice-rich layers (Figs. 4.6b and 4.6c). The majority of scoria fragments in SK-A2 probably represent the low-fountaining component of the eruption column through which pumice fragments were transported to higher levels. This may be caused by density segregation between the denser scoria and lighter pumice clasts—the scoria clasts have an average density of 1.3 g/cm$^3$ while that of the pumice clasts is 0.8 g/cm$^3$; and/or by the preferential positioning of more mafic magma toward conduit walls (Fierstein et al., 1997). The pumice-rich part of the eruption column would have played a critical role in accumulating the main upper part of the initial fallout, and hence the total volume of it would be largely dominated by the pumice component.

### 4.5.2. Eruptive characteristics

#### 4.5.2.1. Tephra volume

In order to investigate the role of caldera collapse and vent widening in the formation of the Ohachidaira caldera, the magma and lithic volumes of the Sounkyo

eruption products were calculated (Table 4.2).

The proximal volume of SK-A (and the distal pumice-fall deposit) was calculated following Pyle (1989) modified by Fierstein and Nathenson (1992). The best fit line on the log of thickness vs. square root of area diagram lies significantly below the plot on the most proximal side (Fig. 4.4), and therefore the extrapolated maximum thickness (To = 46.986 [m]) is thinner than the maximum thickness observed in the field. Note that the estimated thicknesses of plots at the most proximal sites include the scoria-rich layers which may have been transported in different paths than the pumice fragments being responsible for most of the volume of the fallout. This can lead to an overestimation of the thickness of SK-A at the most proximal sites. Due to lack of outcrops farther than ~11 km from the caldera, I applied Eq. 18 of Fierstein and Nathenson (1992) combined with the method of Sulpizio (2005) to estimate the distal volume of the deposit. The total bulk volume of SK-A is then 0.97 $km^3$. This is consistent with the method of Bonadonna and Costa (2012), which calculates the total bulk volume of 1.01 $km^3$.

**Table 4.2:** Volume considerations for the Sounkyo eruption products.

| | Bulk volume ($km^3$) | Lithic* content (vol%) | Lithic volume ($km^3$) | DRE volume ($km^3$) |
|---|---|---|---|---|
| SK-E | 0.03 | 2 | - | 0.02 |
| SK-D | 0.03 | 2 | - | 0.01 |
| SK-C | 0.05 | 60 | 0.03 | 0.01 |
| SK-B | 0.12 | 3.5 | - | 0.07 |
| SK-A | 0.97 | 2 | 0.02 | 0.30 |
| Px-type Ig | 6.39 | 3.5 | 0.22 | 4.69 |
| Total | 7.59 | | 0.28 | 5.10 |

* Lithic content is the mean content of lithic fragments in each unit. Lithic contents in the deposits were semi-quantitatively estimated by comparing, at outcrops, a color index and lithic clasts dispersed in an ash matrix, and the finer (less than a few mm) lithic fragments comprising the ash matrix were ignored. Therefore our estimates of lithic contents will be a minimum.

Because of the scarcity of isopachs of SK-D (Fig. 4.11), I applied the method of Legros (2000) to calculate the minimum volume of SK-D. This method allows calculation of the minimum volume when only one isopach is available. The minimum bulk volume of SK-D is then 0.03 $km^3$.

The present-day volume of the Px-type ignimbrite is estimated in the same way as the Hb-type ignimbrite (see Chapter 3), yielding 3.02 $km^3$. The Px-type ignimbrite is exposed along the river valleys (e.g. the Ishikari River) and has been significantly eroded by the rivers. If I assume that the eroded ignimbrite has had the thickness as much as the thickness of the ignimbrite exposed on the banks of the rivers, the total volume eroded by the rivers is estimated to be 3.37 $km^3$, yielding 6.39 $km^3$ for the total bulk volume of the Px-type ignimbrite.

Bulk volumes of SK-B, -C, and -E were estimated by multiplying the area of distribution by the half of the maximum thickness, yielding 0.12 $km^3$, 0.05 $km^3$, and 0.03 $km^3$, respectively.

Lithic volumes contained in the deposits were calculated with the bulk volume and the mean lithic content, yielding the total lithic volume of 0.28 $km^3$ for the Sounkyo eruption products.

Magma (dense rock equivalent, DRE) volumes were calculated by subtracting the lithic volumes from the deposits and assuming a magma density of 2.5 $g/cm^3$ and an average density of 0.8 $g/cm^3$ for pumice-dominated fallouts (SK-A and the distal pumice-fall deposit), 1.3 $g/cm^3$ for scoria-dominated fallouts (SK-D), 1.5 $g/cm^3$ for non- to weakly welded ignimbrite and breccia units (SK-B, -C, and -E), and 1.9 $g/cm^3$ for moderately to intensely welded ignimbrites (the Px-type ignimbrite). The total magma volume of the Sounkyo eruption products is estimated to be 5.10 $km^3$.

#### 4.5.2.2. Column height and classification of the fallout phases

Eruption column height was calculated for the two fallout units, SK-A2 and -D, following the method of Carey and Sparks (1986). The maximum downwind and crosswind ranges for the lithic isopleth of clast size 6 cm in diameter were plotted on the Carey and Sparks (1986) diagram for 6.4 cm diameter clasts, yielding column heights of 25 km and 16 km, and wind speeds of 30 m/s and 10 m/s, during the eruption

of SK-A2 and -D, respectively (Figs. 4.14 and 4.15). The eruptive style was determined following the classification scheme of Pyle (1989), using the thickness half-distance ($b_t$) vs. the half-distance ratio ($b_c/b_t$), where $b_c$ is the maximum clast size half-distance. From the isopach and isopleth maps, SK-A2 fallout has $b_t$ of 1.97 km and $b_c$ of 3.03 km. These values suggest an eruptive style between subplinian and plinian eruptions, with a column height of 29 km assuming no wind (Fig. 4.16). This contrasts with the column height of 25 km calculated by the method of Carey and Sparks (1986). Pyle (1989) noticed that maximum clast dispersal is increased by a crosswind relative to the still air case. The strong wind speed during the eruption of SK-A2 (30 m/s) may lead to an overestimation of the column height.

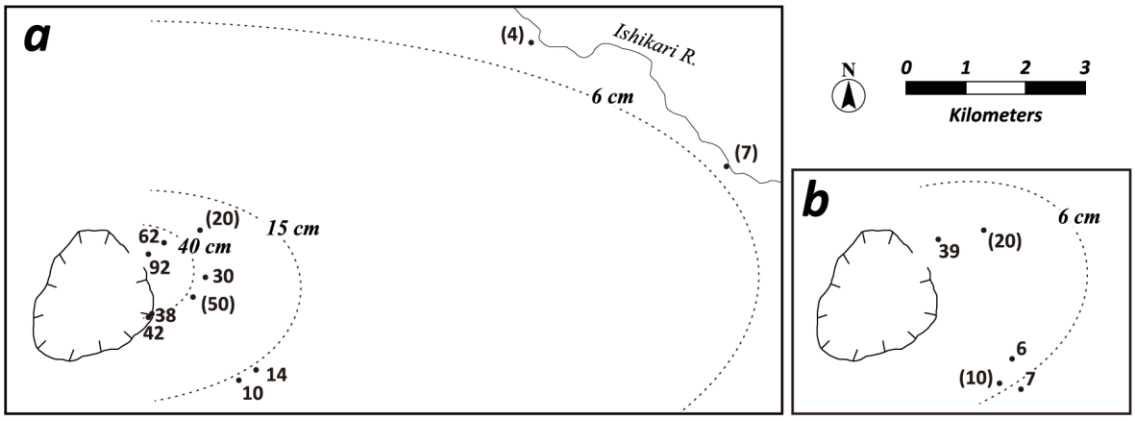


**Figure 4.14:** Lithic isopleth maps of SK-A2 (**a**) and SK-D (**b**). Data are averages of the five largest lithic clasts at each locality, except for numbers in parentheses that are the size of the largest lithic fragment.

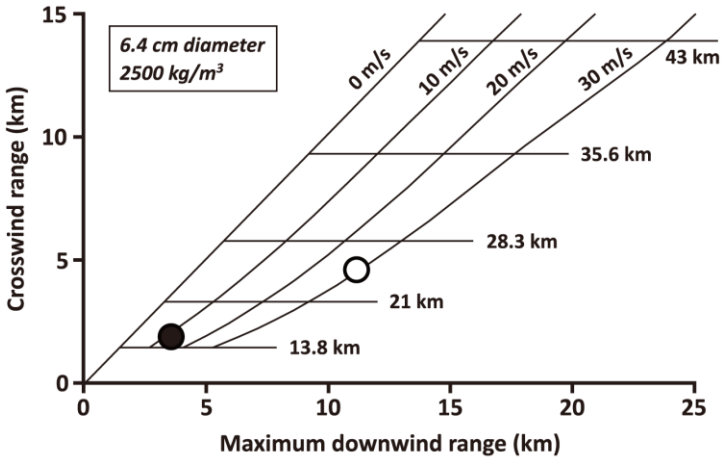


**Figure 4.15:** Crosswind range vs. downwind range for 6.4 cm diameter clasts with a density of 2500 kg/m$^3$ (modified after Carey and Sparks, 1986). Data from SK-A2 (open circle) and SK-D (solid circle) fallouts are plotted.

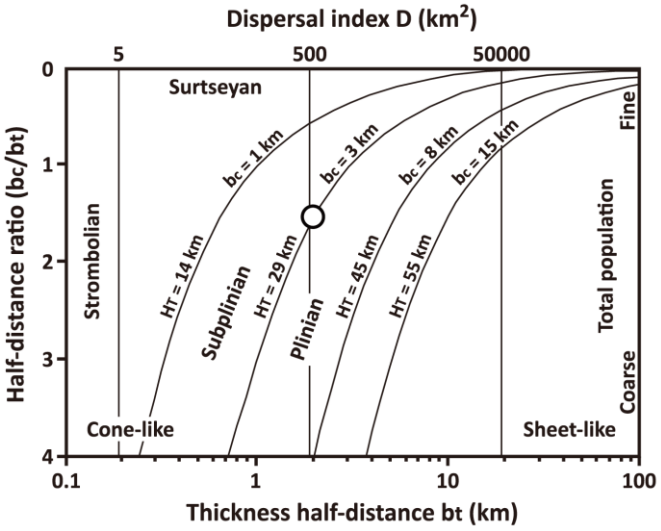


**Figure 4.16:** Classification scheme for fallouts in half-distance ratio ($b_c/b_t$) vs. thickness half-distance ($b_t$) diagram, where $b_c$ is the maximum clast size half-distance (modified after Pyle, 1989). $H_T$ is the maximum column height for eruptions into still air. Data from SK-A2 fallout (open circle) is plotted.

### 4.5.3. Caldera collapse vs. vent widening

Small calderas can be formed by collapse of the roof of a magma chamber due to magma withdrawal, "caldera collapse" (e.g. Pinatubo, Scott et al., 1996, Ceboruco, Gardner and Tait, 2000; Browne and Gardner, 2004, Ksudach, Braitseva et al., 1996; Andrews et al., 2007) or by enlargement of a vent as a result of explosive erosion and failure of the shallow part of conduit walls, "vent widening" (e.g. Nigorikawa, Ando, 1983; Kurozumi and Doi, 2003). The volume of the resulting caldera would be expected to be comparable to that of magma ejected in the former case, or that of lithic fragments ejected in the latter case. A good example of such a relationship is provided by the 1912 Novarupta-Katmai eruption in Alaska, where a ~13 $km^3$ of magma and a ~0.3 $km^3$ of lithic fragments were released from Novarupta 10 km west of Mount Katmai, beneath which the 1912 reservoir actually existed (Hildreth and Fierstein, 2012). This eruption resulted in the formation of a 5.0–5.5 $km^3$ depression on Mount Katmai by caldera collapse and a ~0.2 $km^3$ crater at Novarupta by vent widening (Hildreth and Fierstein, 2012). The volume of the Ohachidaira caldera (0.35 $km^3$) is comparable to that of lithic fragments ejected during the Sounkyo eruption (0.28 $km^3$) and is an order of magnitude less than that of magma ejected (5.10 $km^3$), suggesting that the Ohachidaira caldera was formed mainly by vent widening rather than by caldera collapse. The dominance of the shallow-origin volcanic rocks in the lithic fraction throughout the Sounkyo eruption (Fig. 4.13) supports a flaring funnel-shaped vent developed during the eruption.

The tephra beds of the Mamiyadake Scoria Member exposed in the caldera walls, which was the latest products formed before the Sounkyo eruption, typically dip outward from the caldera, although at some outcrops, they dip inward (Fig. 3.5). This may indicate that the vent had already been enlarged to some extent as the Mamiyadake Scoria Member was formed (see Chapter 3 for more detail), which means that the actual topographic lost volume during the Sounkyo eruption is less than the present-day caldera volume.

### 4.5.4. The origin of lithic breccias associated with caldera-forming eruptions

Coarse lithic-rich breccias in caldera-forming eruption sequences are commonly inferred to mark the timing of caldera collapse (Druitt and Sparks, 1984; Druitt, 1985; Walker, 1985; Druitt and Bacon, 1986; Rosi et al., 1996; Beresford and Cole, 2000; Edgar et al., 2002; Brown and Branney, 2004; Allen, 2005; Palladino and Simei, 2005; Bear et al., 2009; Druitt, 2014; Simmons et al., 2016, 2017ab; Edgar et al., 2017). Caldera collapse may be accompanied by the activation of multiple vents and conduit enlargement along with the subsidence of caldera blocks, which seems to promote the generation of lithic fragments and in turn produce lithic breccias. This idea is so palatable to field geologists that the presence of lithic breccias has been recognized as powerful evidence for caldera collapse even where visible caldera topography is absent (Perrotta and Scarpati, 1994; Sosa-Ceballos et al., 2012; Andrews, 2014). The Sounkyo eruption generated a thick lithic breccia (SK-C) in which as large and abundant lithic blocks are included as the lithic breccias described in other caldera-forming eruptions elsewhere, despite the formation of the Ohachidaira caldera without a major caldera collapse. This casts doubt on the common interpretation that lithic breccias in the deposits of caldera-forming eruptions record caldera collapse.

I believe that lithic breccias ejected in large caldera-forming eruptions are probably generated in association with caldera collapse. The wide variety of lithic types of the lithic breccias, such as at Crater Lake, Phlegraean Fields, and Santorini, may reflect the opening of multiple vents (Suzuki-Kamata et al., 1993; Rosi et al., 1996; Druitt, 2014). Moreover, for large caldera-forming eruptions, the deep-origin lithic fragments tend to appear or become more abundant in the lithic breccias than in the preceding deposits of the same eruption (Table 4.3), indicating rapid conduit erosion not only at shallow levels, but also at depth. This is consistent with the idea that lithic breccias are formed in association with caldera collapse.

For small caldera-forming eruptions, such as at Ohachidaira, Ceboruco, and Ksudach, however, the content of deep-origin lithics in the lithic breccias is lower than or similar with that in the preceding deposits (Table 4.3), and hence the high flux of

lithic fragments into the conduit occurred at shallower depth. This indicates that such lithic breccias reflect a significant change in the shallower conduit system. Considering that SK-C lithic breccia (1) grades downward into SK-B ignimbrite, suggesting that deposition was continuous, (2) is dominated by coarse lithic blocks derived from the walls of the uppermost conduit, (3) is unstratified and ungraded even where >27 m thick, and (4) was followed by an eruptive hiatus as evidenced by the occurrence of the fine-ash layer or reworked deposit sandwiched between SK-C lithic breccia and SK-D fallout, I infer that SK-C lithic breccia marks large-scale failure of the shallow part of conduit walls that (1) produced abundant volcanic lithic fragments, (2) choked the conduit, (3) stopped the eruption, and (4) enlarged the vent. I conclude that the occurrence of lithic breccias within small caldera-forming eruption products does not necessarily reflect the presence and the timing of caldera collapse.

**Table 4.3:** Percentage of deep-origin lithic fragments in the total lithic component for lithic breccias and the preceding deposits.

| | | Preceding deposits | Lithic breccias |
|---|---|---|---|
| *Large calderas* | Santorini (Minoan) [a] | 2.6 | 11.4 |
| | Santorini (Lower Pumice 1) [b] | 0 | 4 |
| | Crater Lake [c] | 0.2 | 4.7 |
| | Vico (Sutri Formation) [d] | 5 | 12 |
| | Las Cañadas (Abrigo ignimbrite) [e] | ? | 9.9 |
| *Small calderas* | Ohachidaira | 16.2 | 2.2 |
| | Ceboruco [f] | 7.5 | 4.5 |
| | Ksudach [g] | 2.7 | 2.6 |

Deep-origin lithic component consists mostly of sedimentary and/or plutonic rocks whcih form the basement in each volcanic field.

[a] Druitt, 2014.

[b] Simmons et al., 2016.

[c] Suzuki-Kamata et al., 1993.

[d] Bear et al., 2009.

[e] Pittari et al., 2008.

[f] Browne and Gardner, 2004.

[g] Andrews et al., 2007.

### 4.5.5. Comparison with other small calderas formed by vent widening

Besides Ohachidaira, small calderas inferred to have formed by vent widening include Novarupta (Hildreth, 1983) and Caldeira in Faial, Azores (Pimentel et al., 2015), all of which show a detailed stratigraphy of tephra from the caldera-forming eruptions, but do not provide direct insight into subsurface structures. However, some Japanese small calderas, Nigorikawa in southwestern Hokkaido (Ando, 1983; Kurozumi and Doi, 2003), Sunagohara in northeastern Honshu (Mizugaki, 1993, 2000), and Gora in the Hakone volcano group (Mannen, 2008, 2014), are well constrained in three dimensions to have a funnel-shaped conduit by geothermal drilling. Here I attempt to correlate the subsurface structures of funnel-shaped small calderas with the stratigraphy of the deposits outside the calderas, proposing a new model for the formation of lithic breccias.

At the Nigorikawa caldera, 3 km in diameter on the ground surface, more than 50 geothermal drill holes delimit the structure of the caldera to depths of ~3 km, showing that inward slopes of the funnel decrease upward from 90° deeper than ~2 km through 70–90° at a depth of 1–2 km to 30–50° shallower than 1 km (see Fig. 4 of Kurozumi and Doi, 2003). The caldera is filled largely by massive lapilli tuff–pyroclastic breccia deposits composed predominantly of lithic fragments of basement rocks in the fine matrix of the same composition, which are capped by lacustrine sediments (Ando, 1983; Kurozumi and Doi, 2003). A similar stratigraphy of the caldera fill is also observed at Sunagohara and Gora. These caldera fills below the lacustrine sediments are essentially landslide breccias (Lipman, 1997) derived from unstable caldera walls, as suggested by (1) the sparseness of juvenile materials, (2) the occurrence of basement fragments derived from shallower depth (Mannen, 2008, 2014), and (3) the upward increase in the content of the shallower-origin basement fragments at the expense of the deeper-origin ones (Ando, 1983; Kurozumi and Doi, 2003), although a part of the caldera fill was inferred to be of fall-back origin (Kurozumi and Doi, 2003).

Another important feature of such funnel-shaped small calderas is that (1) the conduit walls are fractured in situ over horizontal distances of a few m to 500 m (Nigorikawa, Ando, 1983; Kurozumi and Doi, 2003, Sunagohara, Mizugaki, 1993,

2000) and (2) the openings of the fractures are partly filled with lithic and pumice lapilli-tuff that sticks firmly to the fracture surfaces for the case of Nigorikawa (Ando, 1983). Ando (1983) suggested the breakage of the conduit walls by explosions of the eruption and the subsequent penetration of high-temperature eruptive materials into the fractures.

I hypothesize that (1) the shallow part of a conduit has been eroded and enlarged enough for the development of the fractured zone into conduit walls before and during an eruption climax (e.g. SK-A to -B), (2) the subsequent waning of the eruption lead to the collapse of unstable fractured walls and the production of lithic breccias (e.g. SK-C), and (3) the collapsing mixture composed predominantly of fragments of basement rocks with minor eruptive materials contributes, at least in part, its caldera fill. The volcanic lithic fragments in SK-C lithic breccia are often cemented by coarse ash and fine pumice, scoria, and lithic lapilli up to 2 cm in size. This is consistent with the inference that the source of the lithic fragments in SK-C lithic breccia was the fractured conduit walls. The minor volume of magma ejected during the eruption of SK-C lithic breccia, accounting for ~0.3% of the total erupted volume in the Sounkyo eruption, and its lithic-rich nature (usually 50–70 vol%) imply a rapid decrease in eruption intensity (Walker, 1980; Cioni et al., 2008) after the eruption climax.

The ejecta from the 12 ka Nigorikawa eruption (>4 $km^3$ DRE; Kurozumi and Doi, 2003) comprises pyroclastic fall and surge deposits and the overlying three successive units of pyroclastic flows, the second of which is enriched in coarse lithic fragments and appears to be confined to the more proximal area than the other two (Yanai et al., 1992). The lithic fragments are dominated by hornblende andesite which was inferred to have formed a pre-caldera lava dome (Sato, 1968). Kurozumi and Doi (2003) suggested that the caldera fill below the lacustrine sediments was formed contemporaneously with the eruption of the pyroclastic flows, based on similarity in refractive index of hornblende between the caldera fill and the three pyroclastic-flow deposits. The lithic-rich pyroclastic-flow deposit may have formed in the same manner as SK-C lithic breccia described above.

The ~1000-years BP eruption of Caldeira (>0.3 $km^3$ DRE) formed a 2-km-diameter summit caldera, producing a massive to locally diffuse-bedded lithic

breccia rich in lavas at the final phase of the eruption (Pimentel et al., 2015). Pimentel et al. (2015) proposed that the lithic breccia reflects the collapse of the summit into a cored-out central vent during which the caldera was mostly formed. This interpretation is in agreement with my model for the formation of lithic breccias.

At Novarupta, any lithic breccias have not been observed in near-vent (Novarupta) exposures, though the concealed lithic breccias were presumed to underlie the ejecta of the subsequent episode (Hildreth, 1987; Hildreth and Fierstein, 2012). At Sunagohara and Gora, no lithic breccias have been reported, probably due to the absence of proximal exposures in the former case and due to the lack of exact identification of the resulting ejecta in the latter case (Yamamoto and Suto, 1996; Mannnen, 2008, 2014).

### 4.5.6. Reconstruction of the Sounkyo eruption

The 34 ka Sounkyo eruption was the last major explosive event at Ohachidaira volcano of the Taisetsu volcano group, depositing fallout, ignimbrite, and lithic breccia units in proximal and distal areas (Fig. 4.2). The eruption initiated with a column-forming phase. The column heights were relatively low and fluctuating during the earlier phase, forming the thin-bedded, finer-grained, pumice- and scoria-fall succession (SK-A1 and the lower part of the distal pumice-fall deposit; Fig. 4.3). The eruption of SK-A1 was characterized by repeated waxing, waning, and dissipation of eruption columns along with occasional small-scale column collapse, as evidenced by: (1) rhythmic alternation of graded lapilli- and ash-fall layers (Fig. 4.5a); (2) the presence of short time breaks, as suggested by fine-ash layers in the succession; and (3) the occurrence of the thin PDC beds interbedded with fall deposits (Fig. 4.5b).

In the later phase, the eruption became more sustained and more vigorous, and the eruption column reached as high as 25 km (subplinian to plinian), producing the thick, coarse-grained, diffusely stratified, pumice-dominated fallout (SK-A2 and the upper part of the distal pumice-fall deposit; Fig. 4.3). The diffuse stratification due to grain-size variation was most likely produced by slight fluctuations in column height. The lithic component is dominated by the volcanic rocks throughout SK-A (Fig. 4.13),

which reflects a progressive widening of the shallow part of the conduit and vent.

The second phase, the climax of the Sounkyo eruption, was characterized by the collapse of the eruption column and the formation of large-scale PDCs. The PDCs left SK-B ignimbrite in proximal regions, and then traveled down to the east to northeast and south to southwest flanks of the Taisetsu volcano group and infilled the paleovalleys to deposit the Px-type ignimbrite (Fig. 2.4). The presence of the localized lithic-rich base of SK-B ignimbrite (e.g. locality 5; Fig. 4.7a) suggests that the sustained eruption column was overloaded by sudden increase in flux of lithic fragments and then collapsed. The dominance of the volcanic lithic fragments in SK-B implies that the shallow part of the conduit and vent were progressively widened, although the sudden increase of the granodiorite lithic fragments in the middle part of SK-B attests to the breakage of conduit walls at depth (Fig. 4.13). At the end of the phase, the shallow part of the conduit and vent collapsed and widened probably due to the instability of the fractured conduit walls caused by progressive erosion, and dense, very coarse lithic-rich, low-mobile PDCs were generated to form the lithic breccia (SK-C; Fig. 4.8) within the proximal area. The extensive failure of the conduit walls simultaneously choked the conduit itself and in turn stopped the eruption.

After a short hiatus in explosive activity, the eruption resumed with a short-lived fall phase, establishing an eruption column up to 16 km high and producing the scoria-dominated fallout (SK-D) in the vicinity of the source. The stratification marked by variation in grain-size suggests fluctuations in column height. This phase was followed immediately by the generation of PDCs, the final phase, by eruption column collapse to form SK-E ignimbrite in the proximal area. The PDCs may have traveled down to accumulate the Px-type ignimbrite.

## 4.6. Conclusions

The 34 ka Sounkyo eruption provides key information on the eruptive dynamics and formation mechanisms of small calderas. The major conclusion is that lithic breccias associated with caldera eruptions, which are usually regarded as marking caldera collapse, do not reflect the presence and the timing of caldera collapse in small caldera-forming eruptions. Instead, such lithic breccias may be the surface expression of the collapse of the shallow part of conduit walls that has been highly fractured and hence unstable due to progressive erosion prior to and during the climax of the eruption. This is particularly important when modeling the collapse mechanisms of calderas, because some models were developed on the premise that the lithic breccias record the onset of caldera collapse irrespective of caldera size (Roche and Druitt, 2001; Geyer et al., 2006; Andrews and Gardner, 2010; Geshi et al., 2014), which might lead to misinterpretation of the collapse conditions and styles.

# Chapter 5

# Summary

Major advances in understanding the eruptive history of Ohachidaira volcano and the development of its summit caldera and in elucidating formation mechanisms and eruptive dynamics of small calderas have included the following:

1. Since at least 0.6 Ma, Ohachidaira initiated its eruptive activity and produced andesitic to dacitic lavas (Ohachidaira lava) and pyroclastics, forming the lower edifice. Between 80–40 ka and 34 ka, Ohachidaira produced two relatively small explosive eruptions, the Kobachidaira ignimbrite and Mamiyadake Scoria Member. Finally, at 34 ka, the largest Sounkyo eruption occurred in association with caldera formation.
2. While the last largest explosive event (Sounkyo eruption) made a major contribution to the caldera development, the lithic content and assemblages implies that the earlier explosive events (Kobachidaira ignimbrite and Mamiyadake Scoria Member) must have corresponded to vent enlargement to some extent.
3. The 80–40 ka Hb-type ignimbrite (>4.6 $km^3$ in bulk volume), whose source was believed to be the Ohachidaira caldera by some workers (Sato and Wada, 2012), was vented from somewhere in the Taisetsu volcano group rather than the Ohachidaira caldera.
4. The Kobachidaira ignimbrite (0.04 $km^3$ in bulk volume), which was referred to as “lithic pyroclastic deposit” in Metsugi (1987), is described in much more detail. The detailed field mapping demonstrates that the eruptive order of the Kobachidaira ignimbrite and the Mamiyadake Scoria Member is opposed to that suggested by Metsugi (1987).
5. The Mamiyadake Scoria Member (0.08 $km^3$ in bulk volume), which was referred

to as “base-surge deposit” in Metsugi (1987), in fact, includes not only eruptive products of base-surge origin but also those of fall and flow origin.

6. The 34 ka Sounkyo eruption is the latest and largest event at Ohachidaira volcano in the Taisetsu volcano group, which produced 7.6 $km^3$ of tephra (~5 $km^3$ DRE) as fallout, ignimbrite, and lithic breccia units (SK-A to -E and the Px-type ignimbrite).
7. The correlation between the proximal units SK-A to -E and the distal Px-type ignimbrite was achieved by the similarity in paleomagnetic directions, together with their lithological and petrological characteristics.
8. The ChRM directions for the Hb-type ignimbrite, Kobachidaira ignimbrite, Mamiyadake Scoria Member, and Sounkyo Member are distinguishable each other, which confirms the inference from field relations that each eruptive episodes are temporally distinct.
9. The volume of the Ohachidaira caldera (0.35 $km^3$) is comparable to that of lithic fragments ejected during the Sounkyo eruption (0.28 $km^3$) and is an order of magnitude less than that of magma ejected (5.10 $km^3$), suggesting that the Ohachidaira caldera was not essentially formed by caldera collapse and instead formed mainly by vent widening as a consequence of explosive erosion and failure of the shallow part of the conduit during the Sounkyo eruption.
10. The Ohachidaira caldera would be a funnel-shaped small caldera, as seen at Nigorikawa in Japan.
11. The lithic breccia (SK-C) erupted after the climactic ignimbrite (SK-B) marks large-scale wall slumping at the shallow conduit that (1) produced abundant lithic fragments, (2) choked the conduit, (3) stopped the eruption, and (4) enlarged the vent.
12. Although lithic breccias in caldera-forming eruption products are commonly regarded as marking the onset of caldera collapse, this study indicates that the occurrence of lithic breccias in small caldera-forming eruptions does not necessarily reflect the presence and the timing of caldera collapse.
13. Lithic breccias commonly overlie climactic ignimbrite/fallout deposits in small caldera-forming eruptions, and a new model for the formation of such lithic

breccias is proposed; (1) the shallow conduit has been explosively eroded and enlarged with consequent fragmentation and brecciation of the walls before and during an eruption climax, (2) the subsequent waning of the eruption lead to the collapse of unstable fractured walls and the production of lithic breccias, and (3) the collapsing mixture composed predominantly of fragments of basement rocks with minor eruptive materials contributes, at least in part, its caldera fill.

14. Small calderas (<3 km in diameter) may be formed by vent widening rather than by caldera collapse. It seems unlikely that the roof block (or fragmented roof blocks) subsides into the emptying magma chamber along downward narrowing peripheral faults as suggested by some workers (Scott et al., 1996; Browne and Gardner, 2004; Andrews, 2014). Instead, such calderas are formed by explosive erosion and failure of the shallow conduit and vent. The large-scale vent collapse, which may play a significant role in establishing the overall size of the calderas, produces a coarse lithic breccia sheet at the end of the main phase of the explosive sequence.

# Acknowledgments

First of all, I express my sincere thanks to Prof. Keiko Suzuki-Kamata for her enthusiasm for volcanology, which let me in this field. I have had lots of exciting discussion with her to develop ideas described in this thesis. I would like to deeply acknowledge Dr. Eiichi Sato for continued support and wise advice throughout the course of my career in Kobe University. I appreciate Prof. Yoichiro Otofuji for hearty support and his humor that always cheer me up. I am very grateful to Dr. Masako Miki and Prof. Masayuki Hyodo for their wise advice on paleomagnetism. I like to acknowledge Prof. Keiji Wada who gave me a chance to study the Ohachidaira caldera and introduced me to some outcrops. I would like to deeply acknowledge Prof. Hiroaki Sato for valuable comments and helpful suggestions. I would like to thank Dr. Koji Kiyosugi for technical assistance with the XRF analysis. I would like to appreciate Chisato Yamamoto for help with preparation of the reference list and continuous support. I thank Prof. Yoshiyuki Tatsumi, Nobukazu Seama, and Junichiro Makino for their comments that help to improve an earlier version of the manuscript.

For field assistance and comradeship, I am grateful to Dr. Kosuke Ishige. I also would like to thank my field partners, Eri Iizuka, Jumpo Hashimoto, and Dr. Hyeon-Seon Ahn for help with sampling. I thank all of my co-students in Volcanology group of Kobe University for their endless cooperation.

My deepest gratitude goes to Mr. and Mrs. Kawabata who have taken care of me during my stay in Hokkaido, without which I could not finish up the fieldwork. I thank the keepers of mountain huts, Kurodake-ishimuro and Hakuundake-hinan-goya, and the keepers of hotels at Asahidake Onsen for their support and encouragement.

Permission for field access and sampling was granted by the Ministry of the Environment and Agency for Cultural Affairs (Government of Japan). The research was financially supported by the Sasakawa Scientific Research Grant from The Japan Science Society and the Fukada Grant-in-Aid from the Fukada Geological Institute.

Finally I thank my family from the bottom of my heart for their love and support.

# References


Allen, S.R., 2001. Reconstruction of a major caldera-forming eruption from pyroclastic deposit characteristics: Kos Plateau Tuff, eastern Aegean Sea. J. Volcanol. Geotherm. Res. 105, 141–162.

Allen, S.R., 2005. Complex spatter- and pumice-rich pyroclastic deposits from an andesitic caldera-forming eruption: the Siwi pyroclastic sequence, Tanna, Vanuatu. Bull. Volcanol. 67, 27–41.

Allen, S.R., Cas, R.A.F., 1998. Lateral variations within coarse co-ignimbrite lithic breccias of the Kos Plateau Tuff, Greece. Bull. Volcanol. 59, 356–377.

Ando, S., 1983. Structure of the Nigorikawa caldera interpreted from the bore hole data. Earth Mon. 5, 116–121 (in Japanese).

Andrews, B.J., 2014. Magmatic storage conditions, decompression rate, and incipient caldera collapse of the 1902 eruption of Santa Maria Volcano, Guatemala. J. Volcanol. Geotherm. Res. 282, 103–114.

Andrews, B.J., Gardner, J.E., 2010. Effects of caldera collapse on magma decompression rate: An example from the 1800 $^{14}$C yr BP eruption of Ksudach Volcano, Kamchatka, Russia. J. Volcanol. Geotherm. Res. 198, 205–216.

Andrews, B.J., Gardner, J.E., Tait, S., Ponomareva, V., Melekestsev, I.V., 2007. Dynamics of the 1800 $^{14}$C yr BP caldera-forming eruption of Ksudach Volcano, Kamchatka, Russia. Geophys. Monogr. 172, 325–342.

Aramaki, S., 1983. Calderas: A review. Earth Mon. 5, 64–72 (in Japanese).

Aramaki, S., 1984. Formation of the Aira caldera, southern Kyushu, ~22,000 years ago. J. Geophys. Res. 89, 8485–8501.

Bacon, C.R., 1983. Eruptive history of Mount Mazama and Crater Lake caldera, Cascade Range, U.S.A. J. Volcanol. Geotherm. Res. 18, 57–115.

Bear, A.N., Cas, R.A.F., Giordano, G., 2009. The implications of spatter, pumice and lithic clast rich proximal co-ignimbrite lag breccias on the dynamics of caldera forming eruptions: The 151 ka Sutri eruption, Vico Volcano, Central Italy. J. Volcanol. Geotherm. Res. 181, 1–24.

Beresford, S.W., Cole, J.W., 2000. Kaingaroa Ignimbrite, Taupo Volcanic Zone, New Zealand: evidence for asymmetric caldera subsidence of the Reporoa Caldera. N.Z. J. Geol. Geophys. 43, 471–481.

Bonadonna, C., Costa, A., 2012. Estimating the volume of tephra deposits: A new simple strategy. Geology 40, 415–418.

Braitseva, O.A., Melekestsev, I.V., Ponomareva, V.V., Kirianov, V.Yu., 1996. The caldera-forming eruption of Ksudach volcano about cal. A.D. 240: the greatest explosive event of our era in Kamchatka, Russia. J. Volcanol. Geotherm. Res. 70, 49–65.

Branney, M.J., Kokelaar, P., 1994. Volcanotectonic faulting, soft-state deformation, and rheomorphism of tuffs during development of a piecemeal caldera, English Lake District. Geol. Soc. Am. Bull. 106, 507–530.

Brown, R.J., Branney, M.J., 2004. Event-stratigraphy of a caldera-forming ignimbrite eruption on Tenerife: the 273 ka Poris Formation. Bull. Volcanol. 66, 392–416.

Browne, B.L., Gardner, J.E., 2004. The nature and timing of caldera collapse as indicated by accidental lithic fragments from the AD ~1000 eruption of Volcán Ceboruco, Mexico. J. Volcanol. Geotherm. Res. 130, 93–105.

Butler, R.F., 1992. Paleomagnetism: Magnetic Domains to Geologic Terranes. Blackwell Sci., Boston, Mass. 319pp.

Cagnoli, B., Tarling, D.H., 1997. The reliability of anisotropy of magmatic susceptibility (AMS) data as flow direction indicators in friable base surge and ignimbrite deposits: Italian examples. J. Volcanol. Geotherm. Res. 75, 309–320.

Carey, S., Sparks, R.S.J., 1986. Quantitative models of the fallout and dispersal of tephra from volcanic eruption columns. Bull. Volcanol. 48, 109–125.

Chesner, C.A., Rose, W.I., 1991. Stratigraphy of the Toba Tuffs and the evolution of the Toba Caldera Complex, Sumatra, Indonesia. Bull. Volcanol. 53, 343–356.

Cioni, R., Santacroce, R., Sbrana, A., 1999. Pyroclastic deposits as a guide for reconstructing the multi-stage evolution of the Somma-Vesuvius Caldera. Bull. Volcanol. 60, 207–222.

Cioni, R., Bertagnini, A., Santacroce, R., Andronico, D., 2008. Explosive activity and eruption scenarios at Somma-Vesuvius (Italy): Towards a new classification

scheme. J. Volcanol. Geotherm. Res. 178, 331–346.

Costa, A., Folch, A., Macedonio, G., Giaccio, B., Isaia, R., Smith, V.C., 2012. Quantifying volcanic ash dispersal and impact of the Campanian Ignimbrite super-eruption. Geophys. Res. Lett. 39, 1–5.

Del Gaudio, P., Ventura, G., 2008. Mechanical erosion of xenoliths by magmatic shear flow. Geophys. Res. Lett. 35, 1–5.

Doi, S., Konoya, M., Fuziwara, T., Hasegawa, K., 1962. Geology of Kamikawa-cho, Kamikawa Province, Hokkaido. Report of the geological survey of Hokkaido 26, 36 pp (in Japanese).

Druitt, T.H., 1985. Vent evolution and lag breccia formation during the Cape Riva eruption of Santorini, Greece. J. Geol. 93, 439–454.

Druitt, T.H., 2014. New insights into the initiation and venting of the Bronze-Age eruption of Santorini (Greece), from component analysis. Bull. Volcanol. 76, 1–21.

Druitt, T.H., Sparks, R.S.J., 1982. A proximal ignimbrite breccia facies on Santorini, Greece. J. Volcanol. Geotherm. Res. 13, 147–171.

Druitt, T.H., Sparks, R.S.J., 1984. On the formation of calderas during ignimbrite eruptions. Nature 310, 679–681.

Druitt, T.H., Bacon, C.R., 1986. Lithic breccia and ignimbrite erupted during the collapse of Crater Lake Caldera, Oregon. J. Volcanol. Geotherm. Res. 29, 1–32.

Druitt, T.H., Mellors, R.A., Pyle, D.M., Sparks, R.S.J., 1989. Explosive volcanism on Santorini, Greece. Geol. Mag. 126, 95–126.

Edgar, C.J., Wolff, J.A., Nichols, H.J., Cas, R.A.F., Martí, J., 2002. A complex Quaternary ignimbrite-forming phonolitic eruption: the Poris Member of the Diego Hernández Formation (Tenerife, Canary Islands). J. Volcanol. Geotherm. Res. 118, 99–130.

Edgar, C.J., Cas, R.A.F., Olin, P.H., Wolff, J.A., Martí, J., Simmons, J.M., 2017. Causes of complexity in a fallout dominated plinian eruption sequence: 312 ka Fasnia Member, Diego Hernández Formation, Tenerife, Spain. J. Volcanol. Geotherm. Res. 345, 21–45.

Escher, B.G., 1929. On the formation of caldera's. Leidsche Geol. Med. 3, 183–219.

Fierstein, J., Nathenson, M., 1992. Another look at the calculation of fallout tephra volumes. Bull. Volcanol. 54, 156–167.

Fierstein, J., Houghton, B.F., Wilson, C.J.N., Hildreth, W., 1997. Complexities of plinian fall deposition at vent: an example from the 1912 Novarupta eruption (Alaska). J. Volcanol. Geotherm. Res. 76, 215–227.

Filson, J., Simkin, T., Leu, L.K., 1973. Seismicity of a caldera collapse: Galapagos Islands 1968. J. Geophys. Res. 78, 8591–8622.

Fisher, R., 1953. Dispersion on a sphere. Proc. R. Soc. London Ser. A. 217, 295–305.

Fiske, R.S., Tobisch, O.T., 1994. Middle Cretaceous ash-flow tuff and caldera-collapse deposit in the Minarets Caldera, east-central Sierra Nevada, California. Geol. Soc. Am. Bull. 106, 582–593.

Folch, A., Martí, J., 2009. Time-dependent chamber and vent conditions during explosive caldera-forming eruptions. Earth Planet. Sci. Lett. 280, 246–253.

Gardner, J.E., Tait, S., 2000. The caldera-forming eruption of Volcán Ceboruco, Mexico. Bull. Volcanol. 62, 20–33.

Geshi, N., Shimano, T., Chiba, T., Nakada, S., 2002. Caldera collapse during the 2000 eruption of Miyakejima Volcano, Japan. Bull. Volcanol. 64, 55–68.

Geshi, N., Ruch, J., Acocella, V., 2014. Evaluating volumes for magma chambers and magma withdrawn for caldera collapse. Earth Planet. Sci. Lett. 396, 107–115.

Geyer, A., Folch, A., Martí, J., 2006. Relationship between caldera collapse and magma chamber withdrawal: An experimental approach. J. Volcanol. Geotherm. Res. 157, 375–386.

Gregg, P.M., de Silva, S.L., Grosfils, E.B., Parmigiani, J.P., 2012. Catastrophic caldera-forming eruptions: Thermomechanics and implications for eruption triggering and maximum caldera dimensions on Earth. J. Volcanol. Geotherm. Res. 241–242, 1–12.

Global Volcanism Program, 2013. Volcanoes of the World, v.4.6.6. Venzke, E (ed.). Smithsonian Institution.

Hayashida, A., Kamata, H., Danhara, T., 1996. Correlation of widespread tephra deposits based on paleomagnetic directions: Link between a volcanic field and sedimentary sequences in Japan. Quaternary International 34–36, 89–98.

Heiken, G., Goff, F., Stix, J., Tamanyu, S., Shafiqullah, M., Garcia, S., Hagan, R., 1986. Intracaldera volcanic activity, Toledo Caldera and Embayment, Jemez Mountains, New Mexico. J. Geophys. Res. 91, 1799–1815.

Hildreth, W., 1983. The compositionally zoned eruption of 1912 in the Valley of Ten Thousand Smokes, Katmai National Park, Alaska. J. Volcanol. Geotherm. Res. 18, 1–56.

Hildreth, W., 1987. New perspectives on the eruption of 1912 in the Valley of Ten Thousand Smokes, Katmai National Park, Alaska. Bull. Volcanol. 49, 680–693.

Hildreth, W., 1996. Kulshan caldera: A Quaternary subglacial caldera in the North Cascades, Washington. Geol. Soc. Am. Bull. 108, 786–793.

Hildreth, W., Mahood, G.A., 1986. Ring-fracture eruption of the Bishop Tuff. Geol. Soc. Am. Bull. 97, 396–403.

Hildreth, W., Fierstein, J., 2010. Katmai volcanic cluster and the great eruption of 1912. Geol. Soc. Am. Bull. 112, 1594–1620.

Hildreth, W., Fierstein, J., 2012. The Novarupta-Katmai eruption of 1912—largest eruption of the twentieth century: centennial perspectives. U.S.G.S. Prof. Paper 1791, 259pp.

Hiscott, R.N., 1994. Loss of capacity, not competence, as the fundamental process governing deposition from turbidity currents. J. Sediment. Res. A64, 209–214.

Houghton, B.F., Carey, R.J., Cashman, K.V., Wilson, C.J.N., Hobden, B.J., Hammer, J.E., 2010. Diverse patterns of ascent, degassing, and eruption of rhyolite magma during the 1.8 ka Taupo eruption, New Zealand: Evidence from clast vesicularity. J. Volcanol. Geotherm. Res. 195, 31–47.

Ishige, K., 2017. Geology and petrology of Taisetsu volcano group, Japan—Relation between long-term volcanic activity and evolution of magma in the arc-arc junction. Hokkaido University, Ph.D. thesis, 152pp (in Japanese).

Ishige, K., Nakagawa, M., 2017. Late Pleistocene–Holocene volcanic history of Asahidake subgroup of Taisetsu volcano group, central Hokkaido, Japan. J. Geol. Soc. Japan 123, 73–91 (in Japanese with English abstract).

Katsui, Y., Yokoyama, I., Ito, T., 1979. Volcanic geology, volcanic status, and disaster measures, “Asahidake”. Research Report on Volcanoes in Hokkaido. Hokkaido

Disaster Prevention Conference. 7, 42pp (in Japanese).

Kennedy, B., Stix, J., 2007. Magmatic processes associated with caldera collapse at Ossipee ring dyke, New Hampshire. Geol. Soc. Am. Bull. 119, 3–17.

Kennedy, B., Wilcock, J., Stix, J., 2012. Caldera resurgence during magma replenishment and rejuvenation at Valles and Lake City calderas. Bull. Volcanol. 74, 1833–1847.

Kirschvink, J.L., 1980. The least-squares line and plane and the analysis of palaeomagnetic data. Geophys. J. R. Astr. Soc. 62, 699–718.

Kita, S., Nakajima, J., Hasegawa, A., Okada, T., Katsumata, K., Asano, Y., Kimura, T., 2014. Detailed seismic attenuation structure beneath Hokkaido, northeastern Japan: Arc-arc collision process, arc magmatism, and seismotectonics. J. Geophys. Res. Solid Earth 119, 6486–6511.

Kokelaar, P., 2007. Friction melting, catastrophic dilation and breccia formation along caldera superfaults. J. Geol. Soc. London 164, 751–754.

Konoya, M., Matsui, K., Kawachi, S., Kobayashi, T., 1966. Explanatory text of the geological map of Japan, Scale 1:50,000, “Taisetsuzan”. Hokkaido Development Agency. Abashiri-43, 47pp (in Japanese with English abstract).

Kurozumi, H., Doi, N., 2003. Inner structure of the Nigorikawa caldera, Hokkaido, Japan. Bull. Volcanol. Soc. Japan 48, 259–274 (in Japanese with English abstract).

Legros, F., 2000. Minimum volume of a tephra fallout deposit estimated from a single isopach. J. Volcanol. Geotherm. Res. 96, 25–32.

Lindsay, J.M., de Silva, S., Trumbull, R., Emmermann, R., Wemmer, K., 2001. La Pacana caldera, N. Chile: a re-evaluation of the stratigraphy and volcanology of one of the world’s largest resurgent calderas. J. Volcanol. Geotherm. Res. 106, 145–173.

Lipman, P.W., 1976. Caldera-collapse breccias in the western San Juan Mountains, Colorado. Geol. Soc. Am. Bull. 87, 1397–1410.

Lipman, P.W., 1997. Subsidence of ash-flow calderas: relation to caldera size and magma-chamber geometry. Bull. Volcanol. 59, 198–218.

Lipman, P.W., Sawyer, D.A., 1985. Mesozoic ash-flow caldera fragments in

southeastern Arizona and their relation to porphyry copper deposits. Geology 13, 652–656.

Lipman, P.W., Bogatikov, O.A., Tsvetkov, A.A., Gazis, C., Gurbanov, A.G., Hon, K., Koronovsky, N.V., Kovalenko, V.I., Marchev, P., 1993. 2.8-Ma ash-flow caldera at Chegem River in the northern Caucasus Mountains (Russia), contemporaneous granites, and associated ore deposits. J. Volcanol. Geotherm. Res. 57, 85–124.

Macedonio, G., Dobran, F., Neri, A., 1994. Erosion processes in volcanic conduits and application to the AD 79 eruption of Vesuvius. Earth Planet. Sci. Lett. 121, 137–152.

Mannen, K., 2008. Hakone caldera: structure, mode of formation, and role in present-day volcanism. Res. Rep. Kanagawa prefect. Mus. Nat. Hist. 13, 61–76 (in Japanese with English abstract).

Mannen, K., 2014. Post-caldera geology of Gora region in Hakone Volcano Group, Japan. J. Geol. Soc. Japan 120, 117–136 (in Japanese with English abstract).

Metsugi, H., 1987. History of volcanic activity on Ohachi-daira caldera, Daisetu volcano, Hokkaido, Japan. Bull. Sounkyo Mus. Nat. Hist. 7, 1–8 (in Japanese with English abstract).

Miura, D., 1999. Arcuate pyroclastic conduits, ring faults, and coherent floor at Kumano caldera, southwest Honshu, Japan. J. Volcanol. Geotherm. Res. 92, 271–294.

Mizugaki, K., 1993. Geologic structure and volcanic history of Sunagohara caldera volcano, Fukushima, Japan. J. Geol. Soc. Japan 99, 721–737 (in Japanese with English abstract).

Mizugaki, K., 2000. Geologic structure and volcanic history of the Yanaizu-Nishiyama (Okuaizu) geothermal field, Northeast Japan. Geothermics 29, 233–256.

Nairn, I.A., Wood, C.P., Bailey, R.A., 1994. The Reporoa Caldera, Taupo Volcanic Zone: source of the Kaingaroa Ignimbrites. Bull. Volcanol. 56, 529–537.

Nakada, S., 2015. Regularity of volcanic eruptions in terms of Volcanic Explosivity Index (VEI). Bull. Volcanol. Soc. Japan 60, 143–150 (in Japanese with English abstract).

New Energy and Industrial Technology Development Organization (NEDO), 1989. Report on geothermal development promotion survey. No. 16, Kamikawa district.

1032pp (in Japanese).

New Energy and Industrial Technology Development Organization (NEDO), 1990. Report on the distribution and age of volcanic rocks in the Tokachi district, Nationwide geothermal resources exploration project (phase 3), Regional exploration of geothermal fluid circulation system. 490pp (in Japanese).

Newhall, C.G., Dzurisin, D., 1988. Historical unrest at large calderas of the world. U.S. Geol. Surv. Bull. 1855, 1108pp.

Nishiki, K., Ishige, K., Shimada, S., Nakagawa, M., 2017. Fission-track and U-Pb dating of pyroclastic flow deposits around Tokachi caldera in the Biei and Kamikawa areas of central Hokkaido, Japan. Bull. Volcanol. Soc. Japan 62, 83–94 (in Japanese with English abstract).

Ono, K., 1965. Geology of the eastern part of Aso caldera, central Kyushu, southwest Japan. J. Geol. Soc. Japan 71, 541–553 (in Japanese with English abstract).

Ort, M.H., de Silva, S.L., Jiménez, C.N., Jicha, B.R., Singer, B.S., 2013. Correlation of ignimbrites using characteristic remanent magnetization and anisotropy of magnetic susceptibility, Central Andes, Bolivia. Geochem. Geophys. Geosyst. 14, 141–157.

Palladino, D.M., Simei, S., 2005. Eruptive dynamics and caldera collapse during the Onano eruption, Vulsini, Italy. Bull. Volcanol. 67, 423–440.

Palmer, H.C., MacDonald, W.D., 1999. Anisotropy of magnetic susceptibility in relation to source vents of ignimbrites: empirical observations. Tectonophysics 307, 207–218.

Perrotta, A., Scarpati, C., 1994. The dynamics of the Breccia Museo eruption (Campi Flegrei, Italy) and the significance of spatter clasts associated with lithic breccias. J. Volcanol. Geotherm. Res. 59, 335–355.

Pimentel, A., Pacheco, J., Self, S., 2015. The ~1000-years BP explosive eruption of Caldeira Volcano (Faial, Azores): the first stage of incremental caldera formation. Bull. Volcanol. 77, 1–26.

Pittari, A., Cas, R.A.F., Wolff, J.A., Nichols, H.J., Larson, P.B., Martí, J., 2008. The use of lithic clast distributions in pyroclastic deposits to understand pre- and syn-caldera collapse processes: a case study of the Abrigo Ignimbrite, Tenerife,

Canary Islands. In: Gottsman, J., Martí, J. (Eds.), Caldera Volcanism: Analysis, Modelling and Response, Developments in Volcanology 10. Elsevier, Amsterdam, pp. 97–142.

Pyle, D.M., 1989. The thickness, volume and grainsize of tephra fall deposits. Bull. Volcanol. 51, 1–15.

Roche, O., Druitt, T.H., 2001. Onset of caldera collapse during ignimbrite eruptions. Earth Planet. Sci. Lett. 191, 191–202.

Rosi, M., Vezzoli, L., Aleotti, P., De Censi, M., 1996. Interaction between caldera collapse and eruptive dynamics during the Campanian Ignimbrite eruption, Phlegraean Fields, Italy. Bull. Volcanol. 57, 541–554.

Sato, E., Wada, K., 2010. Geological field guide for the Taisetsu volcano. Interpretation of the outcrop for the Taisetsu volcano, central Hokkaido. Part 1: Volcanic products from the 30 ka eruption of Ohachidaira at Obako. Rep. Taisetsuzan Inst. Sci. 44, 1–5 (in Japanese with English abstract).

Sato, E., Wada, K., 2012. Evolution of silicic magma chamber for caldera-forming eruption of Ohachidaira in the Taisetsu volcanic group, central Hokkaido, Japan. Bull. Volcanol. Soc. Japan 57, 177–197 (in Japanese with English abstract).

Sato, H., 1968. The volcanic ejecta from the Nigorikawa caldera, southwestern Hokkaido. J. Geol. Soc. Japan 74, 104 (in Japanese).

Sato, D., Matsuura, H., Yamamoto, T., 2016. Timing of the Late Cretaceous ignimbrite flare-up at the eastern margin of the Eurasian Plate: New zircon U-Pb ages from the Aioi–Arima–Koto region of SW Japan. J. Volcanol. Geotherm. Res. 310, 89–97.

Scandone, R., 1990. Chaotic collapse of calderas. J. Volcanol. Geotherm. Res. 42, 285–302.

Scarpati, C., Sparice, D., Perrotta, A., 2014. A crystal concentration method for calculating ignimbrite volume from distal ash-fall deposits and a reappraisal of the magnitude of the Campanian Ignimbrite. J. Volcanol. Geotherm. Res. 280, 67–75.

Schumacher, R., Mues-Schumacher, U., 1996. The Kizilkaya ignimbrite—an unusual low-aspect-ratio ignimbrite from Cappadocia, central Turkey. J. Volcanol.

Geotherm. Res. 70, 107–121.

Scott, W.E., Hoblitt, R.P., Torres, R.C., Self, S., Martinez, M.L., Nillos, T., 1996. Pyroclastic flows of the June 15, 1991, climactic eruption of Mount Pinatubo. In: Newhall, C.G., Punongbayan, R.S. (Eds.), Fire and Mud: Eruptions and Lahars of Mount Pinatubo, Philippine Institute of Volcanology and Seismology, University of Washington Press, Quezon City, Seattle, pp. 545–570.

Self, S., Rampino, M.R., Newton, M.S., Wolff, J.A., 1984. Volcanological study of the great Tambora eruption of 1815. Geology 12, 659–663.

Self, S., Goff, F., Gardner, J.N., Wright, J.V., Kite, W.M., 1986. Explosive rhyolitic volcanism in the Jemez Mountains: Vent locations, caldera development and relation to regional structure. J. Geophys. Res. 91, 1779–1798.

Simmons, J.M., Cas, R.A.F., Druitt, T.H., Folkes, C.B., 2016. Complex variations during a caldera-forming Plinian eruption, including precursor deposits, thick pumice fallout, co-ignimbrite breccias and climactic lag breccias: The 184 ka Lower Pumice 1 eruption sequence, Santorini, Greece. J. Volcanol. Geotherm. Res. 324, 200–219.

Simmons, J.M., Carey, R.J., Cas, R.A.F., Druitt, T.H., 2017a. High magma decompression rates at the peak of a violent caldera-forming eruption (Lower Pumice 1 eruption, Santorini, Greece). Bull. Volcanol. 79, 1–12.

Simmons, J.M., Cas, R.A.F., Druitt, T.H., Carey, R.J., 2017b. The initiation and development of a caldera-forming Plinian eruption (172 ka Lower Pumice 2 eruption, Santorini, Greece). J. Volcanol. Geotherm. Res. 341, 332–350.

Smith, R.L., Bailey, R.A., 1968. Resurgent cauldrons. Geol. Soc. Am. Mem. 116, 613–662.

Sosa-Ceballos, G., Gardner, J.E., Siebe, C., Macías, J.L., 2012. A caldera-forming eruption ~14,100 $^{14}$C yr BP at Popocatépetl volcano, México: Insights from eruption dynamics and magma mixing. J. Volcanol. Geotherm. Res. 213, 27–40.

Sparks, R.S.J., Walker, G.P.L., 1977. The significance of vitric-enriched air-fall ashes associated with crystal-enriched ignimbrites. J. Volcanol. Geotherm. Res. 2, 329–341.

Spera, F.J., Crisp, J.A., 1981. Eruption volume, periodicity, and caldera area:

relationships and inferences on development of compositional zonation in silicic magma chambers. J. Volcanol. Geotherm. Res. 11, 169–187.

Stearns, H.T., Clark, W.O., 1930. Geology and water resources of the Kau District, Hawaii. U.S. Geological Survey Water-Supply Paper 616, 194pp.

Stix, J., Kobayashi, T., 2008. Magma dynamics and collapse mechanisms during four historic caldera-forming events. J. Geophys. Res. 113, 1–14.

Sulpizio, R., 2005. Three empirical methods for the calculation of distal volume of tephra-fall deposits. J. Volcanol. Geotherm. Res. 145, 315–336.

Suzuki-Kamata, K., Kamata, H., Bacon, C.R., 1993. Evolution of the caldera-forming eruption at Crater Lake, Oregon, indicated by component analysis of lithic fragments. J. Geophys. Res. 98, 14,059–14,074.

Tatsumi, Y., Suzuki-Kamata, K., 2014. Cause and risk of catastrophic eruptions in the Japanese Archipelago. Proc. Jpn. Acad., Ser. B, 90, 347–352.

Valentine, G.A., Wohletz, K.H., 1989. Numerical models of Plinian eruption columns and pyroclastic flows. J. Geophys. Res. 94, 1867–1887.

Valentine, G.A., Groves, K.R., 1996. Entrainment of country rocKI2ring basaltic eruptions of the Lucero volcanic field, New Mexico. J. Geol. 104, 71–90.

Varekamp, J.C., 1993. Some remarks on volcanic vent evolution during plinian eruptions. J. Volcanol. Geotherm. Res. 54, 309–318.

Walker, G.P.L., 1980. The Taupo pumice: product of the most powerful known (ultraplinian) eruption? J. Volcanol. Geotherm. Res. 8, 69–94.

Walker, G.P.L., 1985. Origin of coarse lithic breccias near ignimbrite source vents. J. Volcanol. Geotherm. Res. 25, 157–171.

Watanabe, K., Ono, K., 1969. Geology of the vicinity of Omine on the western flank of the Aso caldera. J. Geol. Soc. Japan 75, 365–374 (in Japanese with English abstract).

Watanabe, Y., Iwata, K., 1987. The Hidaka Supergroup in the Tomuraushi region, Hidaka Belt, Hokkaido, Japan. Earth Science 41, 35–47.

Williams, H., 1941. Calderas and their origin. Univ. California Publ. Depart. Geol. Sci. 25, 239–346.

Williams, H., 1942. The geology of Crater Lake National Park, Oregon. Carnegie Inst.

Washington Publ. 540, 162pp.

Wilson, C.J.N., Walker, G.P.L., 1985. The Taupo eruption, New Zealand I. General aspects. Phil. Trans. R. Soc. Lond. 314, 199–228.

Wright, J.V., Walker, G.P.L., 1977. The ignimbrite source problem: Significance of a co-ignimbrite lag-fall deposit. Geology 5, 729–732.

Yamamoto, T., 2003. Lithofacies and eruption age of Late Cretaceous caldera volcanoes in the Himeji-Yamasaki district, southwest Japan: Implications for ancient large-scale felsic arc volcanism. Island Arc 12, 294–309.

Yamamoto, T., Suto, S., 1996. Eruptive history of Bandai volcano, NE Japan, based on tephrastratigraphy. Bull. Geol. Surv. Japan 47, 335–359 (in Japanese with English abstract).

Yanai, S., Ganzawa, Y., Komori, Y., 1992. The stratigraphy and distribution of the Nigorikawa tephra, latest glacial age time-marker in southwest Hokkaido. J. Geol. Soc. Japan 98, 125–136 (in Japanese with English abstract).

Yasuda, Y., Sato, E., Wada, K., Suzuki-Kamata, K., 2015. Eruption interval between the two pyroclastic-flows from the Ohachidaira caldera of Taisetsu volcano, central Hokkaido, Japan: Estimation from the paleomagnetic directions. Bull. Volcanol. Soc. Japan 60, 447–459 (in Japanese with English abstract).

Yokoyama, I., 1963. Structure of calderas and gravity anomaly. Bull. Volcanol. 26, 67–72.

Yokoyama, I., 1983. Structure and origin of calderas. Earth Mon. 5, 93–100 (in Japanese).

Yokoyama, I., 1993. Evidence for funnel-shaped calderas. Earth Mon. 15, 672–681 (in Japanese).

Yokoyama, I., 2005. A side view of geophysical research of caldera structure for the recent 50 years. Bull. Volcanol. Soc. Japan 50, 59–76 (in Japanese with English abstract).

Yokoyama, I., 2015. Eruption products of the 1883 erup tion of Krakatau and their final settlement. Annals of Geophysics 58, 1–13.

Yokoyama, I., 2016. Origin of calderas: discriminating between collapses and explosions. Annals of Geophysics 59, 1–17.